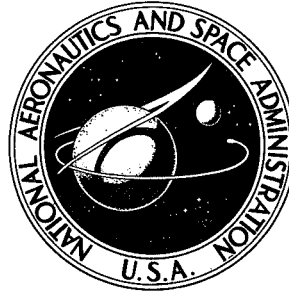


N. 70-30033

NASA TECHNICAL NOTE



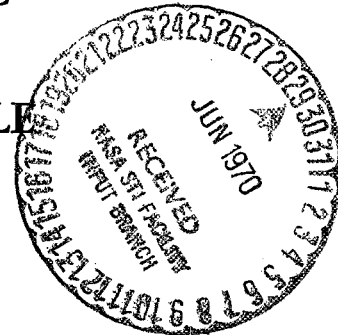
NASA TN D-5831

34567

NASA TN D-5831

CASE FILE
COPY

APPLICATION OF ANALYSIS AND
MODELS TO STRUCTURAL DYNAMIC
PROBLEMS RELATED TO THE
APOLLO-SATURN V LAUNCH VEHICLE



Coordinator: Sumner A. Leadbetter

Langley Research Center

Hampton, Va. 23365

1. Report No. NASA TN D-5831	2. Government Accession No.	3. Recipient's Catalog No.	
4. Title and Subtitle APPLICATION OF ANALYSIS AND MODELS TO STRUCTURAL DYNAMIC PROBLEMS RELATED TO THE APOLLO-SATURN V LAUNCH VEHICLE		5. Report Date June 1970	6. Performing Organization Code
		8. Performing Organization Report No. L-6595	10. Work Unit No. 124-08-13-04-23
7. Author(s) Coordinator: Sumner A. Leadbetter		11. Contract or Grant No.	
9. Performing Organization Name and Address NASA Langley Research Center Hampton, Va. 23365		13. Type of Report and Period Covered Technical Note	
		14. Sponsoring Agency Code	
12. Sponsoring Agency Name and Address National Aeronautics and Space Administration Washington, D.C. 20546		15. Supplementary Notes	
16. Abstract <p>The Langley Research Center has conducted integrated analytical and experimental investigations of potential structural dynamic problems that could contribute to structural malfunctions in the payload section of a launch vehicle. Studies were conducted in support of extensive investigations of an unmanned Apollo-Saturn 502 structural anomaly and results are presented which (1) define the dynamic-response characteristics of components of a model spacecraft, (2) evaluate involved analytical procedures, (3) compare the dynamic behavior of a partial vehicle with that of a full vehicle, and (4) verify the ability of the model spacecraft sandwich structure to withstand a potential failure mode.</p>			
17. Key Words (Suggested by Author(s)) Shell dynamics Structural dynamics Launch-vehicle dynamics Apollo-Saturn V vehicle Vibration modes		18. Distribution Statement Unclassified - Unlimited	
19. Security Classif. (of this report) Unclassified	20. Security Classif. (of this page) Unclassified	21. No. of Pages 105	22. Price* \$3.00

CONTENTS

	Page
SUMMARY	1
I. INTRODUCTION	3
Symbols and Abbreviations	7
Sumner A. Leadbetter	
II. MODELS	11
H. Wayne Leonard and Robert W. Herr	
III. TEST TECHNIQUES	31
H. Wayne Leonard and Robert W. Herr	
IV. LM-SLA COMPONENT DYNAMICS INVESTIGATION	43
William C. Walton, Jr., and Earl C. Steeves	
V. FULL-STACK AND SHORT-STACK STUDIES	65
Larry D. Pinson, John J. Catherines, and Ellwood L. Peele	
VI. COMBINED ACCELERATION LOADS SIMULATION	83
Robert R. Clary, James A. Schoenster, and Lloyd J. Turner, Jr.	
VII. GENERAL CONCLUDING REMARKS	101
Sumner A. Leadbetter	

APPLICATION OF ANALYSIS AND MODELS TO
STRUCTURAL DYNAMIC PROBLEMS RELATED TO THE
APOLLO-SATURN V LAUNCH VEHICLE

Coordinator: Sumner A. Leadbetter
Langley Research Center

SUMMARY

The Langley Research Center has conducted an integrated analytical and experimental effort, utilizing scaled dynamic models, with studies of some potential structural dynamic problems related to the Apollo-Saturn 502 (Apollo 6) launch configuration. Primary efforts have been directed toward understanding the dynamic behavior of the payload structure. Studies have been conducted to define the interactions of the lunar module and the spacecraft lunar module adapter, to evaluate analytical procedures, to compare the dynamic behavior of a short-stack configuration (partial vehicle) with that of a full-stack configuration (total vehicle), to investigate potential longitudinal-lateral coupling mechanisms, and to conduct experiments to verify the probable integrity of the model payload structure under scaled Apollo 6 static and dynamic loads, excluding aerodynamic and thermal loads.

A component-mode analytical approach, used to determine the behavior of the lunar module, the adapter, and the module-adapter assembly, has been developed and yields good agreement with the measured response characteristics of both the payload components and the assembly. A transfer-matrix analysis satisfactorily predicts both the longitudinal and lateral forced response of the short-stack and the full-stack model configurations and was utilized for parametric studies to determine the importance of component dynamic properties, the effects of component damping on coupled response, and the short-stack aft boundary conditions sufficient to produce full-stack payload response levels and lateral center-line deflections.

A mechanism which imposed minimum dynamic restraint to the vehicle was devised and used to apply simulated static acceleration-induced compressive loading to the model full-stack payload components. In addition to the static loads, and excluding thermal loads, combined longitudinal and lateral dynamic loads were applied to the model structure at the scaled levels required for proper simulation of loads at the time of a flight anomaly. The model structure withstood these combined loads without failure.

I. INTRODUCTION

By Sumner A. Leadbetter
Langley Research Center

The structural dynamic characteristics of aerospace vehicles must be accurately known to ensure controllability, structural integrity, and payload protection against the dynamic environment. Longitudinal and lateral vibrations that have occurred during both manned and unmanned flights have, at times, imposed unacceptably severe vibratory loads as a result of dynamic behavior and interactions of various components. One approach to these complex problems is through combined analytical and experimental studies to establish structurally sound configurations that will withstand the dynamic environments. Combined studies are necessary since, in many cases, analytical procedures are not sufficiently comprehensive to define the complex mathematical model required and oversimplified assumptions can lead to unsatisfactory results. Therefore, the validity of theoretical methods must be established with experimental data, often obtained by tests on full-scale hardware. Dynamic models are attractive alternates to full-scale vehicles for obtaining these necessary data for time, cost, and convenience reasons. Test results from properly scaled dynamic models, as discussed in reference I-1, can be valuable in support of analysis in several other ways: (1) provide design information where theory is inadequate, (2) identify problems in new configurations, (3) explore solutions to design problems, (4) develop test techniques for application to full-scale structures, and (5) help to explain anomalies that occur in full-scale flights and tests. However, it is essential that the theoretical and experimental work be closely coordinated in order to achieve maximum understanding of the dynamic responses of these complex aerospace structures. References I-1 to I-4 contain several examples of the application of dynamic models combined with analysis to achieve objectives such as these for the Saturn I and Titan III launch vehicles.

The application of analytical and experimental dynamic model studies to solve a specific operational problem was exemplified during a recent comprehensive investigation of a payload component malfunction that occurred during an unmanned Apollo-Saturn V flight. The second Apollo-Saturn V vehicle (AS-502 or Apollo 6) experienced longitudinal oscillations (pogo) during flight and a local structural failure occurred in the spacecraft lunar module adapter (SLA). (See refs. I-5, I-6, and I-7.) Flight data revealed that the vehicle was vibrating in a coupled first longitudinal mode and a fourth lateral bending (in the pitch plane) mode while experiencing approximately 3.5g axial static thrust acceleration. Vibratory accelerations measured on the lunar module (LM) reached 0.6g at approximately 5.5 Hz in both the pitch and the longitudinal directions. At the same time, in addition to the occurrence of abrupt changes of strain, pressure, and acoustics

and vibration levels in the vehicle third-stage and payload regions, photographs showed that structural pieces separated from the SLA area. Even though the mission was successfully completed, in-depth studies were required by the National Aeronautics and Space Administration (NASA) and its contractors to prevent a repetition of this flight anomaly since the next flight was to be manned.

Several investigations of pogo instabilities, dynamic response, and failure mechanisms, using both full-scale vehicle components and dynamic models, were undertaken at various laboratories to determine the cause of the flight malfunction and to prevent recurrence of the event. Time and cost prohibited ground vibration testing of a complete full-scale Apollo-Saturn V launch vehicle and, accordingly, experimental investigations of flight hardware were limited to static and dynamic tests of components and partial assemblies. The largest assembly tested was the short-stack configuration consisting of the third-stage forward skirt, the instrument unit, and the Apollo payload, including the launch escape system (LES). However, a 1/10-scale dynamic model of the complete flight vehicle that had previously undergone extensive investigation (refs. I-8 and I-9) was available at Langley Research Center (LRC) and could be quickly modified to carry out vibration experiments expeditiously at relatively low cost. Analytical tools, such as reference I-10, were also readily available at LRC for use with the model. Therefore, the Langley Research Center undertook a combined experimental and analytical study of structural dynamic characteristics of the Apollo-Saturn V configuration as part of the total investigation.

This paper presents some salient results from the analytical and experimental dynamic model studies conducted at the Langley Research Center. The general objectives of the studies reported were to:

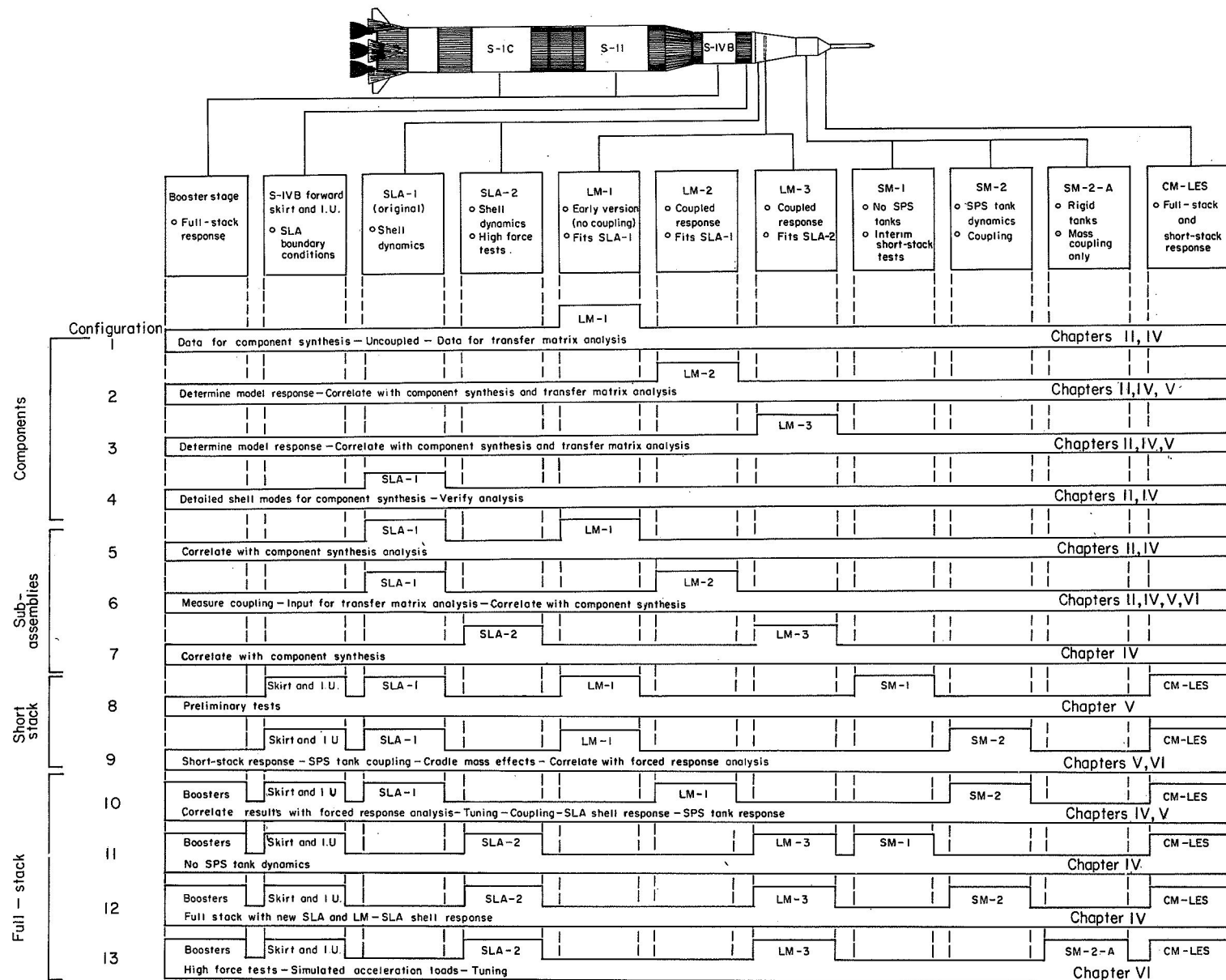
- (1) Provide an understanding of the LM-SLA combination.
- (2) Explore and establish, insofar as possible, the coupling mechanism which caused the large lateral response of the LM-SLA to the longitudinal pogo oscillations.
- (3) Assist with interpretation of full-scale short-stack results in terms of the characteristics of the complete assembled vehicle.
- (4) Verify experimentally the ability or inability of the structure to withstand a postulated failure mode involving the LM-SLA interface structure and the adjacent SLA sandwich structure subjected to combined steady acceleration loads and pogo-induced vibratory loads.

The dynamic-response investigation conducted at the Langley Research Center was a part of a broad program and by itself provided only a partial understanding of the anomaly problem; however, it did provide significant findings in the general area of space-vehicle structural dynamics. Some other phases of the LRC investigation, not reported

herein, provided specific information of value mainly to those directly involved in the anomaly study program, and included information to guide testing of full-scale hardware and to evaluate structural dynamic effects of proposed modifications to the vehicle structure.

The report is given in chapter form, as indicated in the table of contents, each chapter being written by the individuals responsible for the particular work. To assist the reader, the scope of the study and model configurations used in various phases of the LRC structural dynamics investigation are illustrated in table I-1. Across the top of the table and under the sketch of the Apollo-Saturn V are listed the various model components along with a brief statement concerning the part. The bar graphs below this list show the various configurations discussed herein, the subassemblies which comprised each particular configuration, the general objectives for each configuration, and references to pertinent presentations in the text. For example, a short-stack configuration (number 8) consisted of the S-IVB forward skirt, the instrument unit, SLA-1, LM-1, SM-1, and the CM-LES; was used for preliminary studies to develop test techniques and to obtain response data; and is discussed in chapter V. It should be noted that several LM models were studied in an iterative approach, based on experimental and analytical data, to provide a LM model whose overall dynamic characteristics (as affecting the SLA response) approximated those of the full-scale vehicle.

TABLE I-1.- MODEL CONFIGURATIONS INVESTIGATED



Symbols and Abbreviations

A_0, A_n	Fourier coefficients
a	acceleration
B_n	Fourier coefficient
d	LM model dimension (defined in figs. II-9 and II-10)
f	frequency, Hz
g	acceleration due to earth gravity
h', h	LM-2 model dimensions (defined in fig. II-10)
i	imaginary unit, $\sqrt{-1}$
l	length, displacement
m	mass
n	number of full waves on circumference of shell
s', s	LM-2 model dimensions (defined in fig. II-10)
t	LM-2 model dimension (defined in fig. II-10)
W	weight of attached mass on LM-2 cruciform
X, Y, Z	model Cartesian coordinates (positive or negative according to right-hand rule)
x	distance along X-axis
$\bar{x}, \bar{y}, \bar{z}$	Cartesian coordinates for SM-2 center of gravity
θ	phase angle

μ structural damping constant equal to twice the ratio of equivalent viscous damping to critical damping

Subscripts:

c calculated

l longitudinal

m measured

p pitch

rms root mean square

Y refers to attached weights on LM-2 Y-axis

y yaw

Z refers to attached weights on LM-2 Z-axis

Abbreviations:

AS Apollo Saturn

CM command module

IU instrument unit

LES launch escape system

LM lunar module

LRC Langley Research Center

LTA LM test article

NASA National Aeronautics and Space Administration

S-II launch-vehicle second stage
S-IC launch-vehicle first stage
S-IVB launch-vehicle third stage
SLA Saturn LM adapter
SM service module
SPS service propulsion system

References

- I-1. Guyett, P. R.: The Use of Flexible Models in Aerospace Engineering. Tech. Rep. No. 66335, Brit. R.A.E., Nov. 1966.
- I-2. Mixson, John S.; and Catherine, John J.: Experimental Lateral Vibration Characteristics of a 1/5-Scale Model of Saturn SA-1 With an Eight-Cable Suspension System. NASA TN D-2214, 1964.
- I-3. Jaszlics, Ivan J.; and Morosow, George: Dynamic Testing of a 20% Scale Model of the Titan III. AIAA Symposium on Structural Dynamics and Aeroelasticity, Aug.-Sept. 1965, pp. 477-485.
- I-4. Thompson, William M., Jr.: An Investigation of the Response of a Scaled Model of a Liquid-Propellant Multistage Launch Vehicle to Longitudinal Excitation. NASA TN D-3975, 1967.
- I-5. Anon.: Summary of the Problems Encountered in the Second Flight of the Saturn V Launch Vehicle. Hearing Before the Committee on Aeronautical and Space Sciences, U.S. Senate, Ninetieth Congress, U.S. Govt. Printing Office, 1968.
- I-6. Kelly, T. J.: Flight Experience With the Apollo Lunar Module. AIAA Pap. No. 68-1005, Oct. 1968.
- I-7. Saturn V Flight Evaluation Working Group: Saturn V Launch Vehicle Flight Evaluation Report - AS-502 Apollo 6 Mission. MPR-SAT-FE-68-3, NASA George C. Marshall Space Flight Center, 1968.
- I-8. Pinson, Larry D.; and Leonard, H. Wayne: Longitudinal Vibration Characteristics of 1/10-Scale Apollo/Saturn V Replica Model. NASA TN D-5159, 1969.
- I-9. Peele, Ellwood L.; Leonard, H. Wayne; and Leadbetter, Sumner A.: Lateral Vibration Characteristics of the 1/10-Scale Apollo/Saturn V Replica Model. NASA TN D-5778, 1970.
- I-10. Steeves, Earl C.; Durling, Barbara J.; and Walton, William C., Jr.: A Method for Computing the Response of a General Axisymmetric Shell With an Attached Asymmetric Structure. AIAA Structural Dynamics and Aeroelasticity Specialist Conference and the ASME/AIAA 10th Structures, Structural Dynamics, and Materials Conference, Apr. 1969, pp. 302-328.

II. MODELS

By H. Wayne Leonard and Robert W. Herr
Langley Research Center

Scaled models have been widely used to obtain experimental structural dynamics data. (For example, see refs. II-1 to II-3.) An existing 1/10-scale dynamic model of the complete Apollo-Saturn V vehicle shown photographically in figure II-1 was the primary experimental tool used in the present study. This model represented the latest developments in the state of the art in dynamic modeling at the time it was designed in 1964, that is, all the main load-carrying structures of the booster stages were reproduced at 1/10 size of the prototype members. The S-IC, S-II, and S-IVB stages were replica scaled; the Apollo payload portions of the model were dynamically scaled to provide only lateral vibration modes of the assembled structure and were not deemed to be adequate for the present study. Parts of the model payload such as the SLA and SM were, however, of sufficient quality to be utilized as interim hardware while more refined components were being fabricated, but other parts such as the existing LM simulator were totally inadequate and required immediate replacement. A discussion of each of the payload components, the projected test requirements for those components, and the philosophy employed in new component design are presented in the following paragraphs. Figure II-2 shows a schematic of both the full-stack and short-stack configurations and defines the nomenclature of the various model components along with the Cartesian coordinate system employed in the test and analysis program.

Scaling

In general, geometric scale factors associated with physical parameters may be expressed as a length scale factor raised to an appropriate power (see ref. II-4) if similarity of materials is maintained between the model and prototype structures. The physical parameters of importance in the present paper may be expressed in terms of length l , mass m , and acceleration a , and the following table of scale factors for the 1/10-scale model is valid:

Parameter	m-l-a relationship	Ratio of model to full scale	Parameter	m-l-a relationship	Ratio of model to full scale
Length, displacement, etc.	l	10^{-1}	Velocity	$(la)^{1/2}$	1
Mass	m	10^{-3}	Frequency	$(a/l)^{1/2}$	10
Acceleration	a	10	Angular velocity	$(a/l)^{1/2}$	10
Force	ma	10^{-2}	Area moment of inertia	l^4	10^{-4}
Longitudinal stiffness	ma	10^{-2}	Mass moment of inertia	ml^2	10^{-5}
Stress	ma/l^2	1	Bending stiffness	$ma l^2$	10^{-4}
Pressure	ma/l^2	1	Torsion stiffness	$ma l^2$	10^{-4}
Modulus of elasticity	ma/l^2	1			

Command Module (CM) and Launch Escape System (LES)

The 1/10-scale CM-LES structures as originally constructed were dynamically scaled to yield the proper longitudinal mass distribution and lateral bending stiffness; however, the complex CM-SM interface was not dynamically simulated. Since these parts of the payload were not considered to exert other than gross influence on the local payload responses, the existing CM-LES substructure was used throughout the test program.

The original model structure in the service module section of the 1/10-scale model was not sufficiently detailed to satisfy the stringent requirements of the projected test program in regard to the involved lateral-longitudinal coupling mechanisms. The extent that the SM tanks contributed to the coupled response of the flight structure was not known; therefore, it was necessary to modify the model to include simulated tanks. The SM models used during the investigation are described in the next section.

Service Module (SM) Models

SM-1.- The SM-1 service module was part of the original 1/10-scale Saturn V model. External dimensions and mass distribution and overall bending stiffness were scaled from the SM design which existed at the time the 1/10-scale model was constructed. It is a cylindrical aluminum shell bonded to a foamed plastic annular cylinder in which are imbedded ballast weights. This model was used in the early parts of the present study while construction of the SM-2 was pending.

SM-2.- The primary criterion for SM-2 was that it simulate characteristics of the full-scale SM which could contribute to longitudinal-lateral coupling in the flight vehicle. Two prime candidates for coupling appeared to be a mass center of gravity displaced from the SM center line and resonances involving significant motion of SM propellant tanks. The resulting model is relatively stiff in both bending and compression but has realistic simulation of the SM tank masses and attachment flexibilities.

The SM-2 model is illustrated in figure II-3 which also defines the tank numbering system. The four tanks are solid aluminum cylinders with an integral threaded stud extending from the bottom center of each tank.

The basic tank length was 15.3 inches (0.39 m) and the diameters were selected to yield the proper scaled weights. The respective tank masses and diameters are as follows:

Tank	Diameter		Mass	
	in.	m	lb	kg
1	2.396	0.061	6.9	3.13
2	2.675	.068	8.6	3.90
3	3.039	.077	11.1	5.03
4	3.389	.086	13.8	6.26

The lateral resonant frequency of each tank could be tuned by adjusting the spring rates at both the fore and aft ends of the tank. The spring rate at the base of the tank was varied by changing the diameter of the lower spring washers which grip the lower plate. The upper spring was adjustable by positioning of the upper spring rod bearing support. The upper spring rod is a steel shaft pressed into the upper spring bushing which is, in turn, screwed into the upper face of the simulated tank. The spring rod extends upward through a spherical bearing assembly attached inside the upper spring rod bearing support assembly, as shown in the detail sketch in figure II-3. Vertical positioning of the support assembly changes the effective length of the upper spring rod and thus changes the lateral resonant frequency of the tank.

During preliminary tests, the model SM-2 was tuned to have the following response characteristics:

Frequency, Hz	SM-2 tank motions
49.0	Out-of-phase radial motion of tanks 2 and 4
55.0	In-phase radial motion of tanks 2 and 4
69.0	Out-of-phase radial motion of tanks 1 and 3

SM-2 model mass and center-of-gravity locations as compared with scaled values from the AS-503 and AS-504 vehicles as then configured are as follows:

	Model	Scaled AS-503	Scaled AS-504
Mass, lb (kg)	58.0 (26.3)	46.0 (20.8)	50.4 (22.9)
* \bar{x} , in. (m)	7.75 (0.197)	6.60 (0.168)	6.9 (0.175)
\bar{y} , in. (m)	0.61 (0.015)	0.50 (0.013)	0.48 (0.012)
\bar{z} , in. (m)	0.53 (0.013)	0.62 (0.016)	0.66 (0.017)
Center of gravity (from center line), in. (m)	0.81 (0.020)	0.81 (0.020)	0.82 (0.021)

*Measured from bottom of lower plate.

Saturn LM Adapter (SLA) Models

SLA-1.- Although the existing SLA-1 model, described in reference II-5, was inadequate for the flight-loads simulation phase of the anomaly study, it was utilized to evaluate the analyses and to study vehicle dynamic characteristics throughout most of the test program. Although not a replica model, SLA-1 had the correct overall dimensions and was of aluminum honeycomb construction with aluminum face sheets scaled from an

early SLA design. It deviated from flight hardware in the method of attaching the LM, in the physical properties of the LM-SLA interface, and in the longitudinal location of the LM attach ring. Therefore, a new SLA model designated SLA-2 was constructed and is discussed in the following section.

SLA-2.- The 1/10-scale SLA-2 was a near-replica model. Some deviation from replica scaling was allowed in order to permit construction of the model on schedule. Since prohibitive costs and time would be required to manufacture scaled honeycomb for the sandwich core, end-grain balsa was used to simulate full-scale core material. General criteria for the model were as follows:

- (1) All materials, except that for the sandwich core, were the same as full scale
- (2) All face sheet thicknesses were scaled
- (3) Ring frame dimensions and cross sections were scaled
- (4) Particular emphasis was placed on duplication of the LM-SLA interface hardware
- (5) No access hatch simulations were made, but scaled doublers were used around cutout areas near the LM attach points
- (6) Mechanical fastener sizes and patterns were scaled insofar as commercially available fastener sizes permitted
- (7) Full-scale fabrication procedures and structural subassembly divisions were observed wherever applicable.

The resultant SLA-2 model, illustrated in figures II-4 to II-6, consists of two major subassemblies, a forward section and aft section each fabricated from four quarter panels. The LM attach ring frame serves as the boundary between the fore-and-aft sections. Figure II-4 is a photograph of the completed SLA-2 model in the radial response test stand. Figure II-5 is a closeup view of SLA-2 exterior in the area around the +Y LM attach point. The figure gives a general idea of the structural detail observed in constructing SLA-2 and shows the outer skin thicknesses at selected points on the surface. The LM-SLA interface hardware assembly is shown in more detail in figure II-6. Each model LM support assembly consists of a hemispherical ball and a clamp yoke for the attachment of the LM. On the full-scale structure, the clamping action is provided by a spring-piston assembly whereas on the model the clamping action is provided by a screw-press action. Other items included in the LM support assembly and shown in figure II-6 are the clamping yoke, titanium outer cap, LM attach ring, reinforcing doublers, and mechanical fasteners.

Lunar Module (LM) Models

Guidelines for the design of the models used to simulate the dynamic-response characteristics of the LM spacecraft were derived from examination of data obtained during ground vibration tests of the full-scale LM. These tests, conducted by the LM fabrication contractor, are described in reference II-6. The LTA-2 LM spacecraft, which flew on the AS-502 vehicle and which is shown schematically in figure II-7, consisted of a dummy ascent stage having the proper mass and inertial characteristics, and a flight-type descent stage. The descent stage is basically a four-bay cruciform with a propellant tank in each bay and a landing-gear—truss-SLA-attachment-fixture assembly at the end of each cruciform arm. The ground-test results showed that the primary response modes of this spacecraft involved deformations of the cruciform and superimposed propellant tank motions. The ascent stage, in general, behaved as a carried mass. The center of gravity of the complete structure was approximately at the ascent-descent stage interface plane and nearly on the cruciform center line. Although considerable effort was expended to include the dynamics of the descent-stage tankage in the model LM, a reasonable simulation could not be realized. The design criteria called for approximation of the first scaled LM frequency in the pitch (Z) and longitudinal (X) directions. The measured LTA-2 ground-test structural frequencies and mode shapes are shown in figure II-8. Also shown are the LTA-2 flight configuration frequencies obtained by correcting the ground test frequencies to account for differences in onboard liquid masses. The pitch mode, shown as figure II-8(a), was determined by pinning the $\pm Y$ LM-SLA interface points and applying forces in the $\pm Z$ direction. Likewise the yaw mode (fig. II-8(b)) was obtained by pinning the $\pm Z$ end points and vibrating in the $\pm Y$ direction. The longitudinal response (fig. II-8(c)) was determined by pinning all four end points and forcing in the $\pm X$ direction. The model frequency and mode determinations were conducted in a similar manner.

LM-1.— The first LM model, shown in the sketch in figure II-9 and designated LM-1, was designed solely from LTA-2 test frequency and total mass standpoint to be assembled with SLA-1. The design did not attempt to simulate either the ascent stage, the LM component center-of-gravity displacements, or the descent-stage tank dynamics. The model was an aluminum cruciform with a 1-inch-square (0.0254-m) cross section, a total span of 20.62 inches (0.52 m), and rod end bearings extending from the end of each arm. The bearing assemblies were sized to fit mating fixtures attached to the SLA-1. The appropriate scaled mass of the model, but not mass distribution or inertias, was lumped into equal parts on each of the four cruciform arms. The assembly was then attached to rigid posts and the locations of the steel masses were varied to tune the pitch and longitudinal scaled frequencies to approximate the corrected flight-vehicle values.

Yaw frequency simulation was not attempted. The table shown with the sketch in figure II-9 lists frequencies for various positions of the weights. The final model frequencies on posts were as follows: pitch, $f_p = 50.3$ Hz; yaw, $f_y = 45.4$ Hz; and longitudinal, $f_l = 83.2$ Hz. For comparison, the scaled LTA-2 flight-vehicle frequencies were $f_p = 53.5$ Hz; $f_y = 55.7$ Hz; and $f_l = 91.0$ Hz. With this particular LM simulator cruciform, however, it was not possible to raise the pitch frequency above 50.3 Hz since the weights were at the end of the cruciform arm. The free-free frequencies of the final configurations are also listed in the table as general information.

LM-2.- The second LM model was also designed to fit the SLA-1 model. In addition to simulating the mass and frequency characteristics for either the previously flown AS-502 or the then-planned AS-503 LM spacecraft, this model was required to produce a lateral (pitch) force when vibrating in its longitudinal first mode. The resultant configuration, designated LM-2, is shown in figure II-10. The basic aluminum cruciform had a rectangular cross section 1.0 inch (0.025 m) deep and 1.265 inches (0.032 m) wide. The dimensions and locations of the added steel weights and the resultant frequencies for the two configurations are listed in table II-1. The pitch frequency for the AS-502 simulation is identical to the scaled LM (LTA-2) flight frequency and the model longitudinal frequency is high by only 0.2 percent. For vibrations in the longitudinal dishing mode, the centers of mass of the out-of-plane weights are deflected in the same lateral direction to yield a net lateral force. With this type of weight placement, the component will be referred to as a coupled LM model.

LM-3.- The LM model constructed for use with SLA-2 is shown in the sketch in figure II-11(a). The configuration utilized the same basic cruciform-with-weights design as previous LM simulators. The positions of the weights and the cross-section dimensions of each of the opposite pairs of cruciform arms were analytically determined by the procedure described in chapter III with the three basic frequencies as the prime criteria.

A major configuration difference between LM-3 and the previous LM simulators is the LM-SLA interface hardware. Basically, the interface consists of a ball and preload device on the SLA shown in figure II-6 and a mating cup on the LM, as shown in the sketch on figure II-11(b). Also shown in figure II-11 are the measured pitch, yaw, and longitudinal test-stand frequencies for the LM-3.

An uncoupled version of LM-3, wherein the $\pm Z$ weights were equally distributed in the X direction, was also used in some of the component tests.

References

- II-1. Guyett, P. R.: The Use of Flexible Models in Aerospace Engineering. Tech. Rep. No. 66335, Brit. R.A.E., Nov. 1966.
- II-2. Runyan, H. L.; Morgan, H. G.; and Mixson, J. S.: Role of Dynamic Models in Launch Vehicle Development. Experimental Techniques in Shock and Vibration, Will J. Worley, ed., ASME, c.1962, pp. 55-69.
- II-3. Anon.: Proceedings of Symposium on Aeroelastic and Dynamic Modeling Technology. RTD-TDR-63-4197, pt. 1, U.S. Air Force, Mar. 1964.
- II-4. Regier, Arthur A.: The Use of Scaled Dynamic Models in Several Aerospace Vehicle Studies. Paper presented at ASME Colloquium on Use of Models and Scaling in Simulation of Shock and Vibration (Philadelphia, Pa.), Nov. 1963.
- II-5. Leadbetter, Sumner A.; Leonard, H. Wayne; and Brock, E. John, Jr.: Design and Fabrication Considerations for a 1/10-Scale Replica Model of the Apollo/Saturn V. NASA TN D-4138, 1967.
- II-6. Zentgraf, John K.: LTA-2 Vibration Survey at G.A.E.C. Rep. No. LED-520-8, Grumman Aircraft Engineering Corp., Mar. 2, 1965.

TABLE II-1.- LM-2 CONFIGURATIONS FOR SIMULATION

Dimension (see fig. II-10):	Dimensions for -	
	AS-502	AS-503
s_Y , in. (m)	4.75 (0.12)	6.0 (0.15)
s_Z , in. (m)	5.80 (0.15)	4.0 (0.10)
h_Y , in. (m)	2.0 (0.05)	2.0 (0.05)
h_Z , in. (m)	3.0 (0.08)	5.5 (0.14)
t_Y , in. (m)	1.0 (0.025)	1.0 (0.025)
t_Z , in. (m)	1.0 (0.025)	1.0 (0.025)
s'_Z , in. (m)	3.0 (0.08)	4.0 (0.10)
h'_Z , in. (m)	0.5 (0.01)	0.5 (0.01)
d_Y , in. (m)	3.38 (0.08)	5.5 (0.14)
d_Z , in. (m)	0 (0)	0 (0)
Weights:		
Total, lb (N)	26.25 (116.76)	32.0 (142.3)
W_Y , lb (N)	5.37 (23.89)	6.87 (30.56)
W_Z , lb (N)	5.37 (23.89)	6.87 (30.56)
Test-stand frequencies:		
f_p , Hz	53.5	45.7
f_z , Hz	91.2	77.5

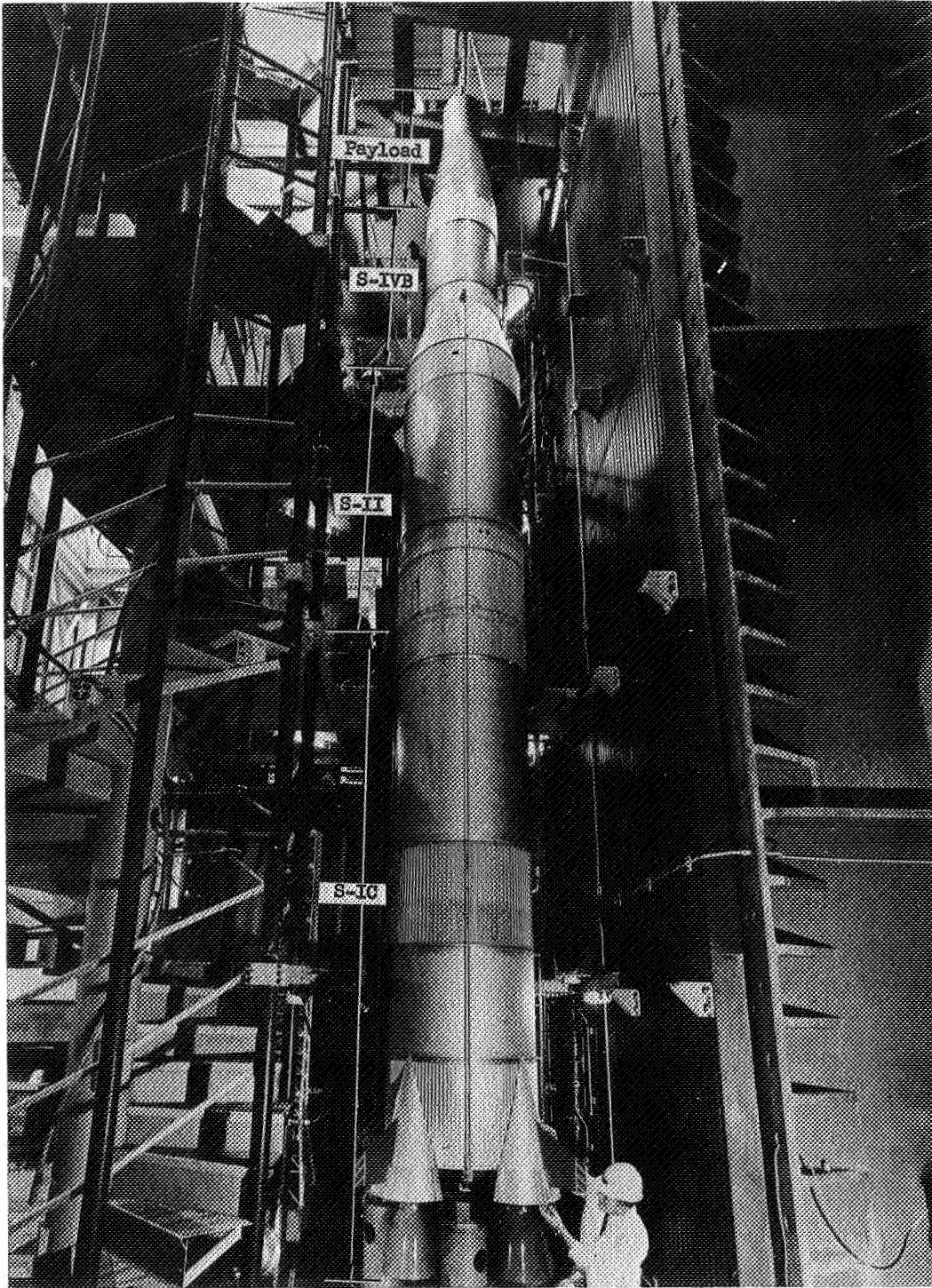


Figure 11-1.- Photograph of 1/10-scale Apollo-Saturn V model.

L-69-1221.1

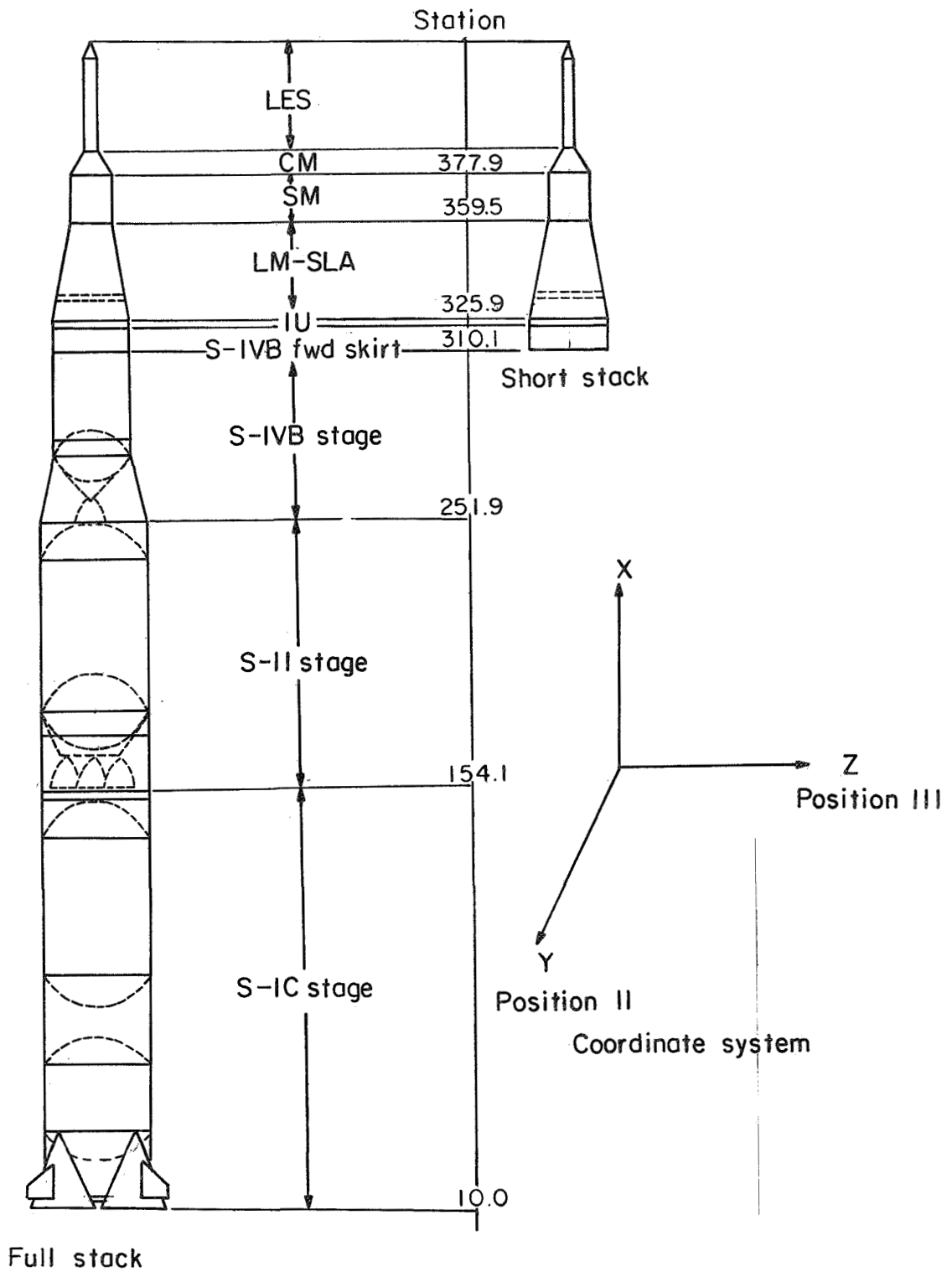


Figure II-2.- Schematic of full-stack and short-stack configurations.

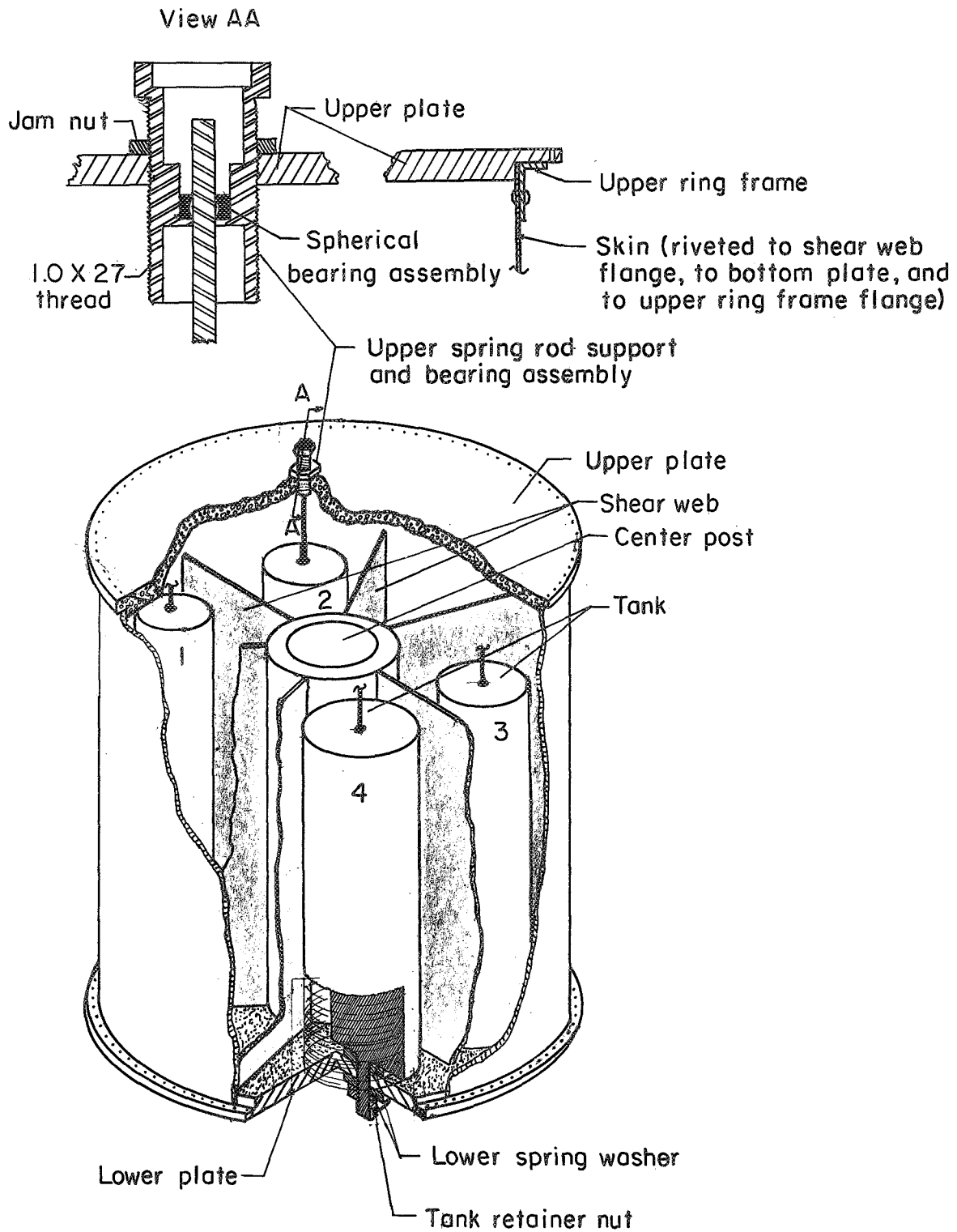


Figure II-3.- Schematic of SM-2.



Figure II-4.- Photograph of SLA-2 model.

L-68-8777

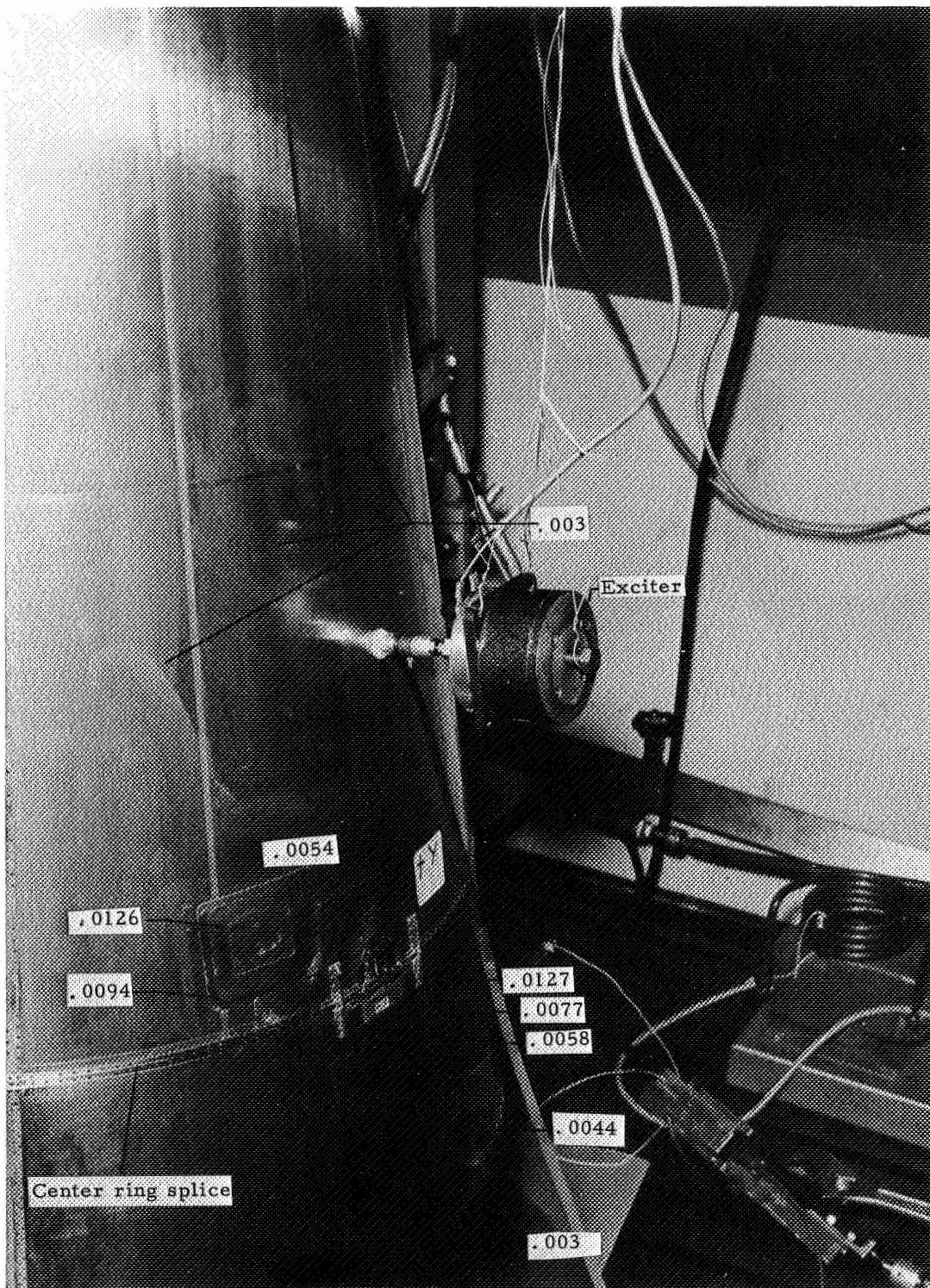
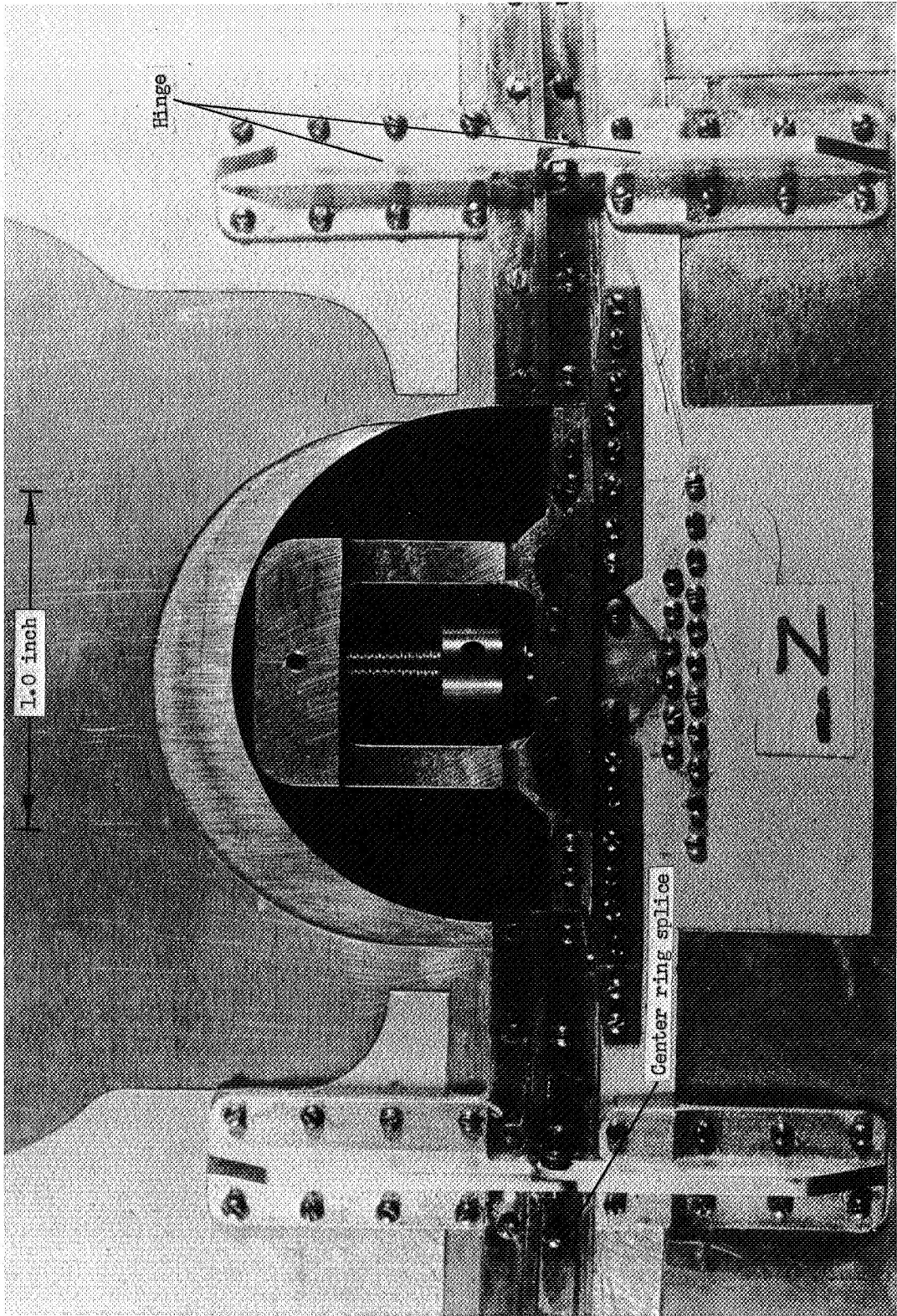


Figure II-5.- LM attach point and forward panel doubler. 1/10-scale SLA-2 model. Numbers indicate skin thickness in inches. L-68-8775.1



L-68-876-1

Figure 11-6.- Exterior view of LM support point. 1/10-scale SLA-2 model.

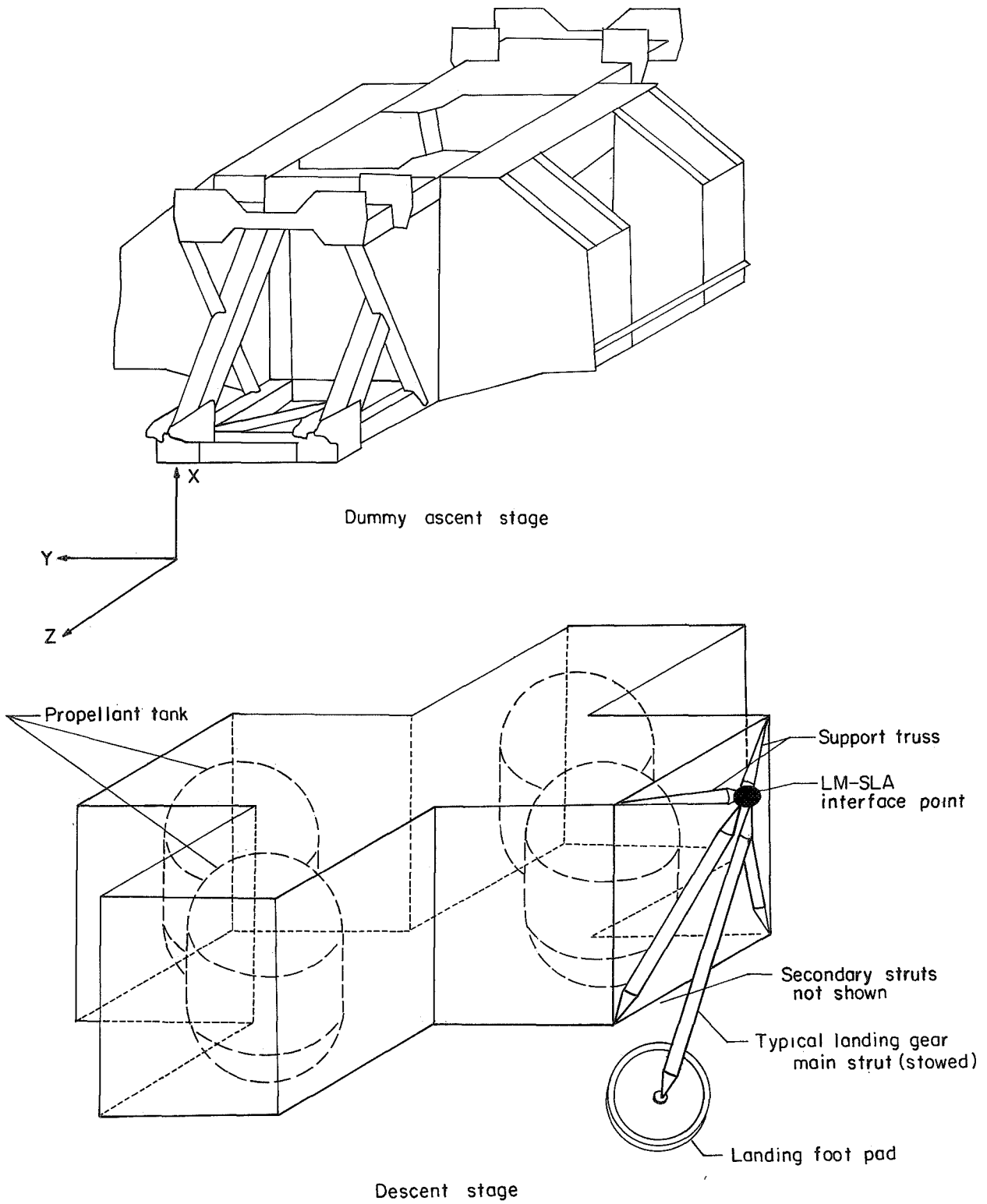
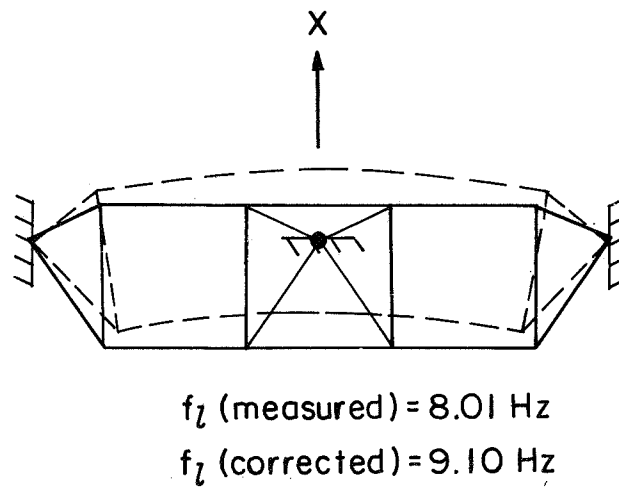
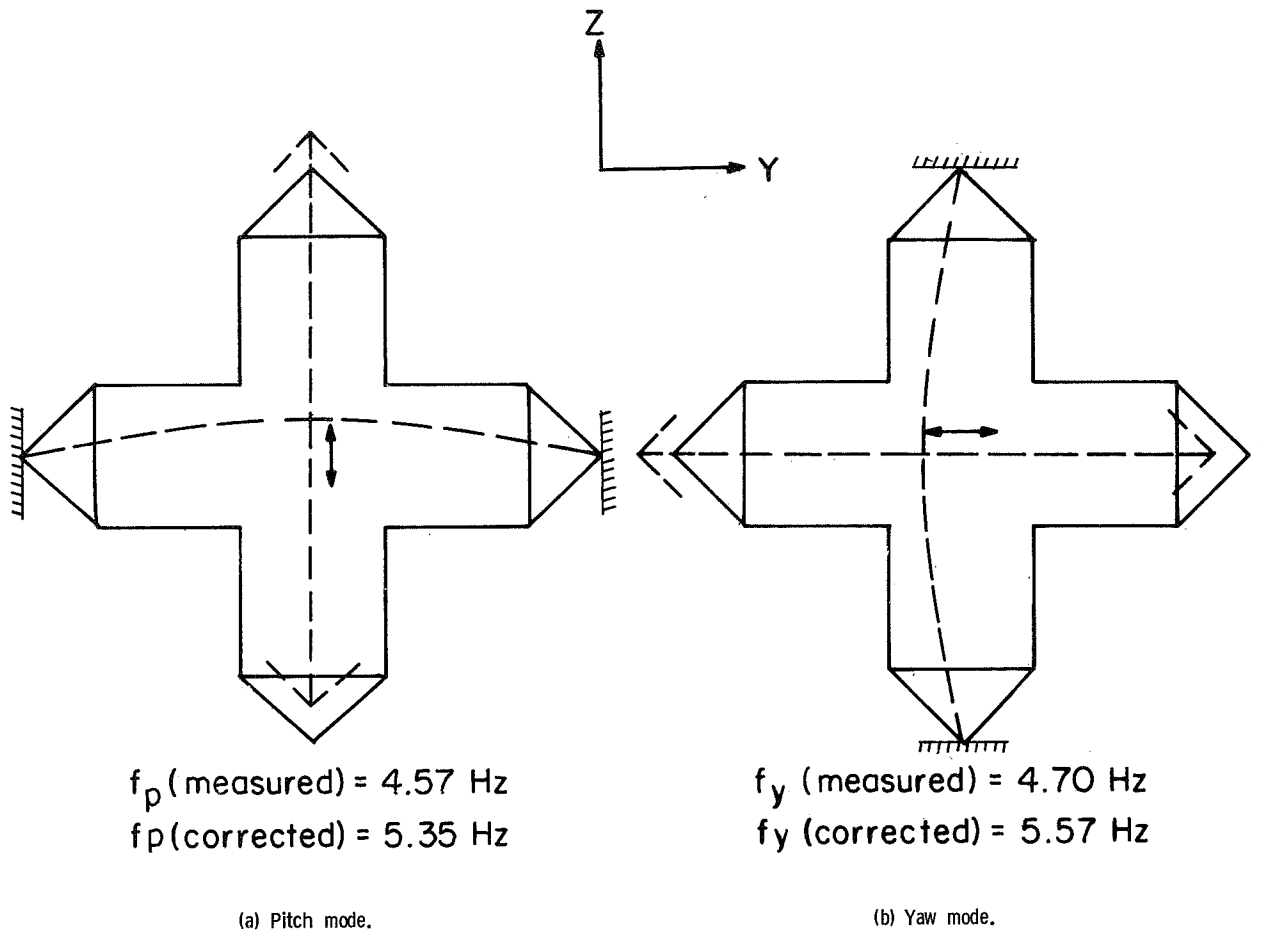
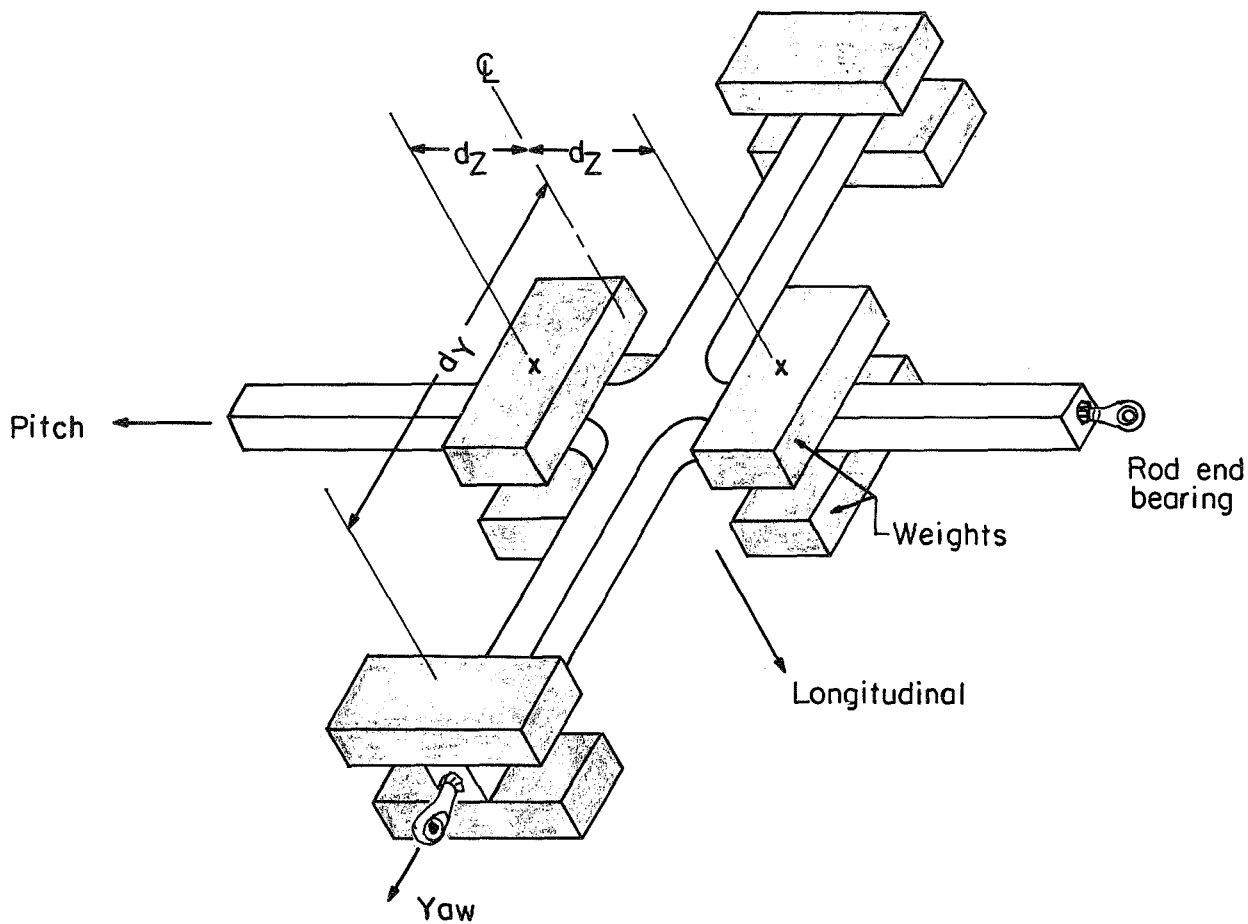


Figure 11-7.- Sketch of full-scale LM spacecraft. LTA-2.



(c) Longitudinal mode.

Figure 11-8.- Measured full-scale LM (LTA-2) deflection shapes and frequencies.



d_z	d_y	On rigid posts			Free - free		
		f_z	f_p	f_y	f_z	f_p	f_y
6.3	6.3	86.0	47.0	—	—	—	—
5.3	5.3	80.0	—	—	—	—	—
4.3	4.3	74.2	45.5	—	—	—	—
4.3	9.3	89.3	—	—	—	—	—
1.7	9.3	83.2	50.3	45.4	105.4	116.3	203.5
9.3	9.3	—	50.3	—	—	—	—

Figure 11-9.- Sketch of 1/10-scale LM-1 model.

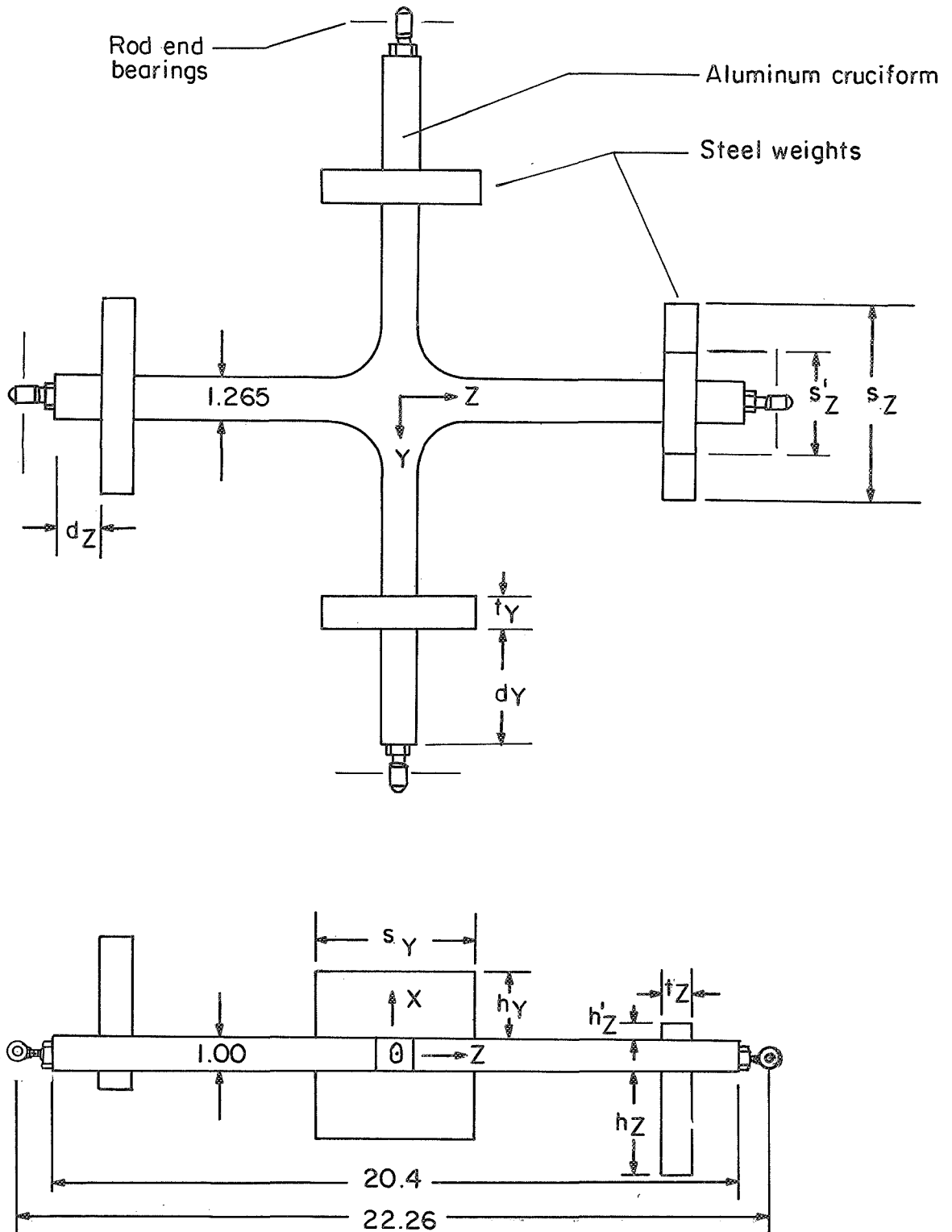
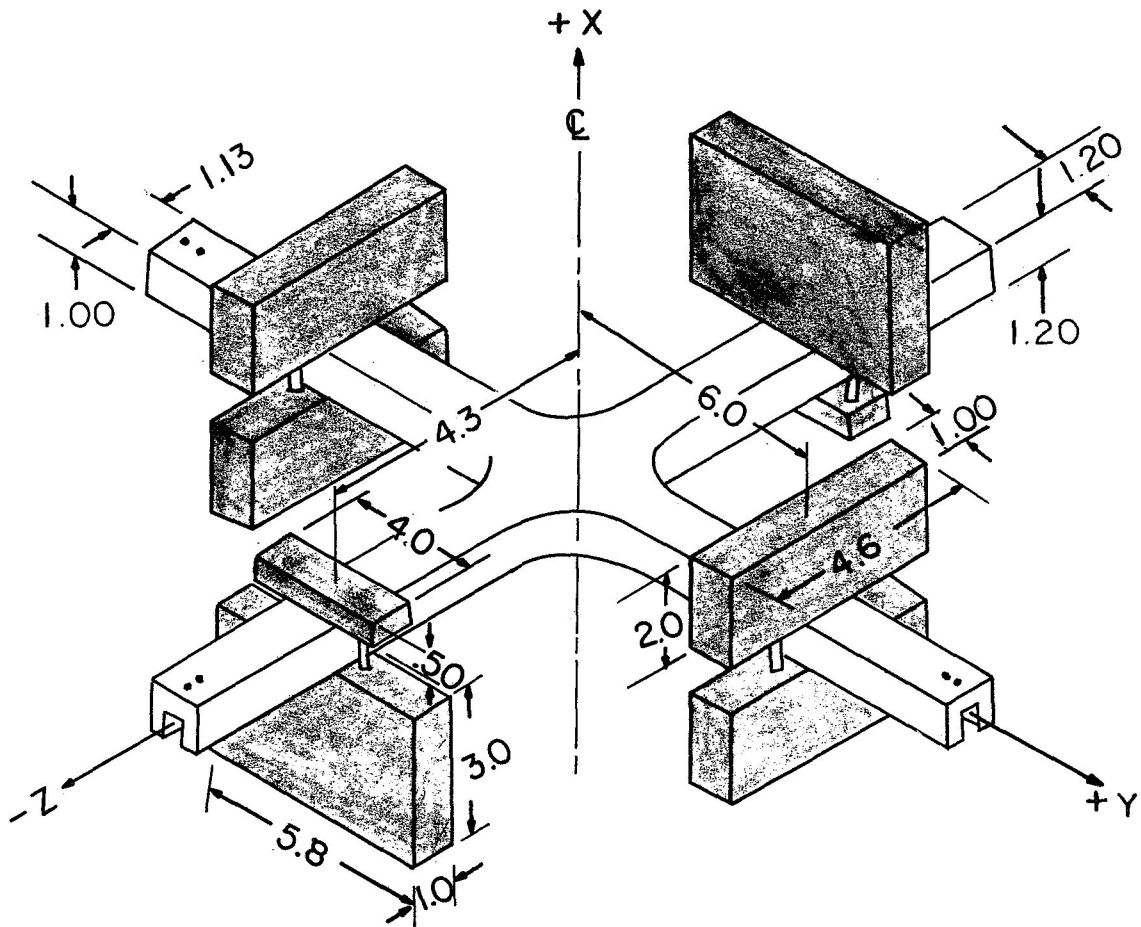


Figure 11-10.- Sketch of 1/10-scale LM-2 model.

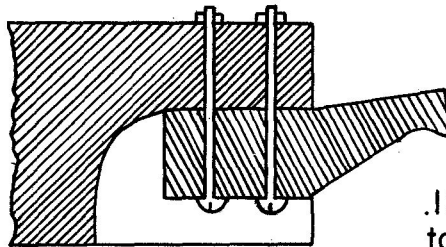


(a) LM-3 configuration.

Cruciform

Frequencies on rigid post, Hz

f_p	53.9
f_y	55.4
f_z	96.0



.125 spherical radius
to match ball in SLA

(b) Detail of socket fixture for LM-3-SLA-2 ball-socket interface.

Figure 11-11.- Sketch of 1/10-scale LM-3 model.

III. TEST TECHNIQUES

By H. Wayne Leonard and Robert W. Herr
Langley Research Center

Load Simulation

The loads acting on the flight structure at the time of the anomaly were assumed to consist only of dynamic loads from vibratory structural deformations and compressive loads from launch-vehicle thrust. No temperature effects were considered. In order to simulate these load conditions, the model had to be tuned to introduce oscillatory stresses from coupled longitudinal and lateral structural responses in addition to static stresses from scaled compressive thrust loads. A unique method, developed and used in the flight-loads simulation, subjected the LM-SLA portion of the model to compressive acceleration loads without interfering with the introduction of vibratory loads.

Static loads.- Duplication in the 1/10-scale model of the overall static stresses existing in the full-scale SLA at the time of the anomaly required that accelerations resulting from vehicle thrust be increased by the scale factor of 10. Thus, the steady longitudinal acceleration of 3.5g for the flight vehicle would require 35g during model tests. Since the model SM-CM-LES weighs 65 pounds (289 N), correct static flight-loads simulation requires a static compressive load of 2274 pounds (10.5×10^3 N) applied to the SLA. It was also necessary to apply a 35g simulated acceleration load to the LM structure. Since the LM model weighs 26 pounds (115 N), this load amounts to an equivalent 910 pounds (4.05×10^3 N). These simulated flight loads must, of course, be applied in such a manner as to introduce negligible constraints to the free-body vibration modes of interest.

The most direct approach would be to suspend weights by means of several elastic cords attached at equal intervals around the circumference at some point above the SLA. However, it was not possible to use this method since the forward skirt of the 1/10-scale model S-IVB stage was not capable of carrying the scaled load because of the use of a lower strength aluminum alloy in model fabrication. The alternate method adopted for simulating flight loads was to apply the steady accelerations to only the SLA-SM section of the model.

The method developed for loading the SLA is illustrated in figures III-1 and III-2, and involved application of the compressive load to the SLA through a dacron line laced alternately between 24 pulleys around the base of the SLA, as shown in figure III-1. The upper pulley-ring assembly (total weight, 0.66 lb (2.9 N)) and lower pulley-ring assembly (total weight, 0.80 lb (3.6 N)) can be seen in figure III-2. The compression load was applied to the SM as well as to the SLA because it was more convenient to attach the upper

pulleys at the CM-SM interface rather than at the SLA-SM interface although the SM is thereby placed in more compression than correct loads simulation requires.

The compression load distributed between 48 cords required a cord tension of approximately 46 pounds (201 N). The tension was applied by using four loading pans – one for each quadrant of the SLA to minimize the cumulative loss of line tension due to pulley friction. One end of each line was attached to a loading pan and the other end was attached to a fixed point on the model. As a check on the friction losses, a calibrated tension gage was placed at the fixed end of each line. Since the cords were of equal length between pulleys, the uniformity of tension could also be checked by plucking the cords and noting the pitch.

The loading harness used to apply the simulated g-load transmitted to the structure by the model LM is illustrated in figure III-3. Four cords, one attached to the LM near each of the four LM-SLA attachment points, were brought outside the vehicle through access holes cut in the skin of the S-IVB forward skirt as may be seen in figures III-3 and III-4. An equal load was applied to each of the four cords by a continuous cable laced through a series of pulleys and attached to a single loading pan. The mechanical advantage of the system was approximately 7.6 so that a loading pan weight of 116.4 pounds (520 N) was required to simulate the 35g load acting on the 26-pound (115-N) dynamic model of the LM. This load was applied to all the structure aft of the LM attach plane. To reduce longitudinal restraint of the vehicle, nylon was used for the loading cords from the point where they emerge from the S-IVB forward skirt. The lateral component of the loading harness restraint was reduced further by attaching horizontal cables between opposite loading cables so that the upper 8 inches (0.202 m) of the loading cables were vertical.

Dynamic loads. - For simulation of measured AS-502 flight loads, the center of the model LM must undergo a dynamic pitch and longitudinal acceleration of 6g at approximately 55 Hz. The body and shell mode shapes must, of course, be similar to those occurring on the flight vehicle at the time of the anomaly. The necessary ratio of lateral response to longitudinal response was attained with a longitudinal input sinusoidal force applied at the S-IC center engine gimbal point and, at the same time and frequency, a properly phased sinusoidal force applied in the pitch direction at the LM-SLA interface point.

Exciter System

The vibratory forces applied to the model were provided by electromagnetic exciters whose size, location, and orientation were determined by particular test requirements. The model short-stack and low-level full-stack vibration tests were conducted by using shakers with capability ranging from 1.5 pounds (6.6 N) to 50 pounds (221 N) force.

Longitudinal vibratory forces were applied to the short-stack configuration by a pair of synchronized 10-pound-force (44.5-N) shakers attached to opposite sides of the support cradle. Lateral short-stack vibrations were introduced by either a 10-pound-force (44.5-N) shaker attached to the support cradle or a 1.5-pound-force (6.6-N) shaker attached at either the support cradle, on the SLA at a LM attach point, or on the SM at the CM-SM interface (model station 378).

In the low-level full-stack tests, longitudinal vibrations were induced through the S-IC center engine gimbal block by a 50-pound-force (221-N) shaker. (See fig. III-5.) Lateral vibratory loads were supplied by combinations of 10-pound-force (44.5-N) shakers at the support cradle and 1.5-pound-force (6.6-N) shakers at either a LM attach point or at model station 378.

The flight loads simulation tests were conducted with a 2000-pound-force (8900-N) shaker acting longitudinally through the S-IC center engine gimbal block and a 50-pound-force (221-N) shaker attached at the LM-3—SLA-2 interface and acting in the pitch direction.

Suspension System

Both short-stack and full-stack tests were performed with the model suspended in a four-cable suspension system. The cables were attached to a support cradle fastened to the bottom of the model. The method of attachment is illustrated in figure III-5 which shows the cradle, cable attachment point, and a portion of the S-IC thrust structure. The length and diameter of the cables were such that the rigid body system frequencies were well separated from the primary structural frequency of interest in the present study (55 Hz). For example, the full-stack configuration with the S-IC stage empty and both the S-II and S-IVB stages full had the following ratio of rigid-body frequency to the 55-Hz frequency of interest: Longitudinal mode, 0.104; pendulum mode, 0.004; and rocking mode, 0.019.

Instrumentation

The on-site instrumentation system provided a means for continuously monitoring the input force and resultant acceleration signals, monitoring and recording the signals from all transducers, and the defining of mode shapes and component response patterns. The general characteristics of the instrumentation system are described in reference III-1.

A sketch of the model showing primary transducer locations and orientations is shown in figure III-6. The orientation of the sensitive axis of each transducer is denoted by the direction of the arrow on the transducer symbol. The external accelerometers were mounted on the surface of the model by attachment brackets and in such a manner

as to permit response shape definition from the collective accelerometer responses. For example, the pitch-sensitive transducers were placed on the yaw axis tangential to the model surface; thus, the effect of radial shell motions on the apparent response shape was minimized.

The internal and external SM, LM, and LM attach-plane transducers are shown separately from the assembly sketch. The external LM attach-plane transducers were used only with SLA-1 configurations. In addition to the primary transducers, vacuum-attached mobile accelerometers were used to measure radial-shell response patterns in the SLA-instrument unit shell area during the stacked tests. The SM tank transducers were mounted on the top of the respective tanks.

For the isolated LM-SLA tests, radial SLA shell motion was measured by a non-contacting, servo-controlled proximity probe shown in figure II-4, which traversed the shell surface in both longitudinal and circumferential directions. This device and the associated electronics are described in reference III-2. The mode shapes of the LM were measured by using a vacuum-attached mobile accelerometer.

Test Procedure

A basic test procedure was employed during the short-stack and full-stack low-force-level tests. A constant-amplitude force of slowly increasing frequency was applied at predetermined force levels, input locations, and frequency ranges. The response of desired transducer groups was recorded for subsequent analysis. Simultaneously, one or more diagrams of amplitude plotted against frequency were recorded as on-site plots. From these plots, and from meters and oscilloscopes, response peaks of interest were determined.

The excitation frequency was manually tuned to the response amplitude peaks of interest. Individual response amplitudes were determined from calibrated meters and the relative phase from Lissajous figures. These readings were recorded and later were plotted in dimensionless form to give deflection shapes. The mobile accelerometer, placed at the intersection of premarked grid lines, was used to map radial SLA response patterns.

Taped frequency sweep data were also played back on a dual channel recorder for interpretation. The response signal recorded from a selected transducer during a frequency sweep was played through one side of a dual-channel tracking filter whereas the input force signal from the same data group was played through the second channel of the filter. The amplitude of the transducer signal was rectified, converted to a logarithmic scale, and recorded on the first ordinate axis of the plotter. The phase angle was determined by a computer that generated an analog signal equal to the phase angle between the two signals from the tracking filter. This signal was simultaneously recorded with the

amplitude signal on the second ordinate axis of the plotter. The abscissa axis of the plotter was driven by an analog signal proportional to the frequency of the input force.

References

- III-1. Pinson, Larry D.; and Leonard, H. Wayne: Longitudinal Vibration Characteristics of 1/10-Scale Apollo/Saturn V Replica Model. NASA TN D-5159, 1969.
- III-2. Naumann, Eugene C.; and Flagge, Bruce: A Noncontacting Displacement Measuring Technique and Its Application to Current Vibration Testing. Preprint No. 16.18-5-66, Instrum. Soc. Amer., Oct. 1966.

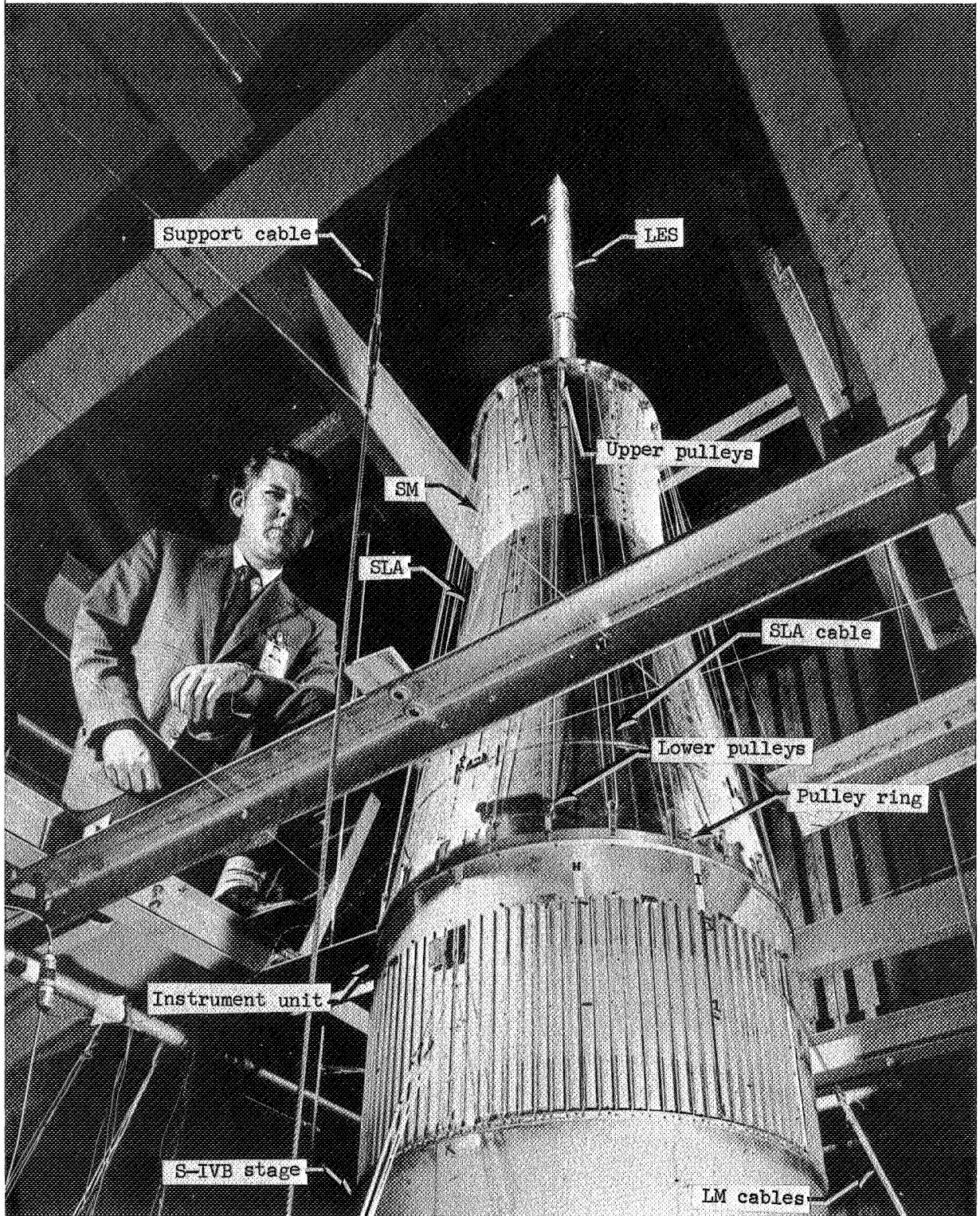


Figure III-1.- 1/10-scale Apollo/Saturn V model with static load device installed.

L-68-9990.1

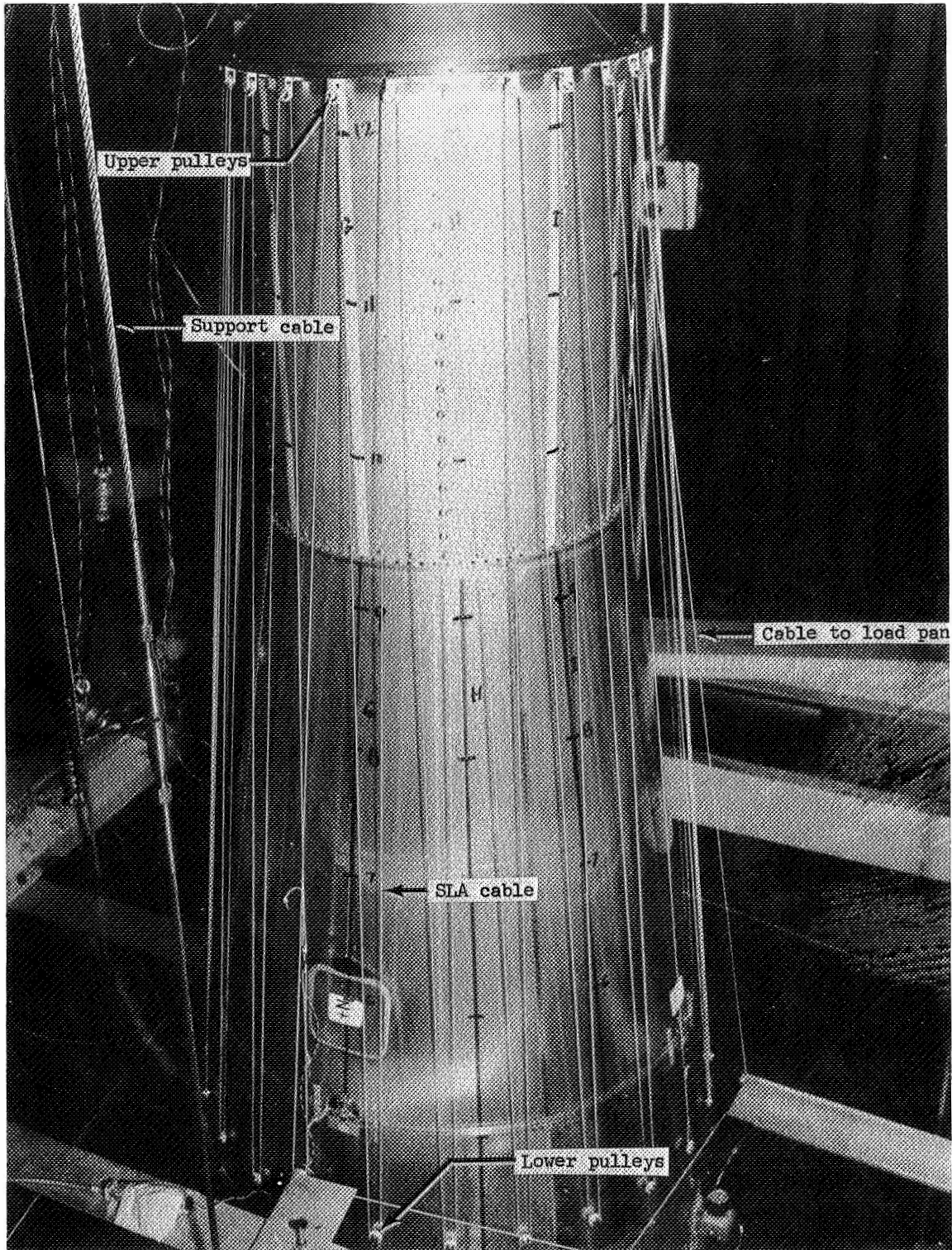


Figure III-2.- 1/10-scale SM-SLA showing static load device.

L-68-9547.1

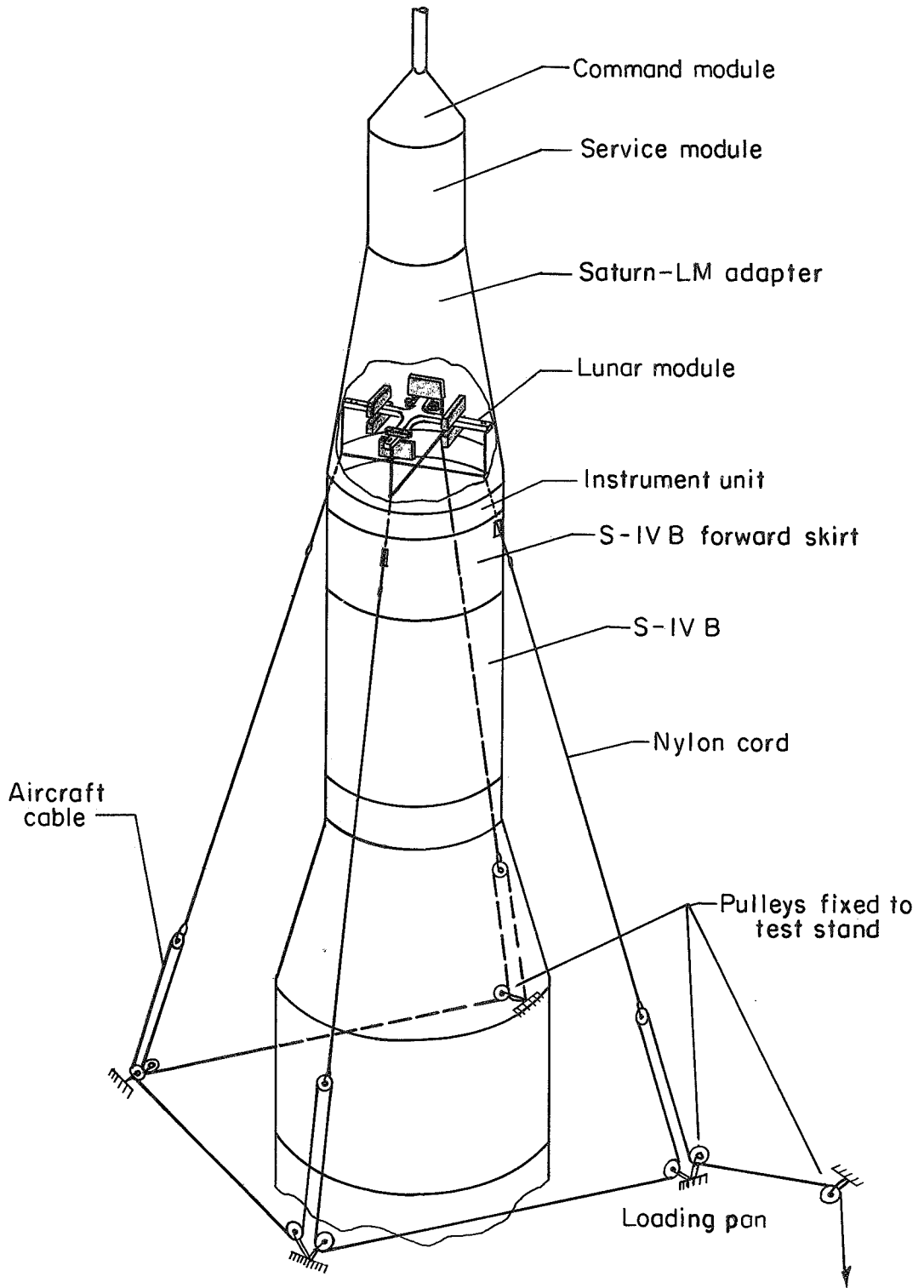


Figure III-3.- Schematic of LM static g-load simulation mechanism.

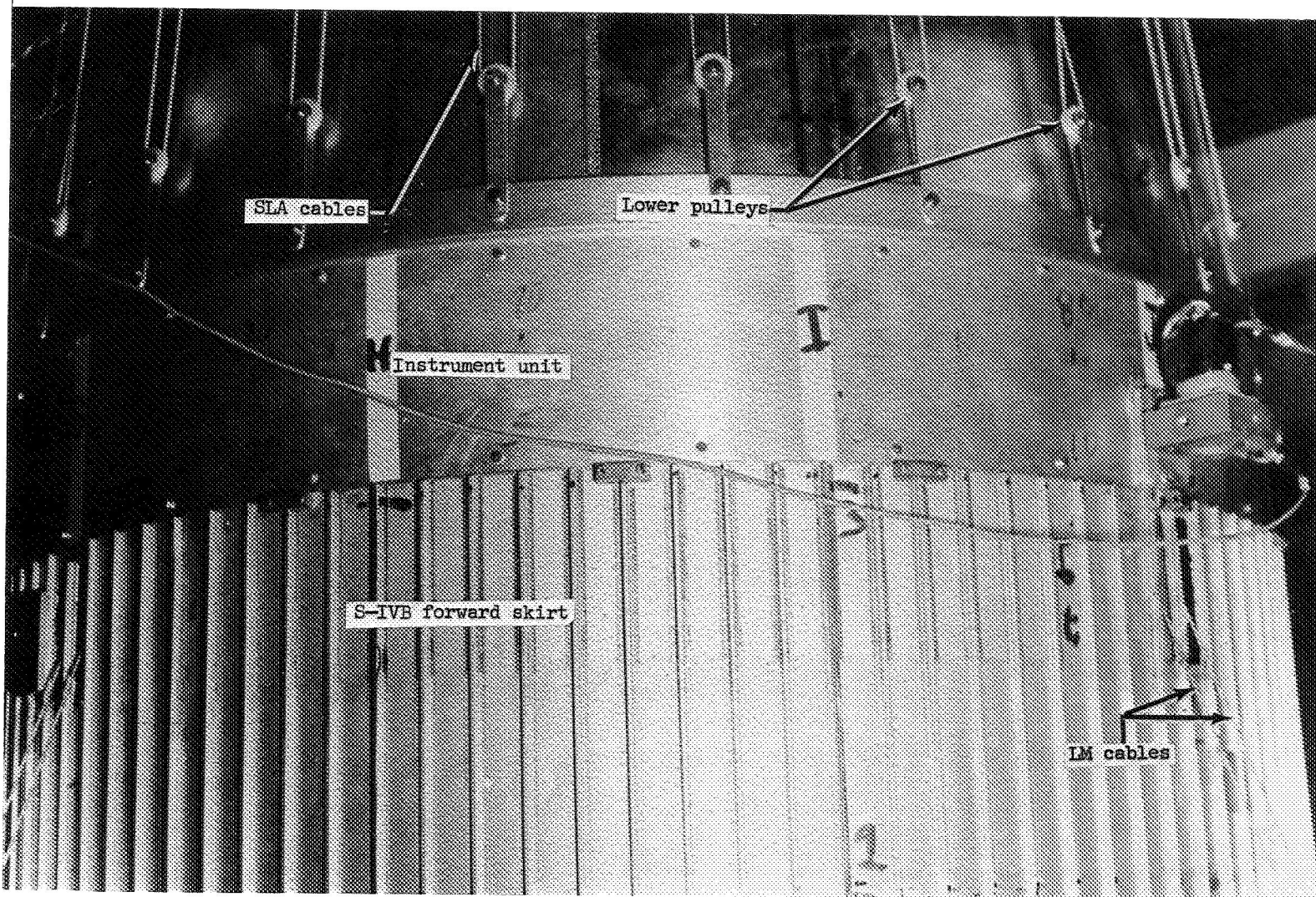


Figure III-4.- SLA lower pulley ring and LM cables. 1/10-scale model.

L-68-9551.1

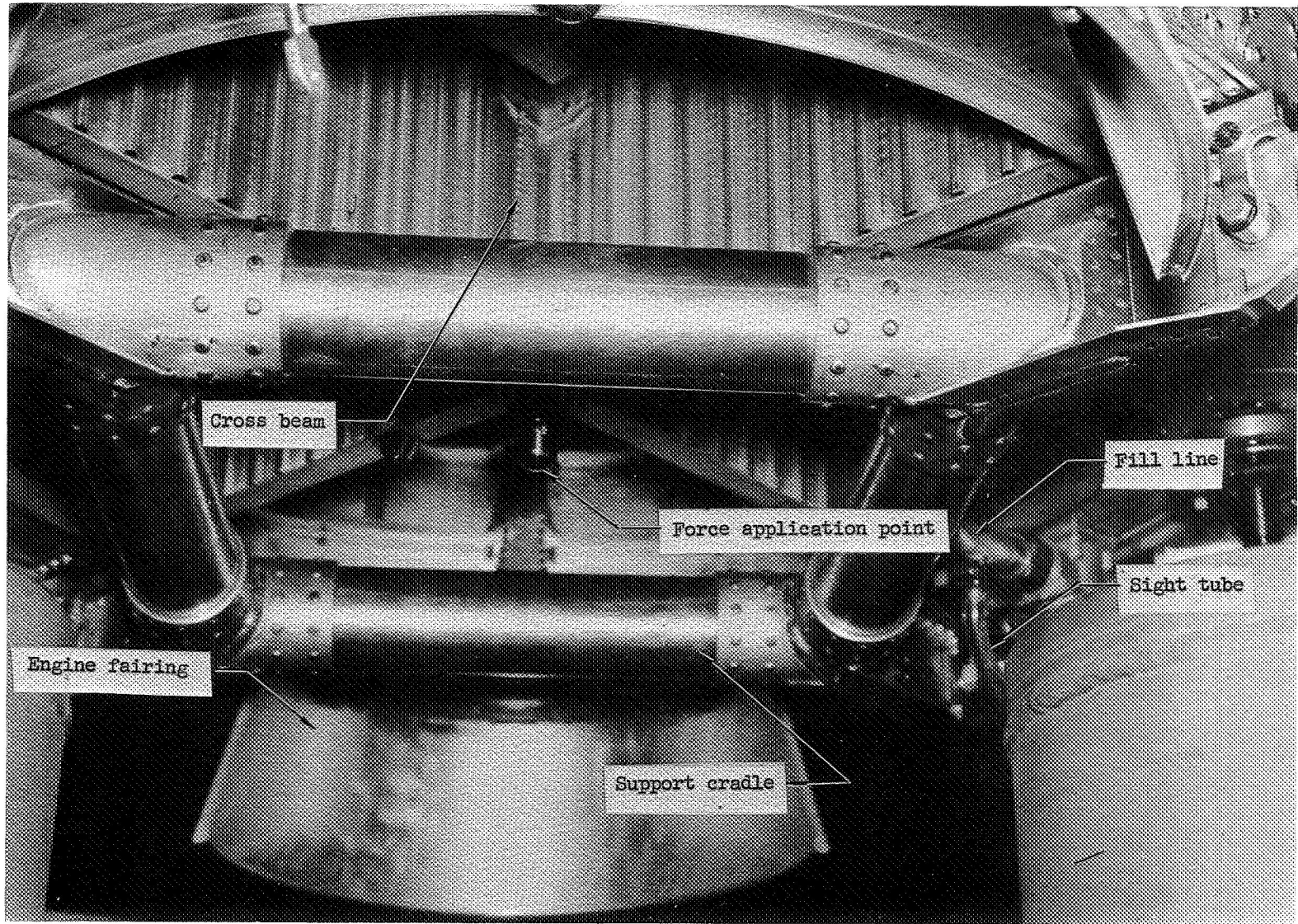


Figure III-5.- S-IC support cradle. 1/10-scale model.

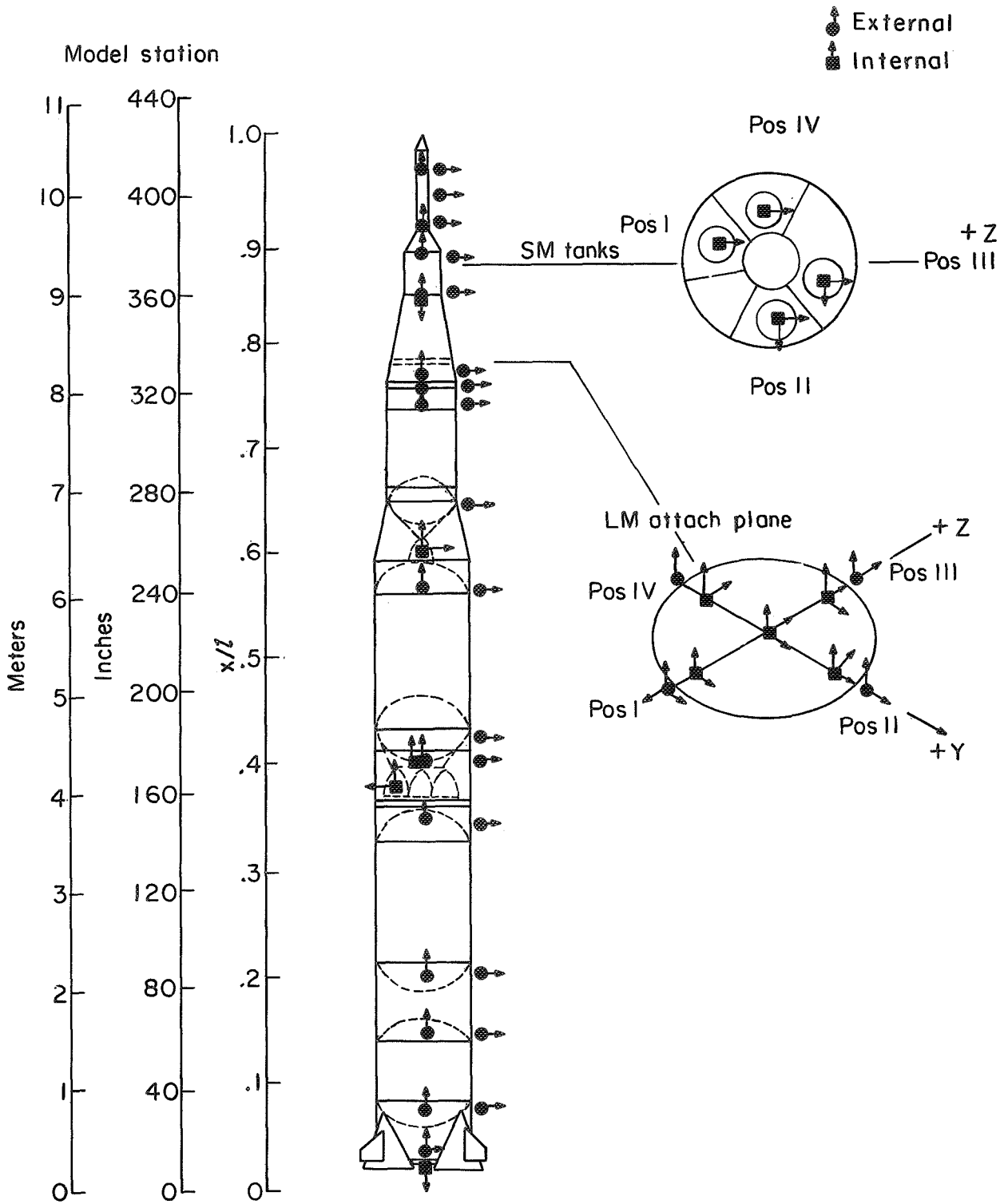


Figure III-6.- Schematic of transducer locations and orientations.

IV. LM-SLA COMPONENT DYNAMICS INVESTIGATION

By William C. Walton, Jr., and Earl C. Steeves
Langley Research Center

Introduction

At the time the structural failure occurred in the LM-SLA component of the AS-502 vehicle, instrumentation indicated substantial LM oscillations in both the pitch and longitudinal directions. The sidewise loading and SLA shell deformations produced by LM pitch oscillations could have contributed to the failure. As part of an effort to understand the mechanism of these oscillations, a combined analytical-experimental study was made to determine the lower frequency vibration modes of the LM-SLA model. Both analysis and experiment had to account for shell behavior of the SLA, three-dimensional elastic characteristics of the LM, and coupling between SLA and LM that could cause asymmetric SLA deformations. The following steps were undertaken:

(1) Establish a procedure based on an appropriate shell theory for calculating natural vibration modes of the SLA.

(2) Establish a procedure for calculating natural vibration modes of the LM-SLA by using the following data:

(a) Vibration modes of the SLA alone calculated by the procedure proposed under (1)

(b) Calculated or measured free-body vibration modes of the LM

(c) Specification of constraints by which the LM is connected to the SLA

(3) Verify the procedures called for under (1) and (2) by correlating analytical and test results for 1/10-scale models of the SLA, LM, and LM-SLA.

An analytical procedure of the type outlined whereby modes of components are determined and then analytically combined to predict the behavior of an entire system is often called component mode analysis.

In this chapter, some of the results obtained from these vibration analyses and tests of 1/10-scale models of the SLA, LM, and the LM-SLA are presented. They are intended to show the character of the vibration modes of these models, to demonstrate the type of results which can be obtained by using the analytical procedures which were developed, and to indicate how longitudinal and lateral motions can couple in a 1/10-scale model of the LM-SLA.

Analyses

SLA-1 analysis.- Free-body natural modes and frequencies of the SLA-1 model were computed by use of the analytical procedure and associated computer program described in reference IV-1. This program was developed especially for systematic accurate calculation of the modes and frequencies of orthotropic thin shells of revolution having general meridional curvature. An idealization of the SLA-1 model leading to input for the aforementioned computer program is described in detail in reference IV-2 and the main assumptions may be summarized as follows: The SLA-1 model was idealized as a thin, axisymmetric, isotropic, conical shell, with rings located at the aft end, at the LM attachment station, and at the forward end. The core, which consisted of aluminum honeycomb and bonding material, was assumed to maintain a constant distance between face sheets, to be infinitely rigid in shear, and to have no bending or stretching stiffness. Bending, torsion, and stretching of the rings was accounted for. Account was also taken of the fact that the elastic centers of the rings were offset from the middle surface of the SLA shell.

LM model analyses.- The analysis to generate natural modes and frequencies for the LM-1 model is discussed in reference IV-2. A similar analysis was made for the LM-2 model. These analyses are summarized as follows: The cruciform members were initially represented as unconnected beams with several lumped masses and rotary inertias. The beams were considered to be infinitely stiff in axial compression and in torsion but could bend in horizontal and vertical planes. Each mass point was allowed four degrees of freedom, a displacement and rotation associated with bending in the horizontal plane, and a displacement and rotation associated with bending in the vertical plane. As additional degrees of freedom, each cruciform member was allowed a rigid-body translation along its axis and a rigid-body rotation about its axis. A mass matrix for each member was readily computed since the masses were lumped, and a straightforward application of Euler beam theory led to stiffness matrices for the members. The masses attached to the cruciform members were initially assigned degrees of freedom appropriate for free masses. Equations of constraint were written for the connection of the cruciform members at their crossing point and for connection of the additional masses to the cruciform members. The equations of constraint were reduced by the method of reference IV-3 leading to stiffness and mass matrices for the systems with all components connected. These stiffness and mass matrices were reduced by standard methods to yield the natural modes and frequencies of the LM models.

LM-SLA analyses.- The computation of the modes of the system consisting of the LM-1 model mounted in the SLA-1 model (LM-1—SLA-1) is discussed in reference IV-2. The same procedure was used to compute the modes of the LM-2—SLA-1 system. An

analytical representation of the entire structure was established in which the displacements within each substructure (LM and SLA) were assumed to be a superposition of relatively few of the vibration modes of the substructure. In formulating this overall representation, constraints were stated in the form of linear algebraic equations requiring the displacements of the SLA and the LM to be equal at the four ball joint connections. The expansion of the component displacements in terms of component normal modes leads to simple diagonal stiffness and mass matrices for each of the components. Reduction of the equations of constraint by the method of reference IV-3 then leads to equations of motion of the system consisting of the components connected together. With the equations of motion in hand, natural modes and frequencies of the system are computed by standard methods.

SLA Modes

Figure IV-1(a) shows measured free-body natural frequencies for the SLA-1 model and the SLA-2 model. Figure IV-1(b) shows a correlation of measured and calculated frequencies for the SLA-1 model. The frequencies are plotted as a function of n , the number of circumferential waves in the mode shape. The three lowest frequencies are shown for each value of n .

The trends of the measured frequencies for the two models differ for mode 1 in that the SLA-2 frequencies show a sharper rise with the circumferential wave number n . For the first mode at $n = 2$, the frequency measured for the SLA-2 model is only slightly higher than the frequency measured for the SLA-1 model. For higher values of n , the first-mode frequencies measured for the SLA-2 model are considerably higher than those measured for the SLA-1 model. For modes 2 and 3, the trends for the two models are similar, and the SLA-2 model frequencies are higher than those of the SLA-1. The analysis for the SLA-1 predicts the trends of the measured frequencies for this model very well; however, the calculated frequencies are somewhat lower than the measured frequencies. The following table in which f_c is calculated frequency and f_m is measured frequency gives deviations for four modes which participate in LM-SLA coupled vibrations:

n	Mode	f_m/f_c
2	1	1.12
2	2	1.15
3	1	1.09
3	2	1.15

The mass distribution of the SLA-1 model used in the analysis was based on a careful weights analysis. Variation of ring stiffness parameters from original estimates by factors up to four had little effect on the results of the calculations. The analysis procedure has been previously demonstrated to yield accurate frequency calculations for conical shells within thin-shell theory. (See ref. IV-1.) Therefore, the low frequencies are attributed to underestimation of the stiffness of the honeycomb wall rather than to misrepresentation of the mass distribution or ring stiffness properties.

Figure IV-2 presents a correlation of calculated and measured modal deflection data for the SLA-1 model. Calculated and measured values of the component of the displacement normal to the surface of the model, are plotted for five of the free-body modes as a function of the normalized slant height, defined to be the slant distance of a point from the top of the model cone divided by the slant height of the cone. The calculated deflections are normalized so that the calculated and measured deflections are equal at the point of maximum deflection in the measured mode. Except for an unexplained bump in the measured mode shape for the first mode at $n = 2$, the calculated deflections reflect the measured deflections well.

It was felt that the correlations which were obtained provided sufficient basis for use of the calculated free-body modes of the SLA-1 model in calculating the LM-SLA coupled modes by a component mode approach.

LM Modes

Figures IV-3 and IV-4 present correlations of calculated and measured frequencies for pitch and longitudinal modes of the LM-1 and LM-2 models with boundary conditions as discussed in the next paragraph. Also shown are the corresponding calculated modal deflections. In the discussion which follows, the member of the basic cruciform perpendicular to the pitch direction is designated member y and the member parallel to the pitch direction is designated member z.

Support conditions were the same for tests of both models. In the test of the pitch mode, the ends of member y were restrained from deflection in any direction but were free to rotate. In the tests for the longitudinal mode, the ends of both members of the cruciform were restrained against motion in any direction but were free to rotate.

In the analysis for both pitch and longitudinal modes, the ends of member y were restrained against vertical and pitch displacements and the ends of member z were restrained against vertical and yaw displacements. For the pitch mode, this restraint represents increased constraint over the test conditions because the ends of member z cannot translate vertically in the analysis. For the longitudinal mode, the analytically assumed conditions represent diminished constraint because the ends of member z are

free to translate in the pitch direction. The analytical conditions were necessary to study pitch-longitudinal coupling in the vibrations of the LM-2 model. The difference between analytical and test support conditions is inconsequential for the LM-1 model because of its symmetry. For the LM-2 model, the differences in support conditions may be expected to have some effect on the correlation.

The following table shows the correlation between measured frequency f_m and calculated frequency f_c for the two LM models:

Model	Pitch mode, f_m/f_c	Longitudinal mode, f_m/f_c
LM-1	0.959	1.04
LM-2	1.03	.920

The correlations indicate no gross misconceptions or errors in determining analytical representations of the LM models. Therefore, it was decided to use calculated free-body modes of the LM models in the component-mode analysis to determine coupled LM-SLA modes.

Longitudinal-Pitch Coupling in the LM-2 Model

The calculated longitudinal mode of the LM-2 model (fig. IV-4) reveals interesting information relating to the attempt to design this model to incorporate coupling of longitudinal and pitch vibrations. An object in the design, leading to the arrangement of eccentric masses on member z, was to achieve a ratio of pitch inertial force to longitudinal inertial force of about 1/7 in the longitudinal mode with the center of gravity displaced in the positive pitch direction when the cruciform members are displaced downward. As figure IV-4 shows when the cruciform members displace downward, the eccentric masses on member z rock so that there is a tendency for the center of gravity of these two masses to move in the positive pitch direction. It was felt that displacements in the pitch direction of other parts of the model would be small and that, therefore, the center of gravity of the system would be shifted in the positive pitch direction. The dimensions of the eccentric masses were sized to give the correct magnitude of the ratio between the pitch and longitudinal forces. However, the analysis indicates that there is a substantial displacement of the two masses on the y member in the negative pitch direction. The inertial force associated with these two masses dominates, and the net displacement of the center of gravity is in the negative pitch direction contrary to the thought in the design. The magnitude of the ratio of pitch force to longitudinal force was calculated to be about 1/10. Thus, if the model is turned around (or equivalently, if the sense of the pitch direction is reversed), the design objectives are met fairly well. Fortunately,

the results of the coupling studies in this section depend only on the existence of some longitudinal-pitch coupling in the LM-2 model and not on the direction of the pitch force relative to the longitudinal force.

LM-SLA Modes

This section presents results of analysis and tests to determine free-body natural vibration modes of the LM-1—SLA-1 and LM-2—SLA-1 assemblies. The calculated results for the first nine modes in each case are shown in figures IV-5 and IV-6. The analysis used LM and SLA component modes as discussed previously. Vibration modes and frequencies were determined experimentally for the LM-1—SLA-1 configuration, but only pitch-longitudinal coupling studies were made experimentally on the LM-2—SLA-1.

The circle in the first row of each figure represents the undeformed circumference of the SLA at the LM plane. The positive pitch direction is to the right. Crossed lines inside the circle represent the undeformed axes of the LM. The ends of these lines do not touch the circle because the ends of the LM members are attached to the SLA through universal joint fixtures that have been accounted for in the analysis. The vertical line to the right of the circle is a side view of member y. With reference to this line, the upward direction, or +x axis, is to the left. The horizontal line below the circle is a corresponding side view of member z. The solid closed curve is the locus of the end points of the LM plane components of the displacement vectors of the points on the LM plane circumference. LM displacements are denoted by the curves superimposed on the various views of the undeformed LM.

Rows 2 and 3 in the figures show the magnitude of the component of the modal displacement normal to the SLA wall as it varies around the circumferences at the top and bottom of the SLA, respectively. At each point on the reference circle, the total normal deflection is plotted radially. The displacements in row 1 and those in rows 2 and 3 are scaled in the ratio of the radii of the respective circles.

The patterns of the nodes of the normal displacement are presented in the bottom row. The positive pitch direction is to the right. The concentric circles represent the undeformed top and bottom circumferences of the SLA cone and the four crosses (not always visible) indicate the LM attachment positions. The superimposed curves are points where the normal displacement vanishes, their radial distance from the small circle being proportional to the slant distance of the point from the top of the SLA. It is emphasized that these curves do not indicate zero motion of the SLA wall at the point; they only mean that there is no motion in the normal direction. Experimentally determined node points where measured are indicated by circular symbols.

LM-1—SLA-1 free body modes. - The free body modes and frequencies of the LM-1—SLA-1 assembly, presented in figure IV-5, are discussed.

In mode 1, LM-1 motions are relatively small. The SLA vibrates in a predominately $n = 2$ mode with relatively large normal displacements along the top circumference and relatively small normal displacements along the bottom circumference. The four meridional node lines and the single circumferential node line pass through the LM attachment points.

In mode 2, lateral motions of the LM are relatively small. Some longitudinal motion of the LM can be detected in which the LM assumes a "saddle" configuration. That is, member y is concave downward while member z is concave upward. (One of the lower frequency calculated free-body modes of the LM-1 model exhibited such a saddle deformation.) The SLA vibrates in a predominately $n = 2$ mode with normal displacements generally very large compared with the maximum LM displacement. The nodal pattern resembles the nodal pattern of mode 1 rotated 45° .

Longitudinal motions of the LM are relatively small in mode 3. Substantial displacements of the LM in the LM plane result in a "scissoring" deformation of the LM. The SLA deforms into a predominately $n = 2$ mode shape. In contrast to modes 1 and 2, the larger normal displacements are in the lower regions of the SLA. As in mode 1, there are four meridional node lines, one through each of the LM attachments. A node line also runs around the SLA in the upper regions although it is not circumferential since its radial distance from the upper circumference is not constant.

Mode 4 is the "pitch" mode of interest in the anomaly study. In the LM plane, member y deforms into a shape similar to the first mode of a free-free beam whereas member z translates as a rigid body in the pitch direction. There is relatively little longitudinal motion of the LM. However, a slight rocking of member z is detectable in its side view and LM deformations are comparable in magnitude to those of the SLA. The SLA deformation involves a substantial $n = 3$ mode component. For this mode, the larger normal deflections of the SLA are in the lower regions.

Mode 5 is the "longitudinal" mode that is also of interest in the anomaly study. Relatively large deflections of the LM in the longitudinal direction result in a "dishing" deformation. Consistent with the symmetric design of the LM-1 model, there is no detectable horizontal motion of the LM. Substantial normal displacements of the SLA indicate a significant $n = 2$ mode component near the top and some contribution from an $n = 0$ mode component at the bottom.

In mode 6, a relatively small bending of member z appears in the LM plane along with a slight rocking of member y. In both modes 6 and 7, the SLA deforms in a

predominately $n = 3$ shape with relatively large normal deflections at the bottom. The deflection shape of mode 7 is roughly similar to mode 6, but is rotated 45° .

Mode 8 is the "yaw" mode which is similar to the pitch mode. Member z bends in the LM plane whereas member y translates as a rigid body but with a slight rock. However, the rigid translation of member y is small so that there is relatively little displacement at its attach points whereas in the "pitch" mode (mode 4) substantial translation of member z resulted in relatively large horizontal displacements of the SLA at its ends. Normal deflections of the SLA have a strong $n = 3$ component, the deflections at the bottom being the larger.

Mode 9 has no longitudinal motion of the LM. In the LM plane, the LM displacements consist of a rigid body spin about the longitudinal axis accompanied by some bending of member z. The normal deflections of the SLA are relatively small along the top circumference and large along the bottom circumference with a strong $n = 4$ component.

In the frequency range from 52.1 Hz to 143.5 Hz, eight distinct resonant frequencies were detected experimentally. These frequencies were associated with the calculated modes by comparing mode shapes and are also shown in figure IV-5. The following table shows the ratio of measured frequency f_m to calculated frequency f_c for each mode:

Mode	1	2	3	4	5	6	7	8
f_m/f_c	1.13	1.11	0.951	1.16	1.002	1.16	1.16	0.893

Differences of up to 16 percent are indicated. Since modes 3, 4, and 8 involve substantial deformation of the LM, errors for these modes are felt to stem from errors in the LM model component analysis. Errors in modes 1, 2, 5, and 6 are felt to result from errors in the SLA model component analysis as indicated by the correlation of measured and calculated free-body SLA natural frequencies in figure IV-1. The correlation between measured and calculated nodal patterns is good with the possible exception of mode 7. For mode 7, the measured and calculated nodal patterns have the same number of meridional node lines but are rotated with respect to each other.

LM-2—SLA-1 free-body modes.— Modes calculated for the LM-2—SLA-1 are shown in figure IV-6. Modes 1, 2, 5, 6, and 8 of this system have essentially the same frequencies and shapes as modes 1, 2, 6, 7, and 9, respectively, of the LM-1—SLA-1. Since there is relatively little motion of the LM in these modes, the differences in the two models would not be expected to affect the results significantly. Also, the third modes of the two systems, in which the LM undergoes a scissoring deformation in the LM plane, appear to be nearly the same. However, modes 4 and 9 of the LM-2—SLA-1 model indicate effects of longitudinal-pitch coupling in the LM-2 model. Mode 4 may be described

as a pitch mode in the sense that the largest deflections are in the pitch direction with member y bending and member z translating as a rigid body. However, longitudinal deflections occur as well; thus, this mode can be excited by a longitudinal driving force. The largest deflections in mode 9 are in the longitudinal direction and exhibit the dish configuration associated with a "longitudinal" mode. Again, pitch deflections occur as well.

LM-2—SLA-1 longitudinal-pitch coupling.- Figure IV-7 shows results from a test to determine whether pitch responses could be excited by longitudinal excitation. The LM-2—SLA-1 model was suspended on soft rubber bands and a sinusoidal force was applied longitudinally near the center of the LM-2 model. The force amplitude was held constant and the frequency varied. The plots show the absolute values of the accelerations in g units in the longitudinal and pitch directions as registered by accelerometers mounted at the top center of the LM-2 model. Both responses exhibit peaks at frequencies of approximately 117 Hz and 148 Hz. For the pitch response, there was a 90° phase difference between acceleration and input force at each of the response peaks. For the longitudinal response, the phase did not change at 117 Hz, but shifted 90° at 148 Hz. The peak at 117 Hz is associated with the resonance of mode 4, the pitch mode of figure IV-6, with a calculated frequency of 102.6 Hz, and the peak at 148 Hz is associated with resonance of mode 9, the "longitudinal" mode of figure IV-6, with a calculated frequency of 153.5 Hz. These associations, although reasonable, cannot be made with certainty because the response shapes were not surveyed in sufficient detail and because more than one mode is responding at 117 Hz. The response plots show, however, that pitch response of the LM-2 model comparable with the longitudinal response can be excited by a longitudinal driving force in this configuration. In the vicinity of 117 Hz, the pitch response is even somewhat greater than the longitudinal response.

Concluding Remarks

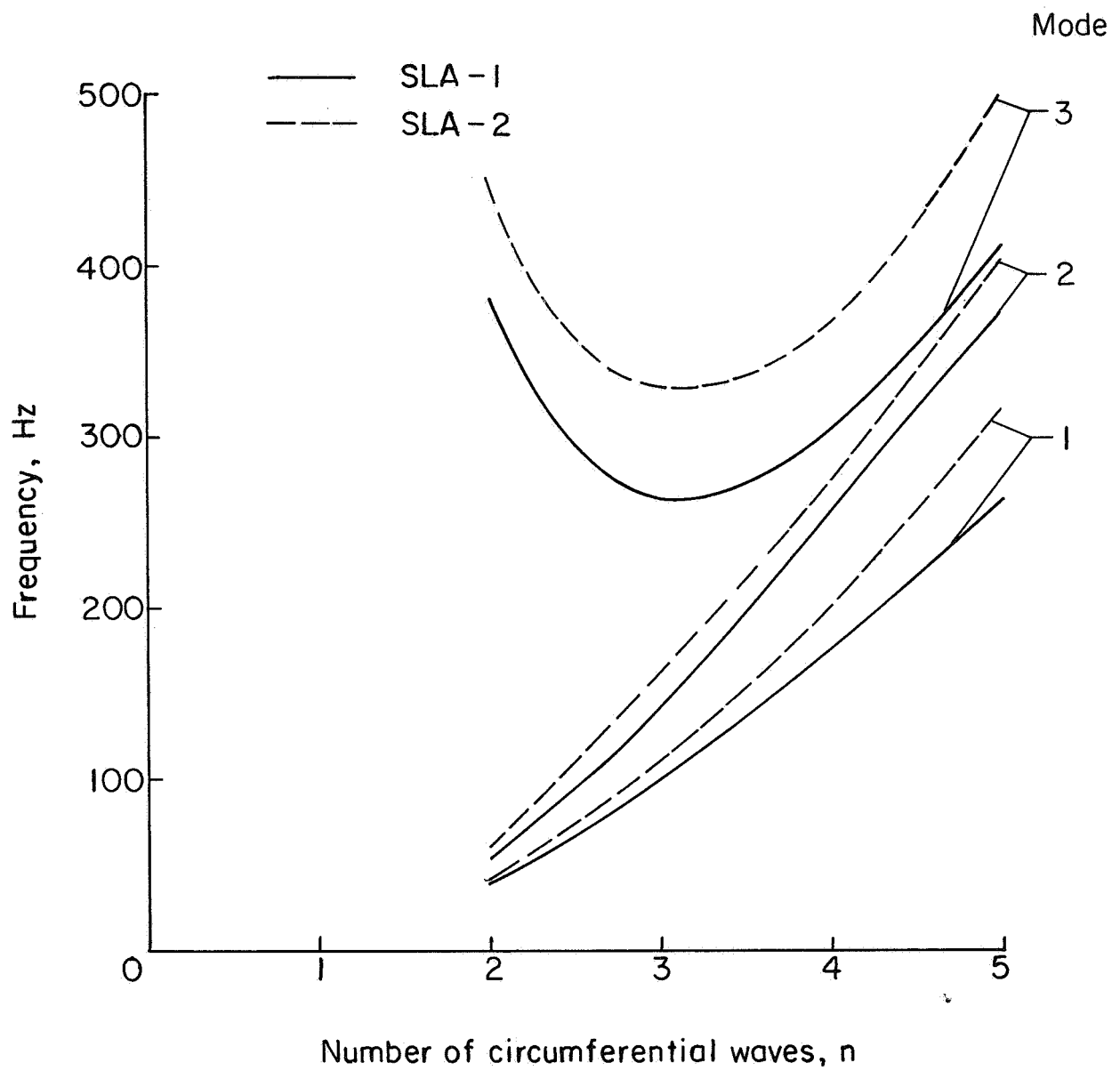
An analytical and experimental study has been conducted to further the understanding of full-scale LM-SLA structural dynamic properties through the use of 1/10-scale dynamic models of the LM, SLA, and LM-SLA. Calculated frequencies and mode shapes are presented for a model of the SLA, called the SLA-1 model, with two different models of the LM mounted within. One of the LM models (LM-1) is designed to have uncoupled lateral and longitudinal vibration modes and the other (LM-2) is designed to introduce a degree of coupling between the lateral and longitudinal modes. Results of a vibration test to determine modes of the LM-1—SLA-1 model are correlated with corresponding analytical results. In addition, results are shown from analyses and tests to demonstrate lateral to longitudinal coupling observed during studies of the LM-2 model while isolated and studies of the LM-2—SLA-1 model.

In general, these studies have enabled an improved understanding of the LM-SLA component dynamics and have demonstrated that the component mode approach can be advantageous provided individual component modes are adequately defined. For the considered case, existing analytical procedures were adequate for predicting the modes of the LM models and for determining, particularly in the low frequency range, the trends of the SLA shell modes. For the assembled LM-1—SLA-1, a comparison of analytically and experimentally determined modes reveals that the calculations give estimates of natural frequencies that are within 16 percent of experimental results and provide good definition of nodal patterns. These results indicate that the analytical predictions can serve as a useful guide to tests and as a basis for representing structures such as the LM-SLA component in dynamic analysis of an entire complex launch-vehicle system.

In the analysis of the LM-2 and LM-2—SLA-1 models, calculated modes showed coupling of lateral and longitudinal vibratory motions of the LM-2. In these tests, it was shown that substantial motion of the LM-2 center in the pitch direction could be excited by a longitudinally applied force.

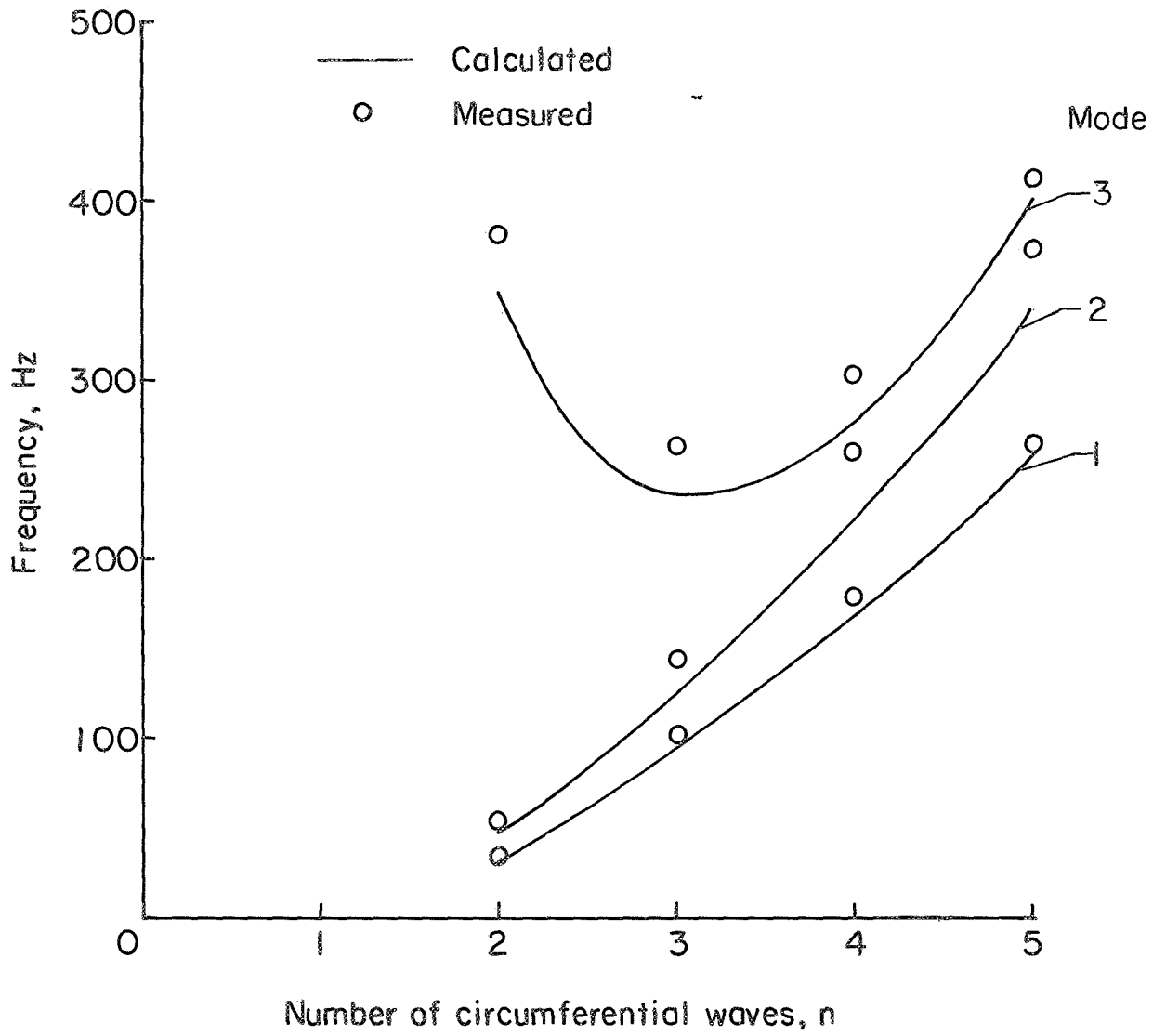
References

- IV-1. Adelman, Howard M.; Catherines, Donnell S.; and Walton, William C., Jr.: A Method for Computation of Vibration Modes and Frequencies of Orthotropic Thin Shells of Revolution Having General Meridional Curvature. NASA TN D-4972, 1969.
- IV-2. Steeves, Earl C.; Durling, Barbara J.; and Walton, William C., Jr.: A Method for Computing the Response of a General Axisymmetric Shell With an Attached Asymmetric Structure. AIAA Structural Dynamics and Aeroelasticity Specialist Conference and the ASME/AIAA 10th Structures, Structural Dynamics, and Materials Conference, Apr. 1969, pp. 302-328.
- IV-3. Walton, William C., Jr.; and Steeves, Earl C.: A Practical Computational Method for Reducing a Dynamical System With Constraints to an Equivalent System With Independent Coordinates. Paper presented at Air Force Second Conference on Matrix Methods in Structural Mechanics (Wright-Patterson Air Force Base, Ohio), October 15-17, 1968.



(a) SLA-1 and SLA-2, measured.

Figure IV-1.- 1/10-scale SLA free-body frequencies.



(b) SLA-1, calculated and measured.

Figure IV-1.- Concluded.

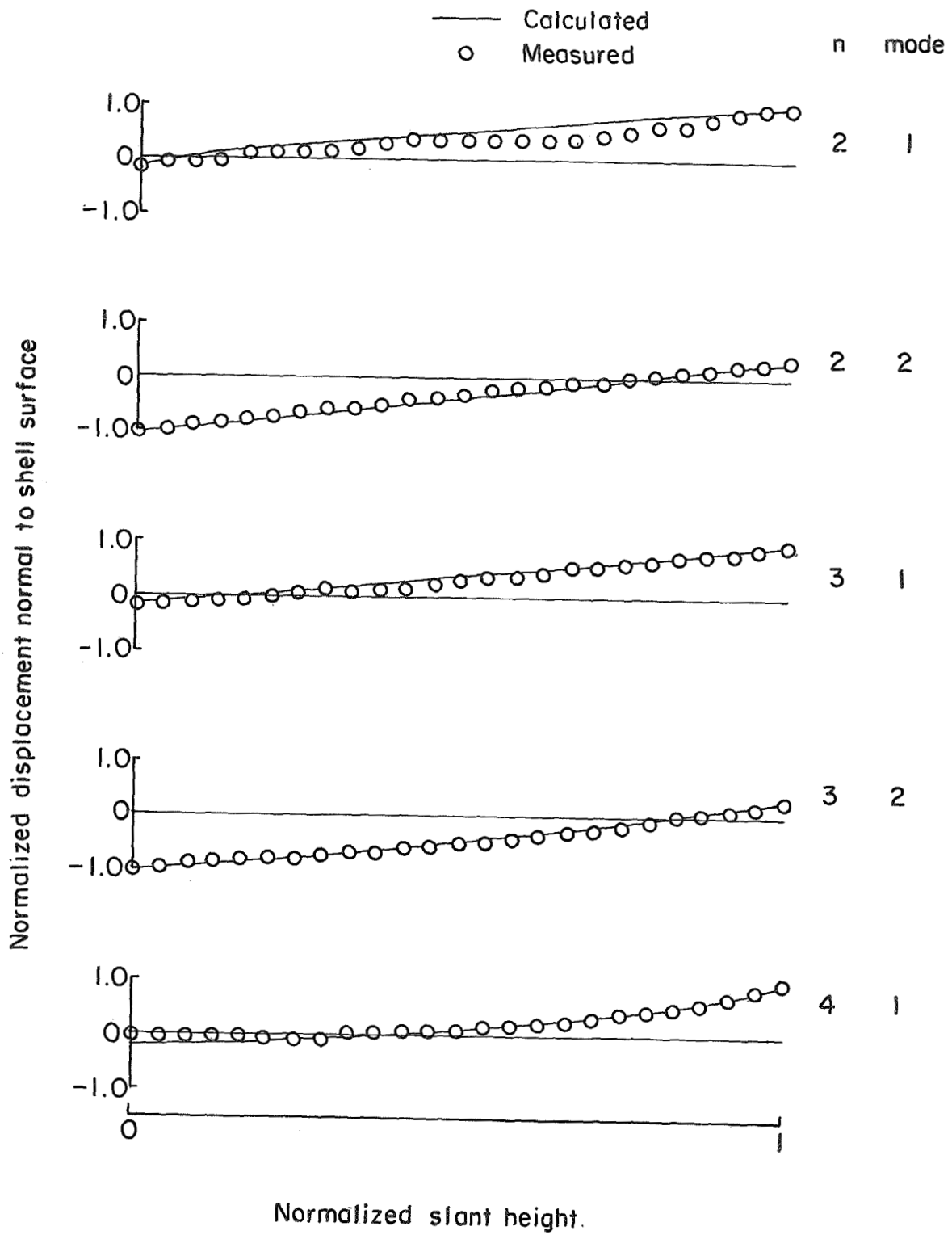


Figure IV-2.- Correlation of calculated and measured free-body modal deflections for the 1/10-scale SLA-1 model.

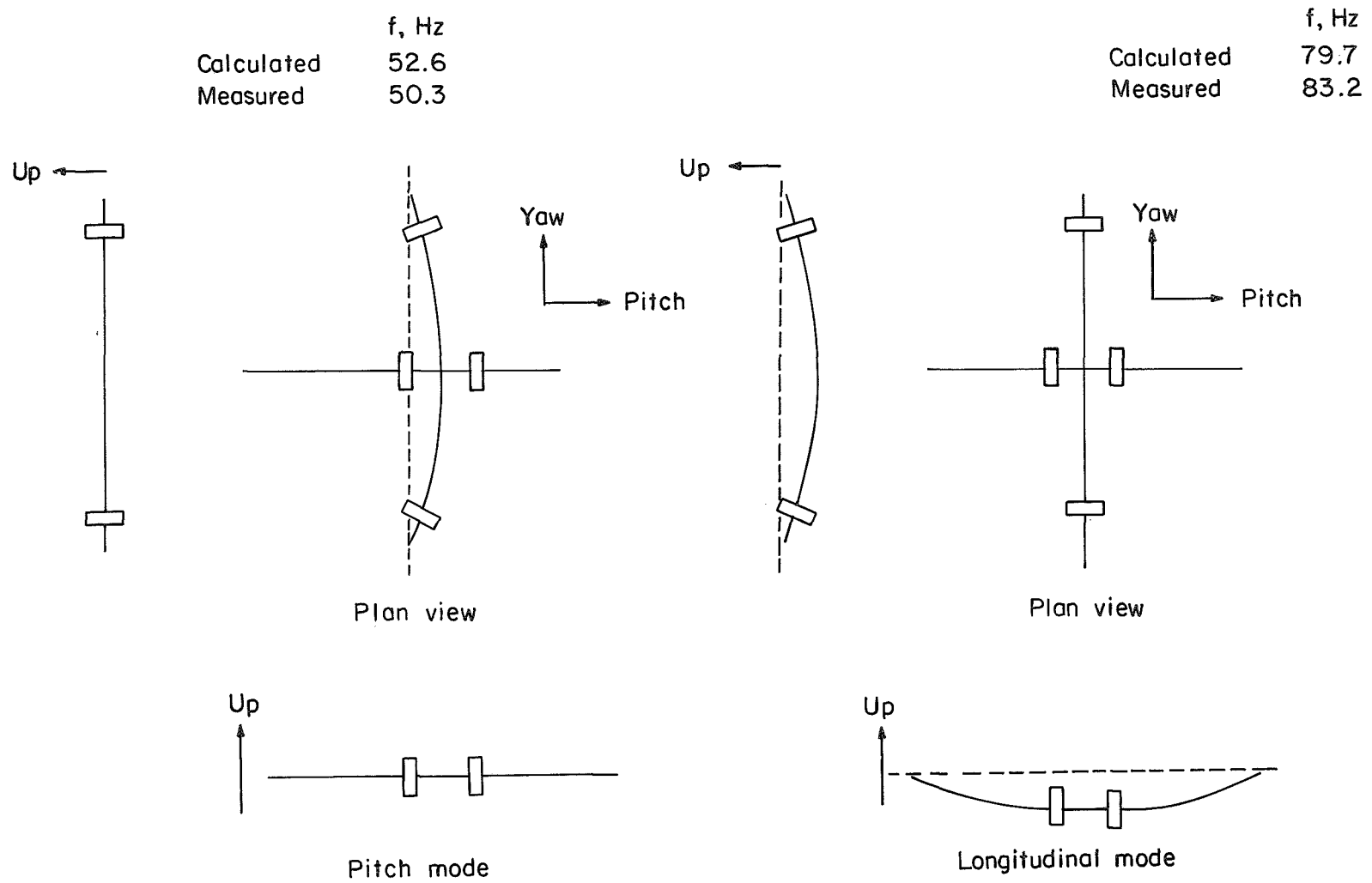


Figure IV-3.- Correlation of calculated and measured frequencies for the 1/10-scale LM-1 model.

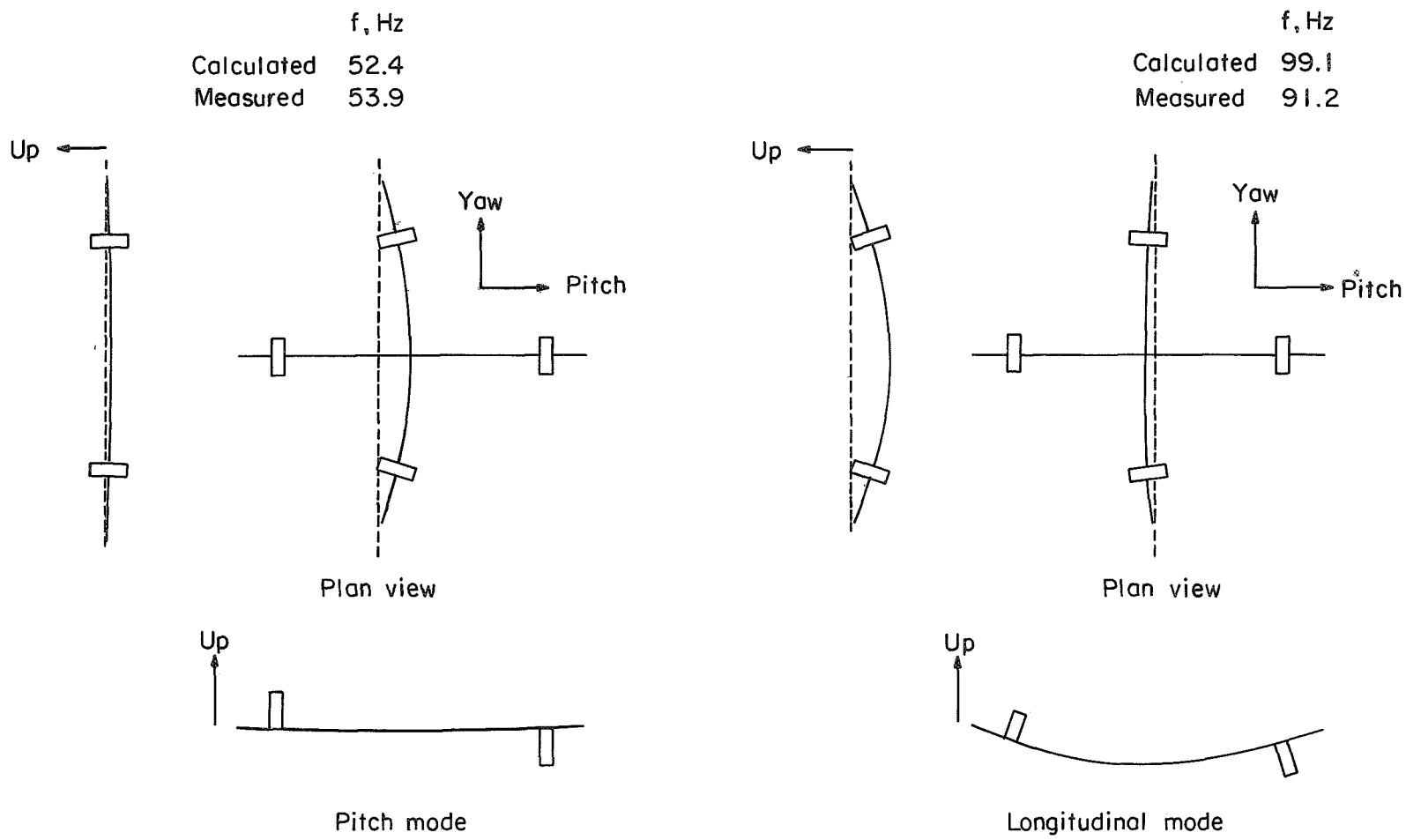
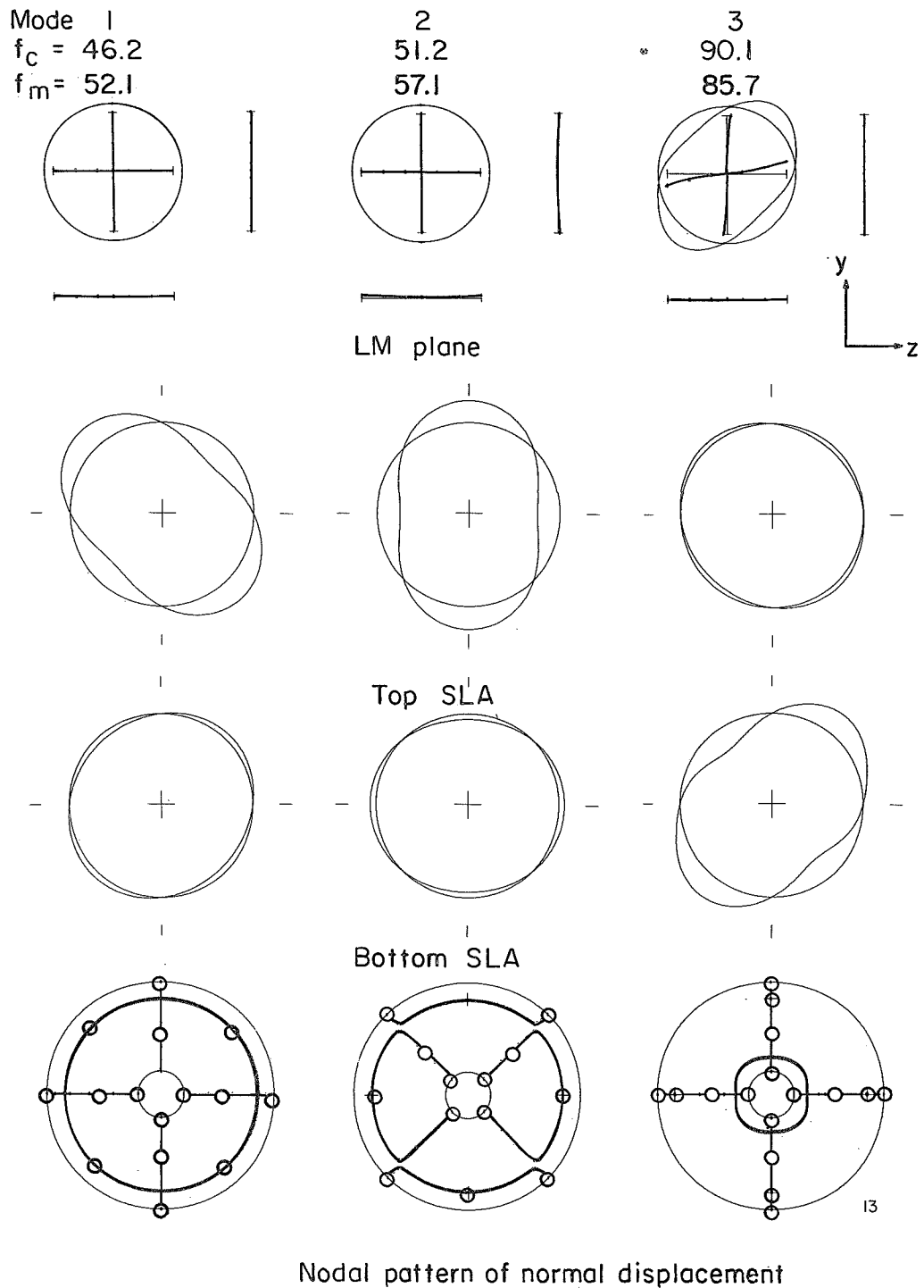


Figure IV-4.- Correlation of calculated and measured frequencies for the 1/10-scale LM-2 model.



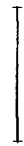
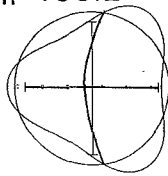
(a) Modes 1 to 3.

Figure IV-5.- Modal data for LM-1/SLA-1 model. f_c , calculated frequency, Hz; f_m , measured frequency, Hz.

Mode 4

$f_c = 90.6$

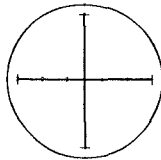
$f_m = 105.2$



5

122.6

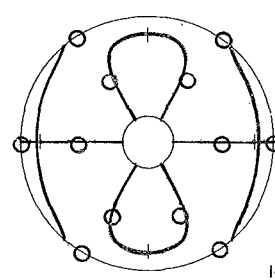
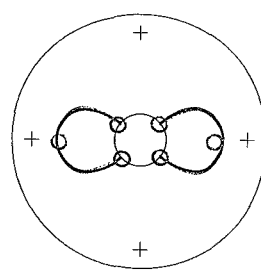
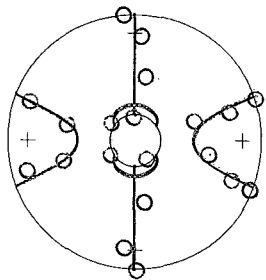
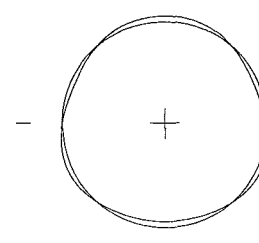
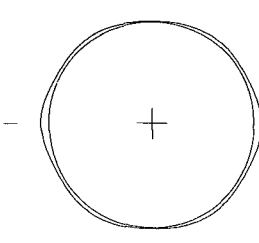
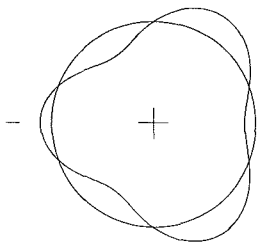
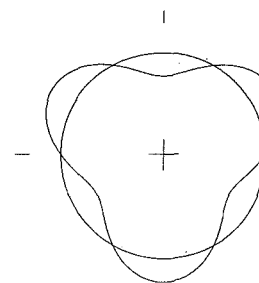
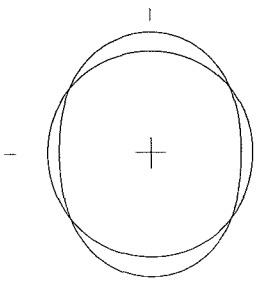
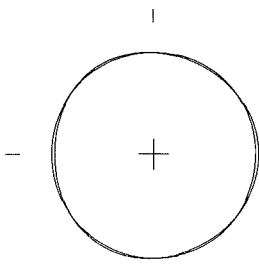
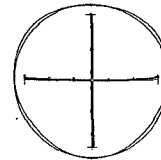
122.8



6

123.5

143.3



14

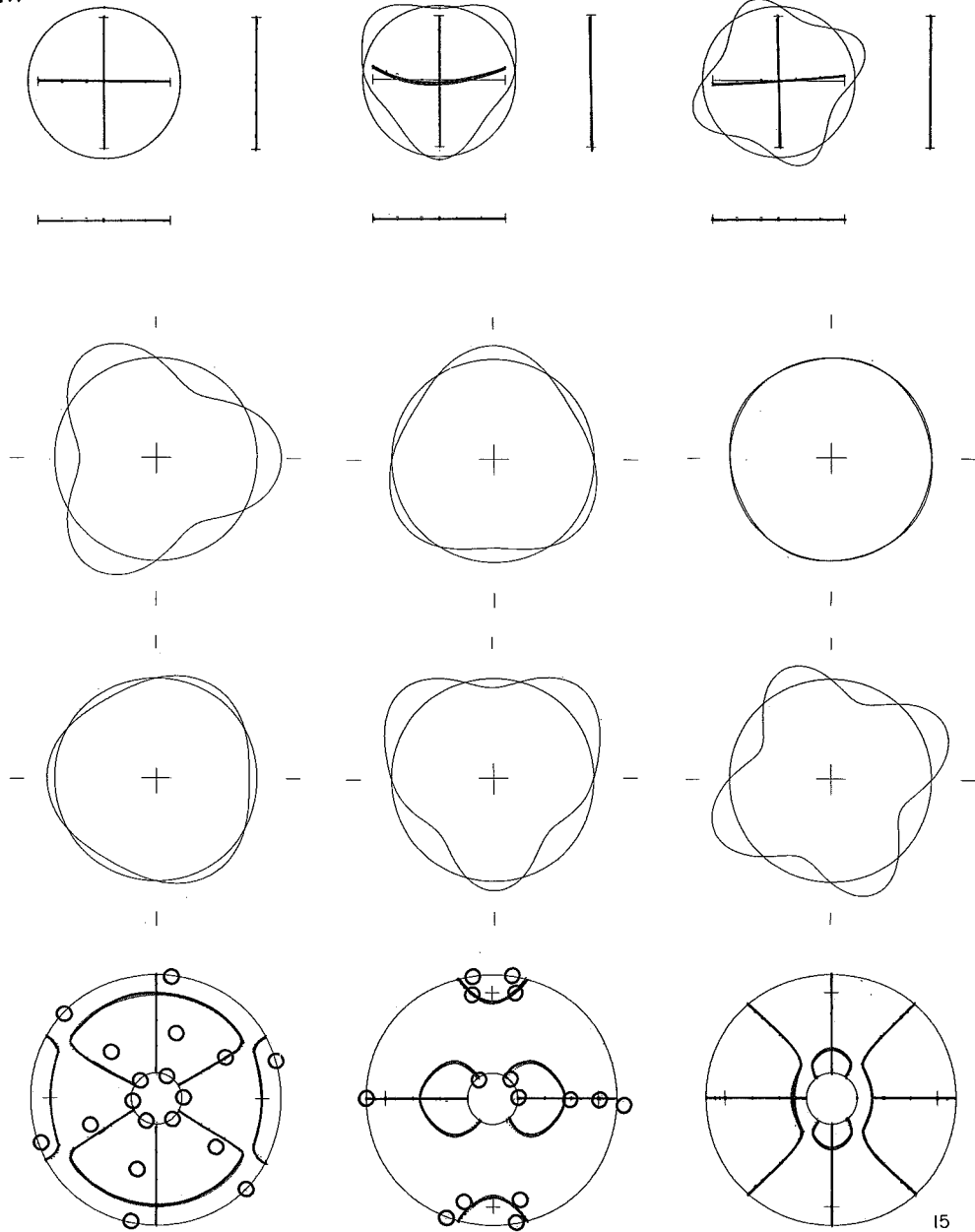
(b) Modes 4 to 6.

Figure IV-5.- Continued.

Mode 7
 $f_c = 124.0$
 $f_m = 143.5$

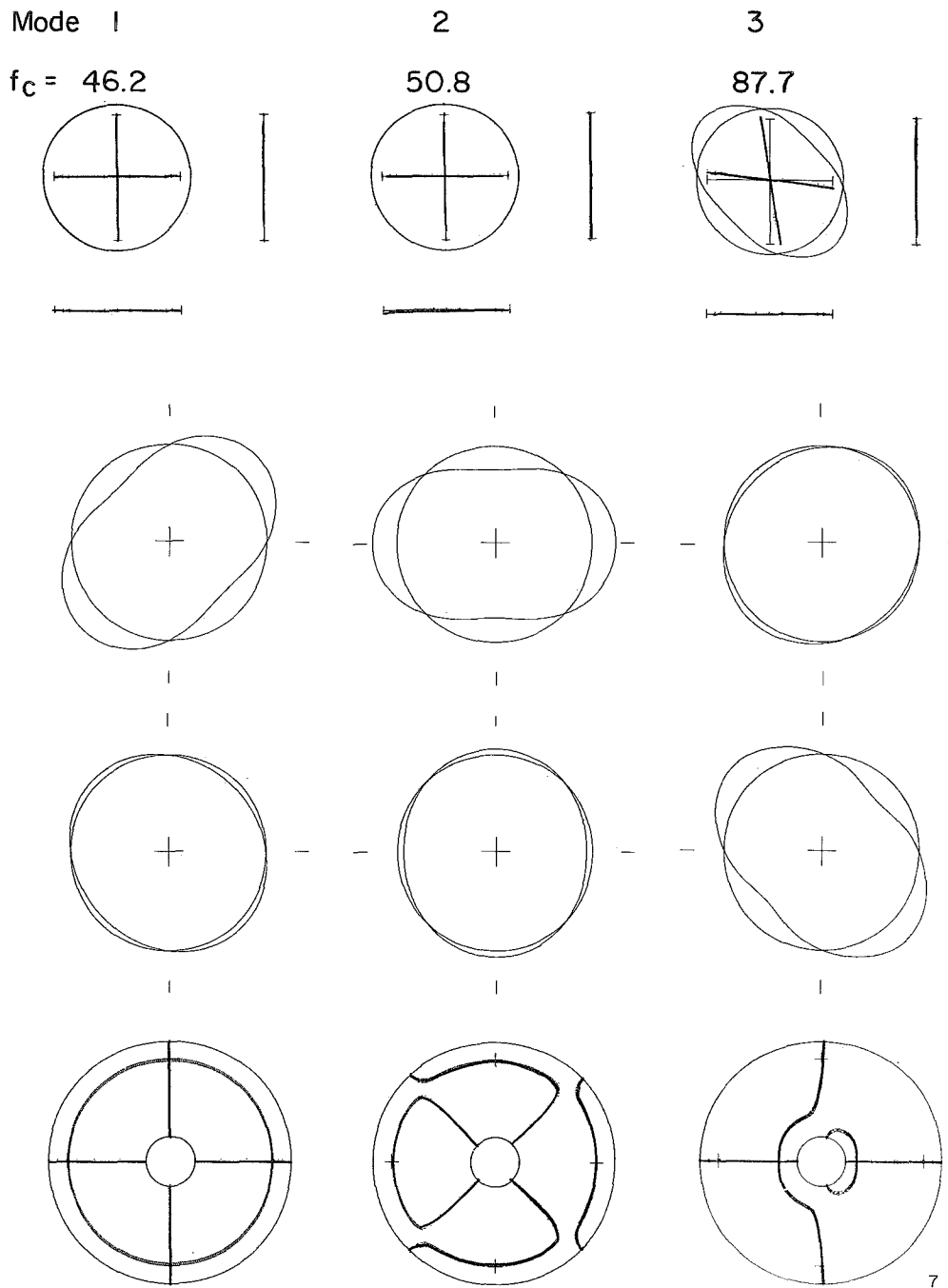
8
 128.2
 114.5

9
 150.9



(c) Modes 7 to 9.

Figure IV-5,- Concluded.



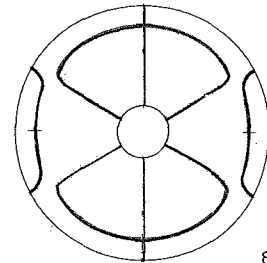
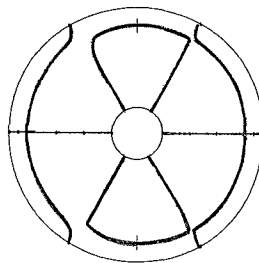
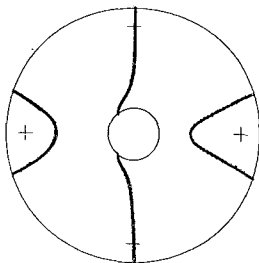
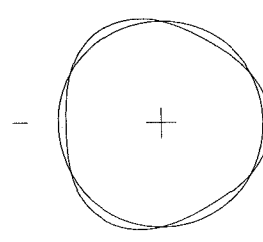
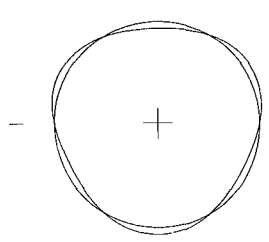
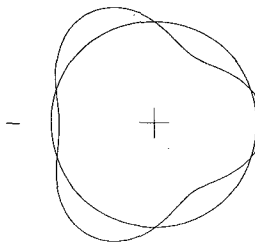
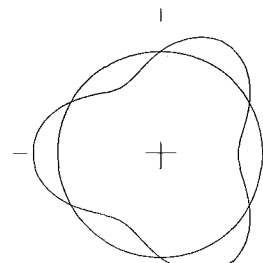
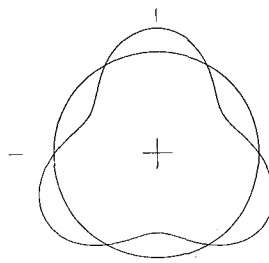
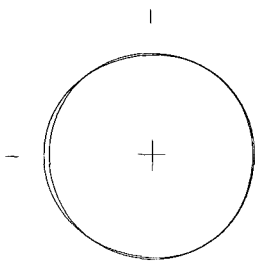
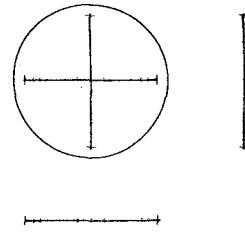
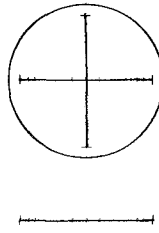
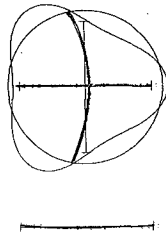
(a) Modes 1 to 3.

Figure IV-6.- Modal data for LM-2-SLA-1 model. f_c , calculated frequency, Hz.

Mode 4
 $f_c = 102.6$

5
123.8

6
123.9



8

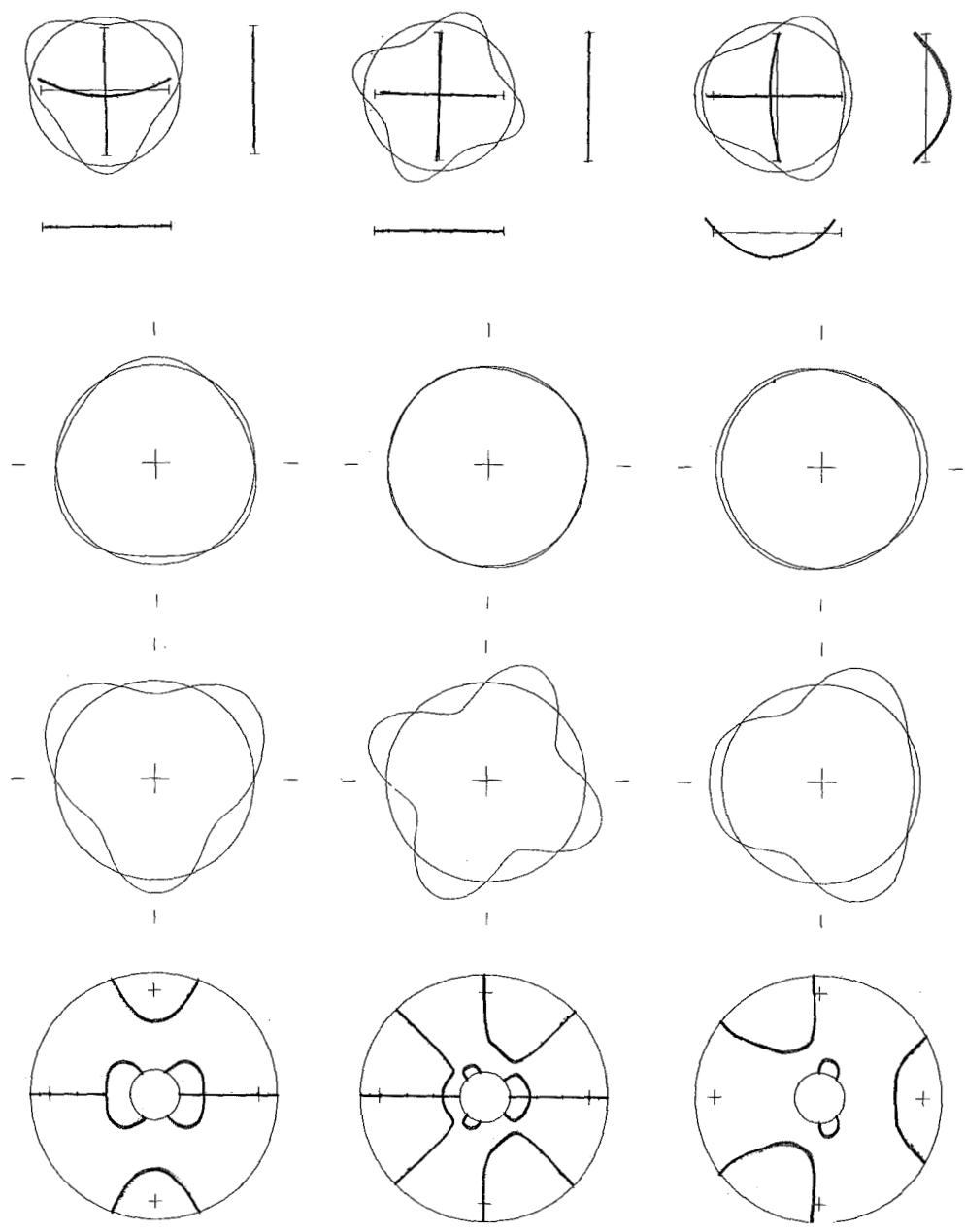
(b) Modes 4 to 6.

Figure IV-6.- Continued.

Mode 7
 $f_c = 131.5$

Mode 8
 $f_c = 144.9$

Mode 9
 $f_c = 153.5$



(c) Modes 7 to 9.

Figure IV-6.- Concluded.

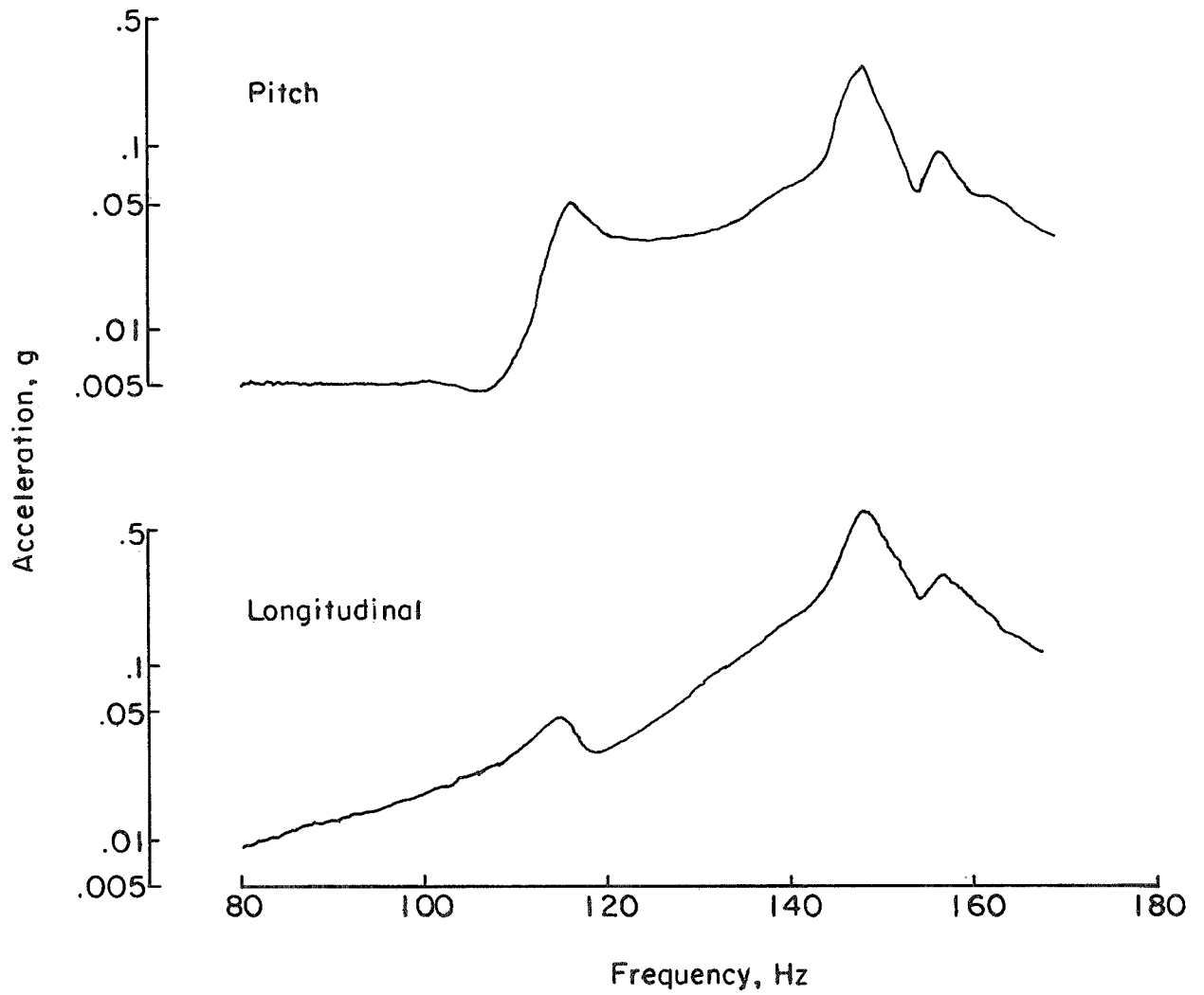


Figure IV-7.- LM center-line pitch and longitudinal amplitude as functions of frequency for free-free LM-2—SLA-1 model excited longitudinally near the LM center line.

V. FULL-STACK AND SHORT-STACK STUDIES

By Larry D. Pinson, John J. Catherines,
and Ellwood L. Peele
Langley Research Center

Introduction

The largest full-scale assembly available for experimental studies during the AS-502 anomaly investigation was the short-stack configuration defined in chapter II. Since there was no full-stack full-scale assembly, the Langley 1/10-scale dynamic model provided the only opportunity to obtain directly comparable data on both full-stack and short-stack configurations. The question arose of the feasibility of adjusting the boundary conditions of the short-stack tests to produce a dynamic deformation shape which approximated that of the full-stack configuration in the payload area for a particular frequency. The addition of an appropriate mass was suggested as one possible method. Therefore, one objective of studies discussed in this chapter was to determine a suitable way of obtaining this full-stack dynamic deflection shape in the payload area from a short-stack test. Other objectives of these studies were to assess differences in longitudinal-lateral coupling between full-stack and short-stack configurations, and to assess differences in the detailed vibratory characteristics in the LM-SLA area of the short-stack and the full-stack configurations. Since dynamic response during the anomaly was at model frequencies near 55 Hz, studies were limited to the responses in that frequency range. Results are presented and discussed from parametric studies as well as comparisons from analytical and experimental results from studies of short-stack and full-stack configurations. Both full-stack and short-stack analytical studies were performed by using a configuration comprised of the 1/10-scale Saturn V model with SLA-1, LM-1, and SM-2. Because of requirements for tuning longitudinal and lateral resonances, full-stack results were obtained with S-IC stage engines removed, no first-stage propellants, and no second stage (S-II) simulated lox.

Analysis

For calculations of stiffness, the short-stack and full-stack configurations, illustrated in figure II-2, were idealized as beams with vehicle mass lumped at convenient locations and with attached branch systems. Shear deformation and rotatory inertia effects were included. The transfer matrix method, extensively discussed in reference V-1, was used to describe the dynamic behavior of the mathematical model. For the current study, an existing computer program for determining lateral natural frequencies and mode shapes was extended to compute forced response from sinusoidal inputs

and to include coupled lateral-longitudinal motion resulting from noncoincident mass and elastic axes.

Figure V-1 indicates the idealization used. The short-stack mass was lumped at 26 locations and the full-stack mass was lumped at 55 locations. The short-stack model, except for the added mass and inertia of the support structure, possessed the same stiffness and inertial properties as the full-stack model from model station 310 forward. The lateral and longitudinal stiffness properties of the full-stack structure are given in reference II-5. The state vector at each station consisted of six elements: shearing force, bending moment, longitudinal force, rotation, lateral deflection, and longitudinal deflection. Since structural damping was included in the forced-response calculations, each element of the state vector is, in general, complex.

The mass moment of inertia and eccentricity of each SM tank was determined from drawings. Since the SM tanks were restrained primarily at their base with only vernier tuning accomplished by the forward restraint, each tank was assumed to be a rigid bar cantilevered from a torsional spring located at the base of the SM with only longitudinal and pitch motions allowed. Torsional spring constants were obtained from test data. The service-module-tank fixed-base natural frequencies are: tank 1, 90.0 Hz; tank 2, 50.0 Hz; tank 3, 67.9 Hz; and tank 4, 43.0 Hz.

The simulated LM was represented as an attached spring-mass system with elasticity and inertia in the longitudinal and pitch directions. Its fixed-base natural frequencies were derived by a Rayleigh-Ritz procedure by assuming sine waves for all bending beams. These frequencies agreed closely with measured values. An equivalent ring around the LM cruciform was assumed to account for the restraint of the shell on the LM although it provided only a small part of the total stiffness of this system. The resultant analytical LM fixed-base natural frequencies with the ring restraint included are: pitch direction, 54.0 Hz; longitudinal direction, 77.9 Hz.

The engines in the S-II and S-IVB stages were represented in a manner similar to that of the SM tanks. No mass eccentricity was allowed for any of the engines and torsional spring constants were empirically determined from measured data in the same way as those for the SM tanks.

Dynamics of Full-Stack Configuration

The analysis and measured data for the full-stack configuration are compared in this section. Results are included to show effects of SM tanks and S-II and S-IVB engines on vehicle response characteristics.

Forced-response shapes.- Figure V-2 compares analytical and experimental lateral forced-response amplitudes for the lower of two full-stack resonances present in the

frequency range of interest. As shown in the figure, sinusoidal pitch forces of 3.0 pounds (13.35 N) at the base of the model and 0.5 pound (2.23 N) at the CM-SM interface were applied. In the analysis a damping value of 2 percent of critical was assumed. Damping is included by multiplying the stiffness by $1 + i\mu$ where i is the imaginary unit and μ is the structural damping coefficient equal to twice the ratio of damping to critical damping. The amplitude of the analytical response is generally lower than that obtained experimentally. However, the response shapes agree reasonably well whereas the frequencies differ by 5 percent. The solid horizontal lines connect analytical points whose phase angles, with respect to that of a reference displacement, were too close to 90° to be plotted as either positive or negative. The difference between the experimental LM leg and LM center deflections represents dynamic deformation of the LM.

Figure V-3 compares analytical and experimental longitudinal forced response. The response shape and amplitude agreement are considered to be good except for some discrepancies in the payload joint areas where the model appears to be softer than the analytical representation. The analytical frequency is higher by approximately 10 percent than that found experimentally. Tests in which the model was incrementally loaded to simulate flight acceleration levels indicate that much of the frequency discrepancy is due to relatively high joint compliance, an effect not considered in the analysis. The inset of figure V-3 illustrates the effect of compressive axial load on the experimental frequency of this mode. These incremental load tests are discussed in chapter VI. The plot shows model longitudinal resonant frequency as a function of simulated axial g-loading. The data show an increase in frequency with compressive load. At the point where the joint can be assumed to be fully effective, the increase is about 8 percent over the initial value. Static tests performed on the original model and reported in reference V-2 also show significant joint compliance. Although the analysis was performed on the SLA-1—LM-1 configuration and the g-load tests were made with SLA-2—LM-3, the trends support the joint compliance hypothesis.

Effects of component flexibilities. - At the frequencies of interest certain model components responded at high amplitudes. The significance of some of these component responses relative to overall vehicle response was investigated analytically by altering the magnitude of the component stiffness. For example, figure V-4 shows the effect of the SM tank flexibilities on the overall response in the higher of the two lateral resonances present. This system resonance occurs near the resonant frequency of the LM in pitch both analytically and experimentally. The force is 1 pound (4.45 N) at the base in the pitch direction and the damping is 2 percent of the critical damping value throughout. In this case, the lateral-response amplitude is not greatly changed by considering the tanks to be rigidly attached.

The effect of changing from rigid to flexible connections for the S-II and S-IVB engines is shown in figures V-5 and V-6. Figure V-5 presents the analytical lateral forced-response amplitude in the higher resonance region with the engines rigidly attached but with the SM tanks flexibly connected, and compares these results with results from studies with forced-response amplitudes calculated with all components flexibly attached. The solid curves in figures V-4 and V-5 represent the same data whereas the dashed curve in figure V-5 is the calculated shape for the rigid engine case. The response shape including the SM tank and LM response amplitudes is significantly changed when the engine attachment flexibility is made zero. Figure V-6 shows the analytically determined lateral frequency response at the forward end of the LES for both rigidly and flexibly attached engines. These curves also show significant changes in frequency response due to engine dynamic characteristics.

Lateral-longitudinal coupling through SM tanks.- The only coupling considered in the analysis was the mass eccentricity of each SM tank which was present even with rigidly attached tanks. The effect of tank mounting flexibility on coupling in the full-stack configuration is shown in figure V-7 as the ratio of longitudinal to lateral LM deflection amplitude as a function of forcing frequency for a unit longitudinal sinusoidal force at the base of the S-IC stage. The S-II and S-IVB stage engines are attached flexibly in these calculations. The results indicate that attaching the tanks rigidly decreases the peak-frequency coupling amplitude. The frequency at which the peak coupling occurs is also decreased. In addition, when the tanks are rigidly mounted, a small secondary peak in the coupling ratio at 56 Hz indicates that the flexibly mounted tanks have a vibration absorber effect at this frequency.

Since only one coupling mechanism is considered in this analysis, the coupling studies in this chapter are presented only to indicate trends. Other coupling mechanisms were considered in the LM-SLA studies in the preceding chapter and for the flight-loads simulation in the following chapter.

Dynamics of Short-Stack Configuration

A comparison of analytical and experimental data on the short-stack configuration is presented in this section along with the results of a coupling study.

Forced response.- Figure V-8 is a comparison of the analytical free-free lateral forced response with experimental data for the 1/10-scale short-stack configuration with 43 pounds (191 N) additional weight at the aft end of the assembly. (As shown subsequently, 43 pounds (191 N) of added weight is nearly optimum for duplicating the full-stack deflection at the base of the short-stack configuration.) No longitudinal response data for the short-stack configuration is presented because no longitudinal resonance occurred in the frequency range of interest. The experimental data were harmonically

analyzed. The experimental phase angles are denoted by numerical values and the suffix E and the analytical phase angles are indicated by numerical values and the suffix A. A structural damping constant of $\mu = 0.04$ or 2 percent of the critical value was assumed throughout the structure for this analysis. Some discrepancy in phase and amplitude occurs near the base but other parts of the structure are in very good agreement. Correlations forward of model SM were not made because of loss of data signal for the forward transducers. However, the analysis and experiment overall are in excellent agreement for this complex structure.

Effects of damping on lateral-longitudinal coupling.- The results of an analytical coupling study on the short-stack configuration are presented in figure V-9. The ratio of lateral to longitudinal LM deflection amplitude as a function of forcing frequency for a longitudinal force at the base of the short-stack configuration is shown. Damping in various portions of the structure was a parameter. These variations in damping are shown in the table associated with the figure. The nominal damping in the structure was assumed to be $\mu = 0.04$ or 2 percent of the critical value except where noted in the table. The maximum reduction in coupling occurs when damping is doubled in the SM tanks, LM, and structure, as might be expected. The coupling ratio is reduced more by doubling damping in the SM tanks than by doubling damping in the LM and again emphasizes the significance of SM tank-mounting flexibility relative to LM coupling. In all cases maximum coupling occurs at about 56 Hz. In the full-stack study, the maximum coupling occurred near 50 Hz. As in the full-stack study, these coupling results should be regarded only as trends since only one coupling mechanism was considered in the analysis. However, the study indicates the effects of the presence of various proportions of damping in selected areas of the structure. The versatility of the analytical approach used in the study is also demonstrated.

Full-Stack and Short-Stack Model Comparisons

Previous sections have established the general validity of the mathematical model for predicting the response of both the full-stack model and the short-stack model in the direction of the applied force by comparing analytical and experimental results. Therefore, analytical comparisons between full-stack and short-stack results should be valid. Specifically, the short-stack end conditions required to duplicate full-stack dynamic response in the LM-SLA area can be established with some confidence. This section presents the short-stack end conditions necessary to permit the short-stack model to behave as if it were part of the full-stack model based on these analyses.

Figure V-10 shows the effects of added weight at the base of the short-stack model on the analytical shear, moment, rotation, and deflection amplitudes for the two principle resonances in the 45 Hz to 60 Hz range along with the corresponding values from the

full-stack configuration. The values are for model station 310 which is the base of the short-stack configuration. The moment of inertia of the added weight was calculated by assuming that all the mass was concentrated in a ring that had the same diameter as the forward skirt of the third stage. The dashed lines of the figure give the shear, moment, rotation, and deflection for the full-stack model with a lateral sinusoidal input force at the base of the short-stack model (station 310). On the basis of deflection, the optimum additional weight is 43 pounds (191 N) for the 56 Hz resonance. However, the other boundary conditions of rotation, moment, and shear are not matched by this one parameter.

The effect of not matching rotations at the base of the short-stack configuration is shown in figure V-11. Figure V-11(a) compares analytical results and figure V-11(b) compares experimental data. In figure V-11(a), the solid curve is the full-stack deflection shape from the base of the short-stack configuration forward. The dashed curve in figure V-11(a) is the calculated short-stack deflection shape, the same as the analytical part of figure V-8. Although the deflections at the base of the short-stack model match, as figure V-10 indicates they should, the deflection shapes for the remainder of the structure are very different. A similar result is indicated by the experimental data in figure V-11(b). When the moment of inertia of the added mass was arbitrarily increased by a factor of six, the third curve of figure V-11(a) was obtained. It is in qualitative agreement with the full-stack mode shape but the amplitude is large by about a factor of two. The figure indicates, however, the importance of the moment of inertia of the added mass in attempting to match the short-stack and full-stack deflection shapes and the necessity of matching more than one boundary condition.

Since the simulated LM was represented as an attached spring mass system with its fixed-base frequencies derived by a Rayleigh-Ritz procedure and with the SLA shell restraint represented by a spring determined from an equivalent ring, this analysis did not enable a qualitative evaluation of how the LM pitch mode was affected by the absence of the booster stages of the launch vehicle. Results from analytical studies, reported in chapter III, indicate the presence of LM-pitch-type modes, having $n = 3$, with the isolated LM-SLA configuration. It was determined experimentally that for the frequency range of interest, the LM pitch mode and the resulting SLA deformation, having a mode shape similar to that indicated in chapter IV, is essentially unchanged in either frequency or basic shape.

Concluding Remarks

Results of analytical parametric studies for both the full-stack and short-stack configurations and comparisons with experimental data have been presented. In the analysis the vehicle is modeled as a beam whose mass is concentrated at selected locations. Shear deformation, rotatory inertia, longitudinal mass, and longitudinal

elasticity are included. Coupling between longitudinal and lateral motion due to non-coincident mass and elastic axes is also included. Damping may be varied in selected areas of the structure.

Matching the dynamic deformation shape of the short-stack model to that of the full-stack model by the addition of appropriate mass at the base of the short-stack model was attempted both analytically and experimentally without success. It was shown analytically that addition of mass alone was insufficient; an appropriate additional mass moment of inertia at the base of the short-stack model is also necessary.

The analysis satisfactorily predicts the lateral response of both the short-stack and full-stack configurations of the 1/10-scale Saturn V model. However, the longitudinal response prediction for the full-stack configuration has a 10-percent frequency discrepancy. This discrepancy is attributed to significant compliance at certain joints in the structure which was not accounted for in the analysis.

The dynamics of the S-II and S-IVB engines produces the largest effect on the overall response of the full-stack model of all the branch components.

Doubling the damping in the SM tanks affected the ratio of lateral to longitudinal deflection of the LM more than doubling the damping in the LM.

A greater ratio of lateral to longitudinal LM deflection occurred in the short-stack model than in the full-stack model for longitudinal excitation. The peak value of this ratio occurred at 56 Hz in the short-stack analysis whereas the full-stack analysis showed the peak at about 50 Hz. A small secondary peak in this ratio occurred at 56 Hz in the full-stack analysis when the SM tanks were attached rigidly to the main structure but did not occur when the tanks were elastically attached; this result suggests a vibration absorber effect from the elastically supported tanks in the 56 Hz region.

The frequency and shape of the LM pitch mode was relatively unchanged between short-stack and full-stack tests with only the added weight on the short-stack model.

References

- V-1. Pestel, Eduard C.; and Leckie, Frederick A.: Matrix Methods in Elastomechanics. McGraw-Hill Book Co., Inc., c.1963.
- V-2. Pinson, Larry D.; and Leonard, H. Wayne: Longitudinal Vibration Characteristics of 1/10-Scale Apollo/Saturn V Replica Model. NASA TN D-5159, 1969.

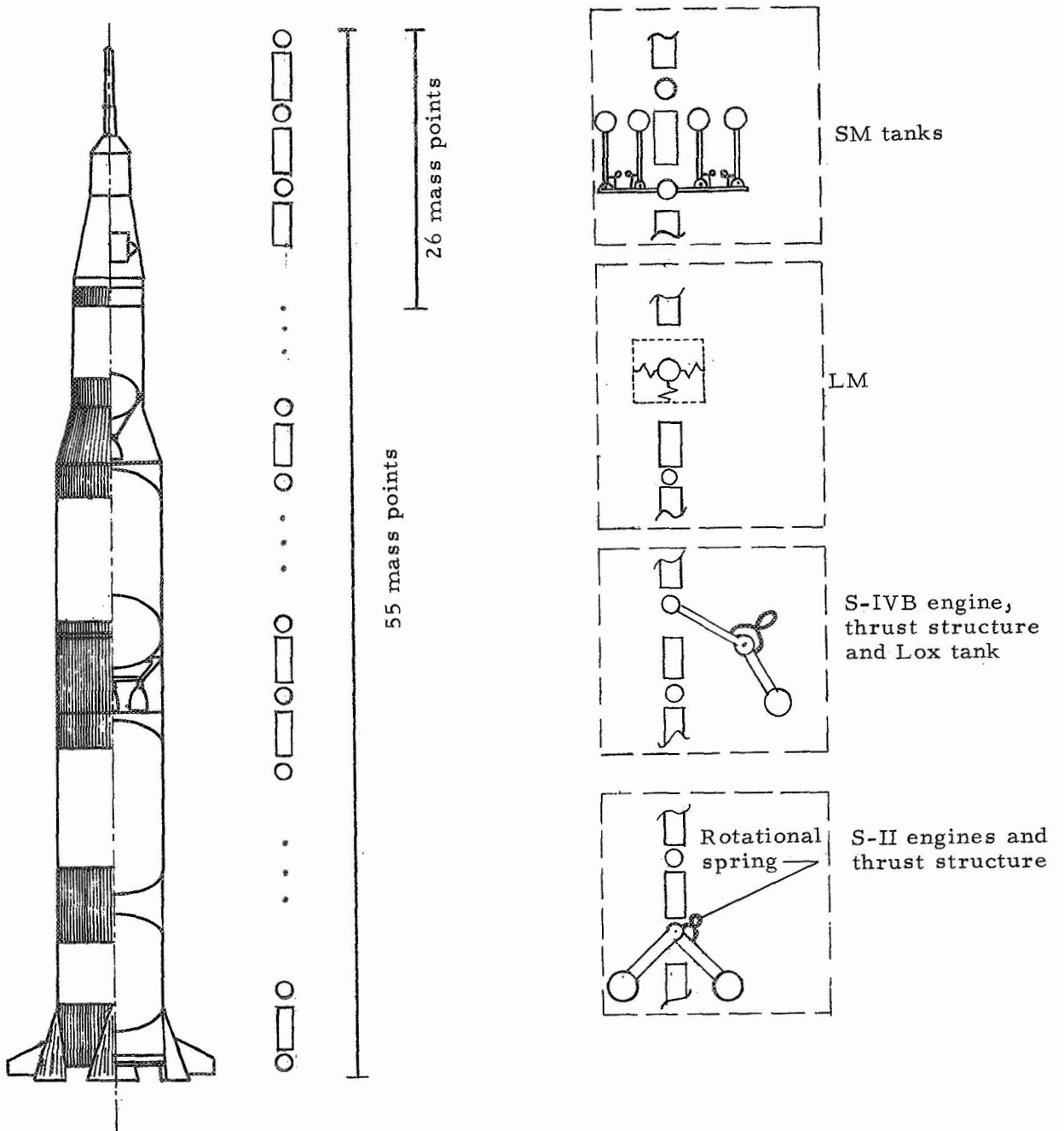


Figure V-1.- Schematic of mathematical idealization, 1/10-scale model.

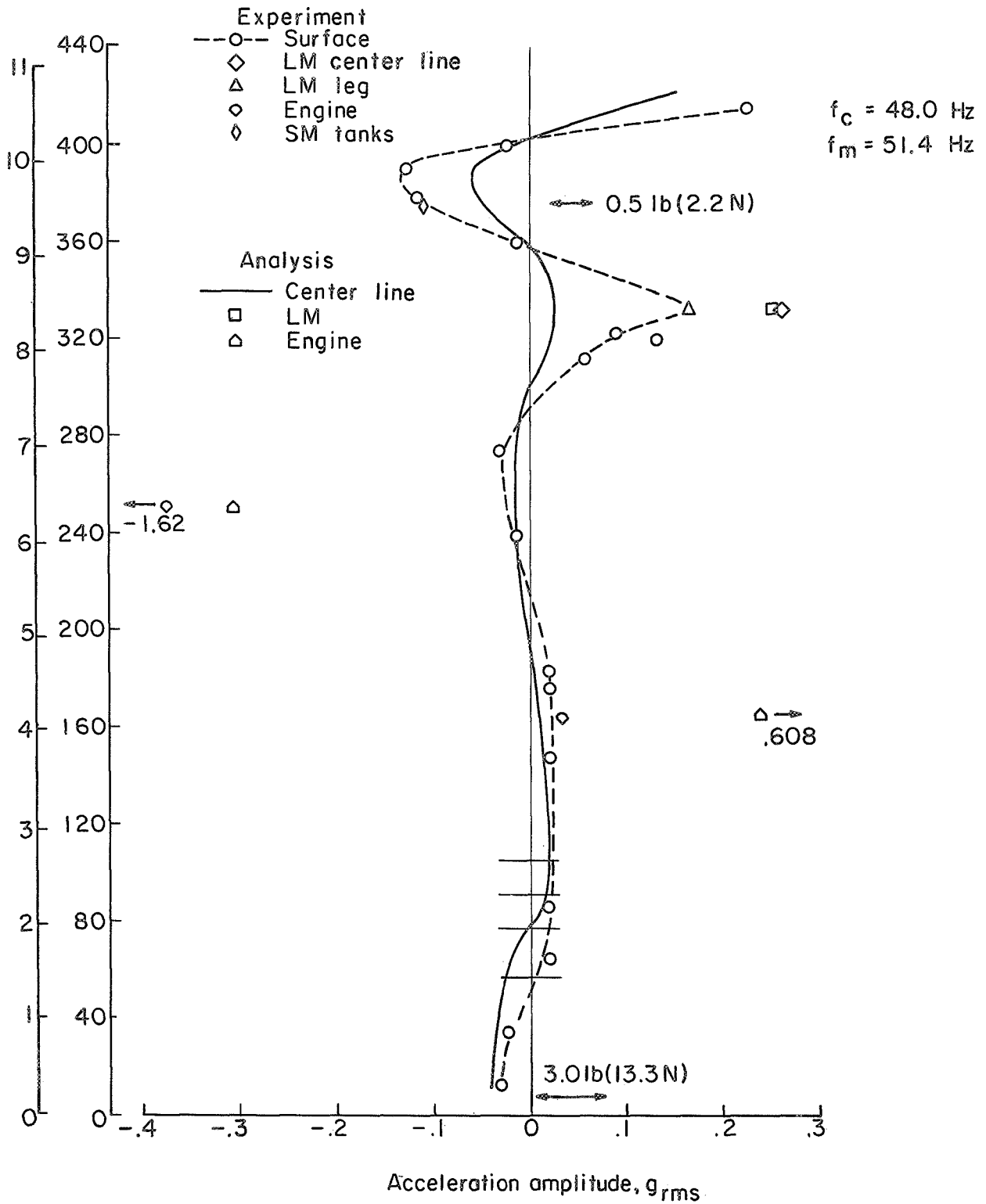


Figure V-2.- Lateral analytical forced response compared with experiment for 1/10-scale full-stack configuration. $\mu = 0.04$.

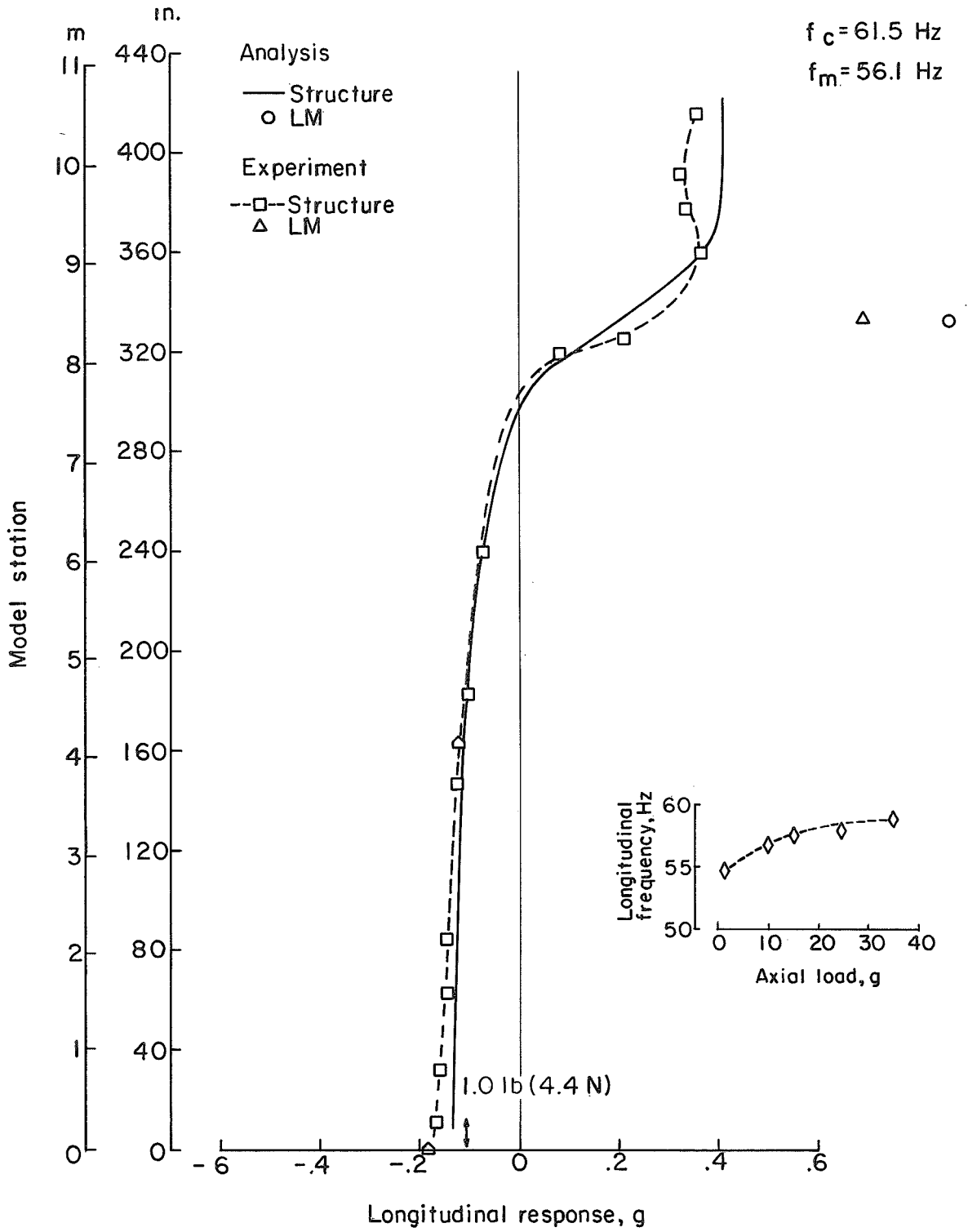


Figure V-3.- Longitudinal analytical forced response compared with experiment for 1/10-scale full-stack configuration. $\mu = 0.04$.

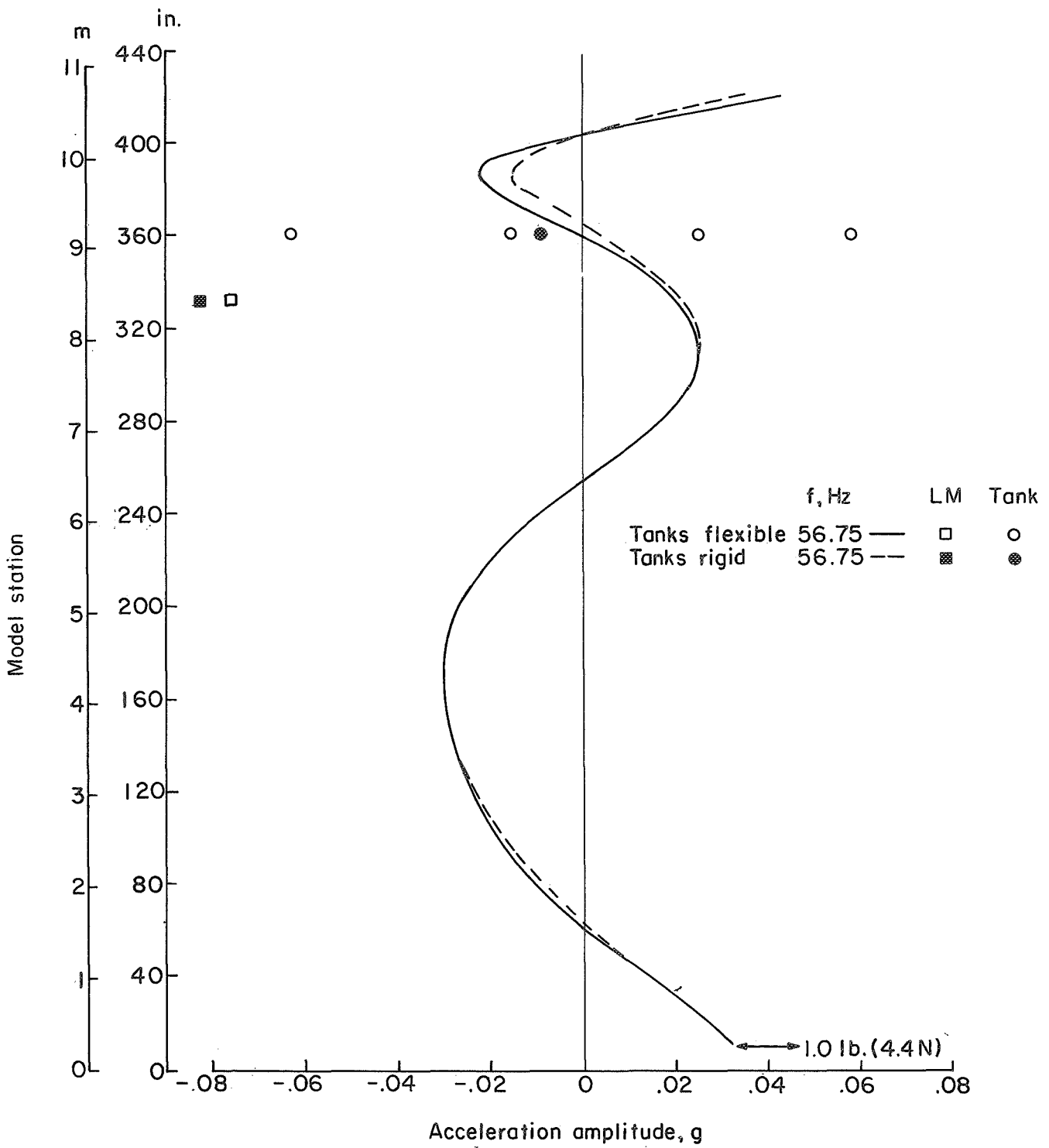


Figure V-4.- Effect of SM tank dynamics on 1/10-scale full-stack analytical lateral forced response ($\mu = 0.04$). Unit force at model station 12; $\mu = 0.04$.

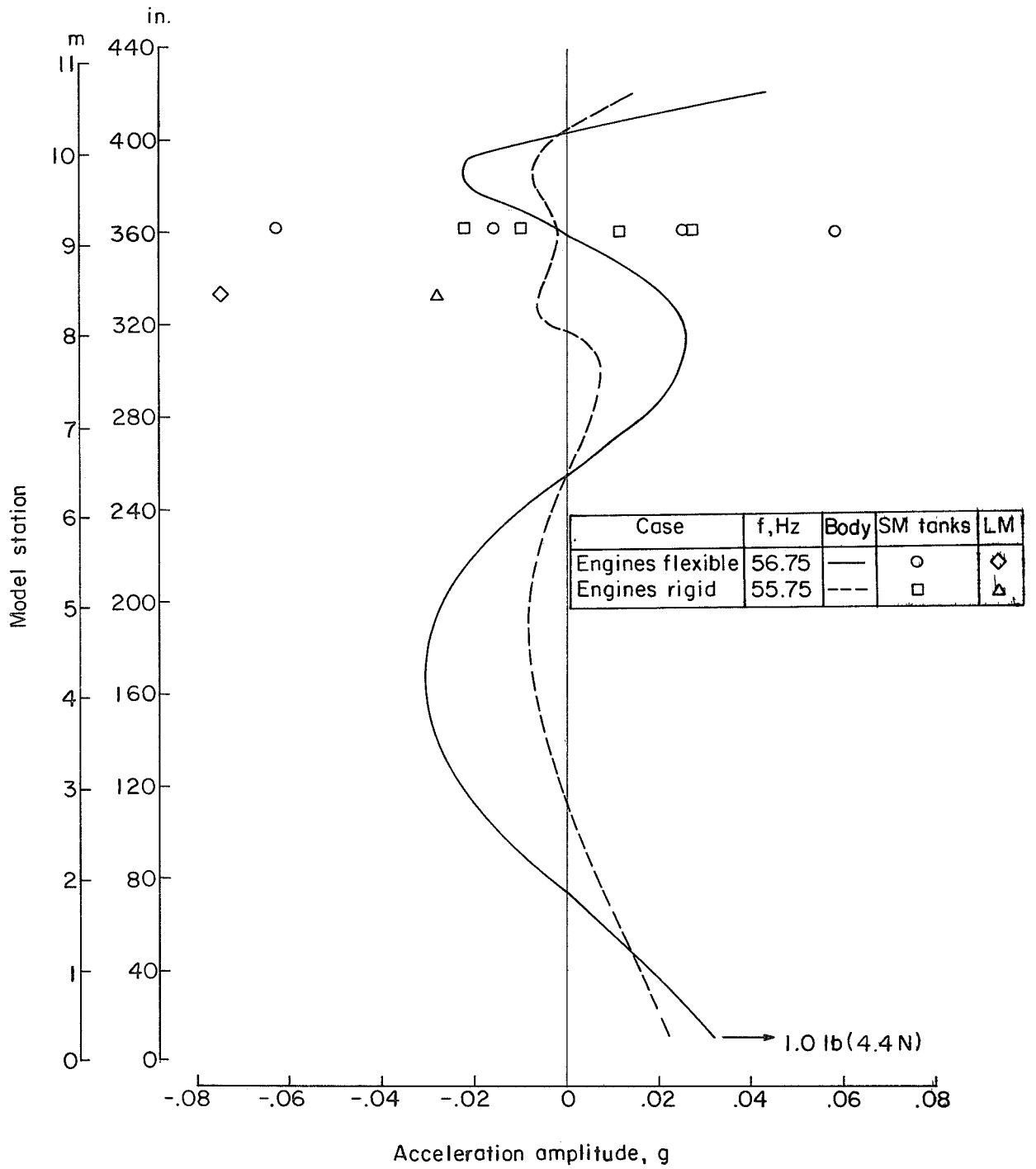


Figure V-5.- Effect of engine dynamics on 1/10-scale full-stack analytical lateral forced response. $\mu = 0.04$.

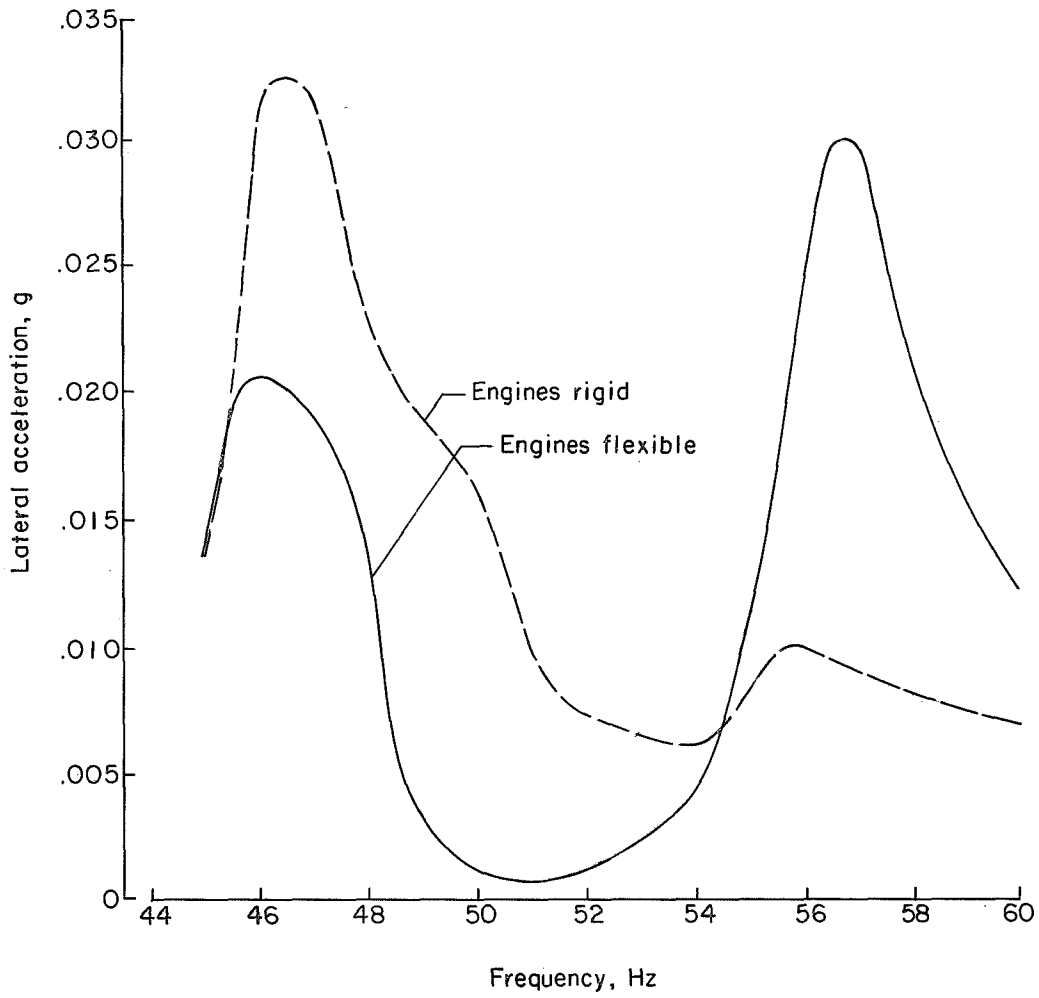


Figure V-6.- Effect of engine dynamics on analytical lateral frequency response at model station 421. Unit force at model station 12; $\mu = 0.04$.

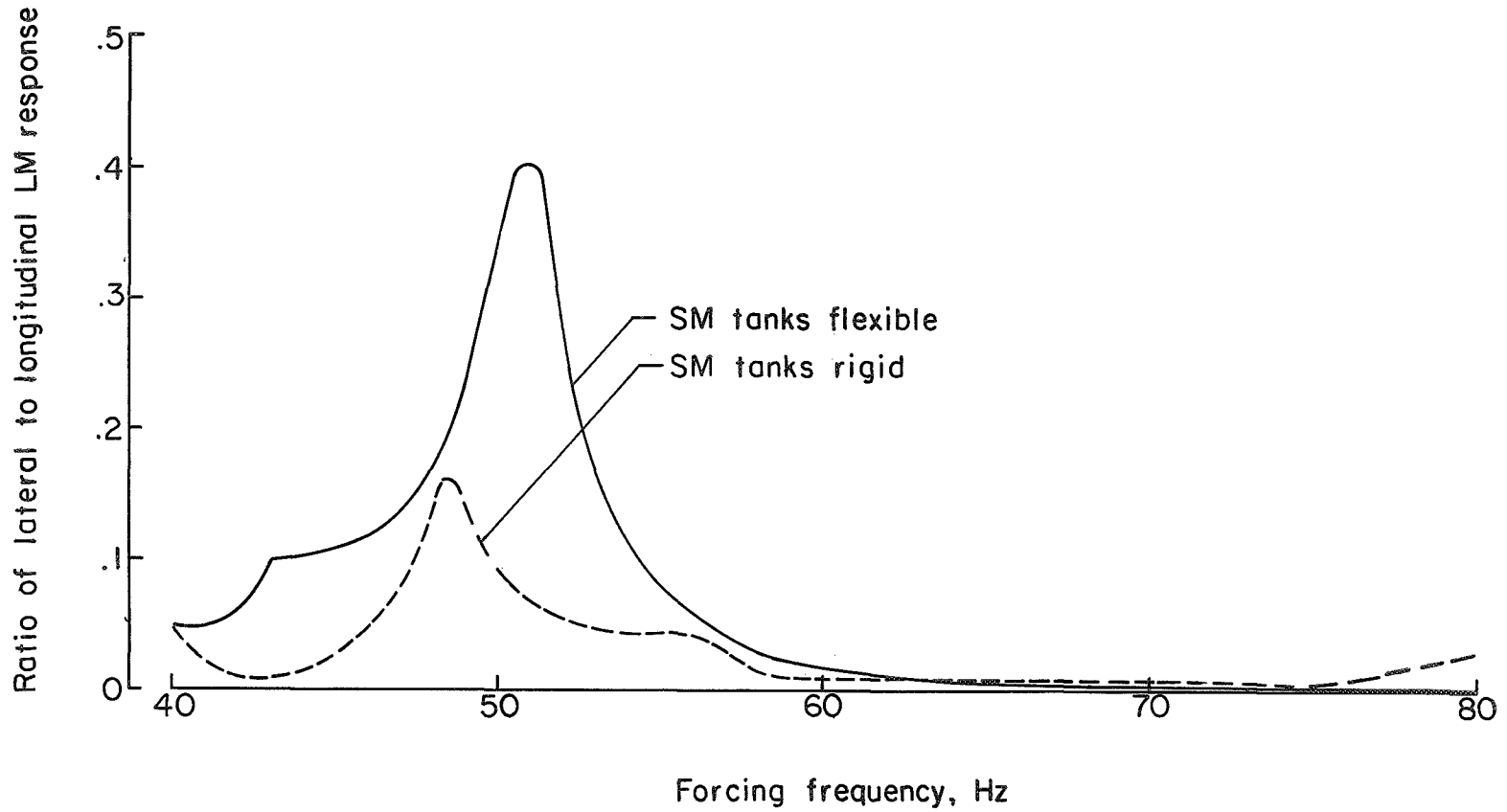


Figure V-7.- Effect of SM tank dynamics on analytical LM lateral to longitudinal response ratio. Unit longitudinal force at model station 12; $\mu = 0.04$.

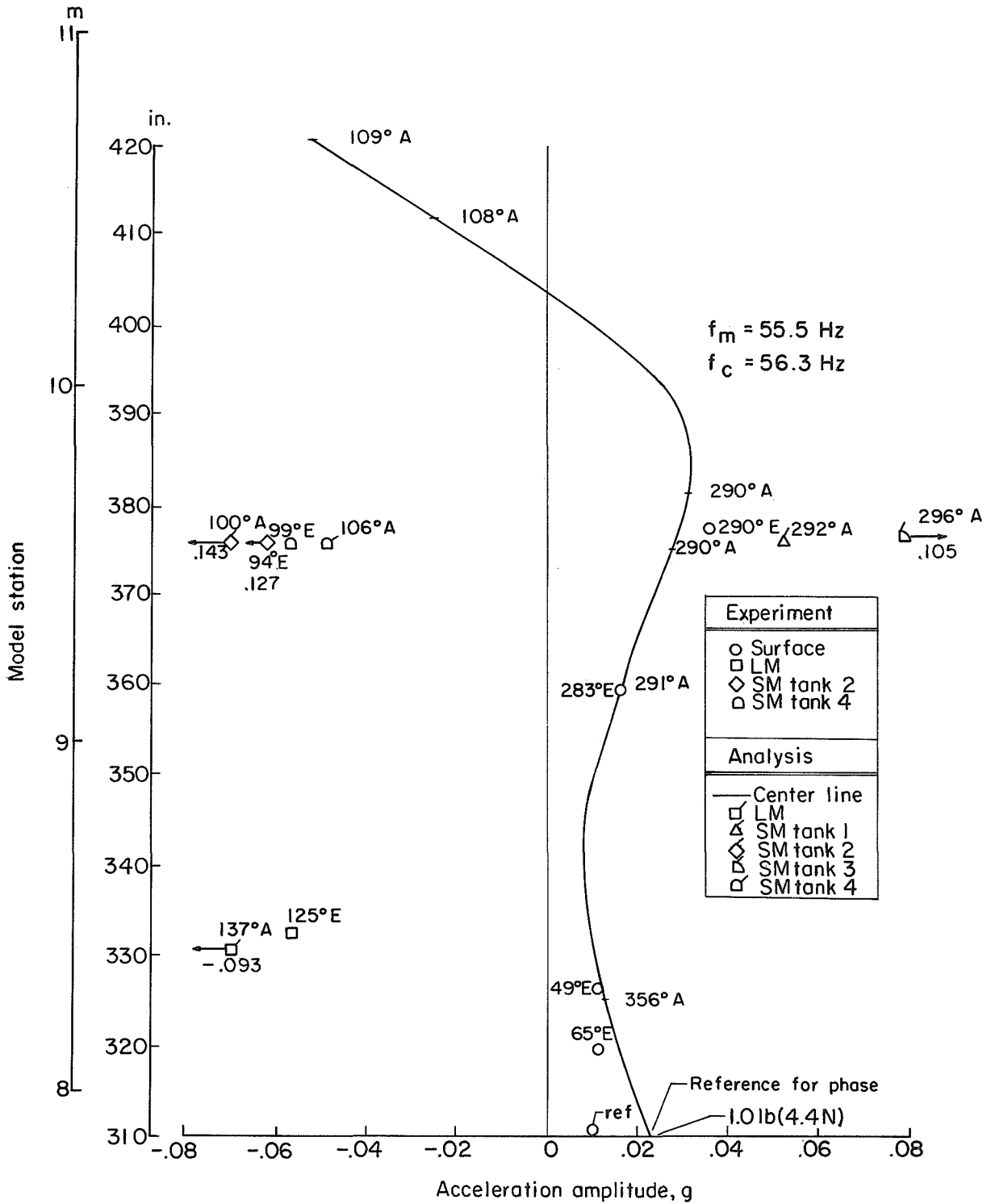


Figure V-8.- Comparison of experimental and analytical lateral forced response of 1/10-scale short stack with 43 pounds (191 N) added weight at aft end. Unit force at station 310; $\mu = 0.04$. E denotes experimental value; A, analytical.

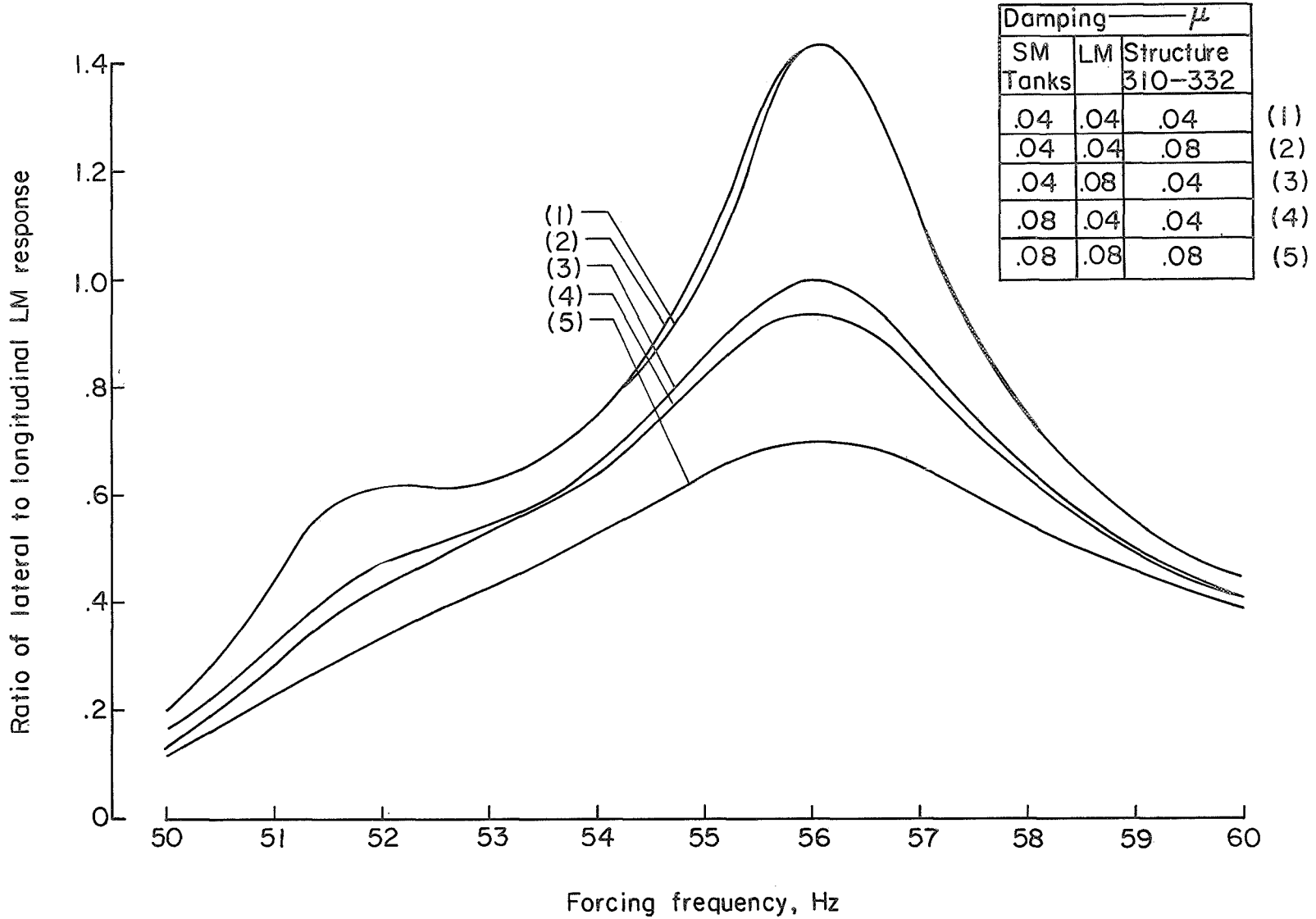


Figure V-9.- Effect of component damping on analytical ratio of lateral to longitudinal LM response. Unit longitudinal force and 43 pounds (191 N) added weight at base of short-stack model.

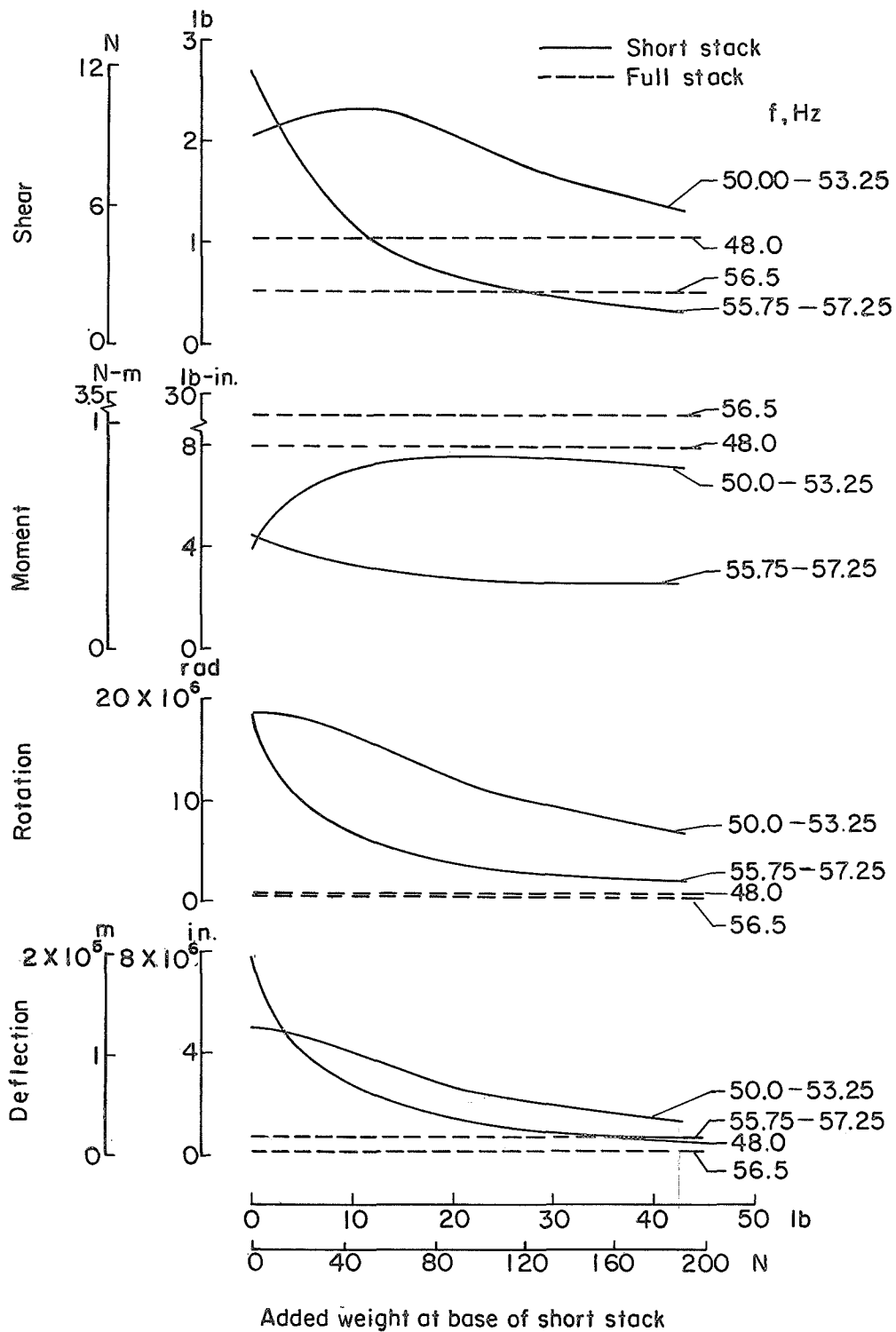
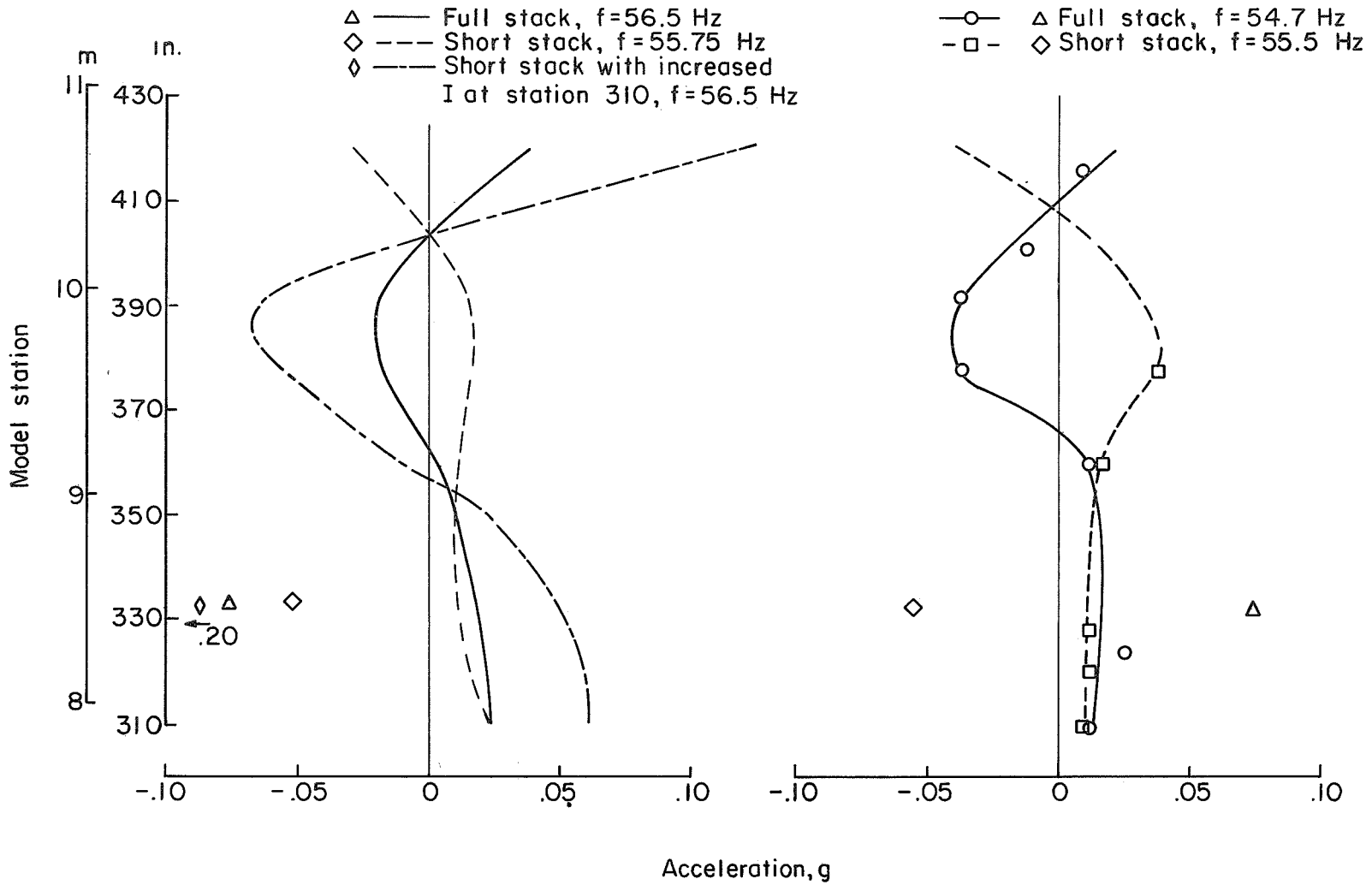


Figure V-10.- Calculated state vector at base of short-stack configuration (model station 310) for various added weights. Unit lateral force at station 310; $\mu = 0.04$.



(a) Analysis.

(b) Experiment.

Figure V-11.- Comparison of 1/10-scale model full-stack and short-stack deflection shapes.

VI. COMBINED ACCELERATION LOADS SIMULATION

By Robert R. Clary, James A. Schoenster,
and Lloyd J. Turner, Jr.
Langley Research Center

Introduction

During accelerated flight, a launch vehicle may be subjected to longitudinal compressive forces which may, with the superposition of accompanying vibratory loads that result from vehicle dynamic responses, impose local stresses which exceed the design capability of the involved structure. Since a launch vehicle is, in fact, a highly efficient structure, relatively small dynamic loads can thereby result in unacceptable flight anomalies. For example, it has been postulated that the local failure which occurred in the SLA sandwich structure during the AS-502 flight may have been due to inability of the structure to withstand combined thrust acceleration loads and induced vibration loads.

The purpose of this chapter is to discuss an experimental investigation conducted with the 1/10-scale Apollo-Saturn V model with selected components subjected to combined static and vibratory loads. Loads resulting from thermal effects were not included. These tests were conducted in an effort to demonstrate either the structural integrity or the failure mode of a carefully scaled dynamic model of the SLA.

Simulation Requirements

In order to simulate, with proper scaling, the combined acceleration loads experienced in the AS-502 flight on the 1/10-scale model, the following test conditions were necessary:

(1) The model should be tuned so that the first longitudinal mode, a bending mode in which the response of the model in the payload area is similar to the vehicle fourth bending mode response measured during the AS-502 flight, and the LM-SLA pitch mode all have frequencies near 55 Hz.

(2) The vibratory response of the model LM, at its center, should be 6g at a frequency of about 55 Hz in both the pitch and longitudinal directions.

(3) The model SLA and LM should be subjected to static compressive loads equivalent to 35g axial acceleration.

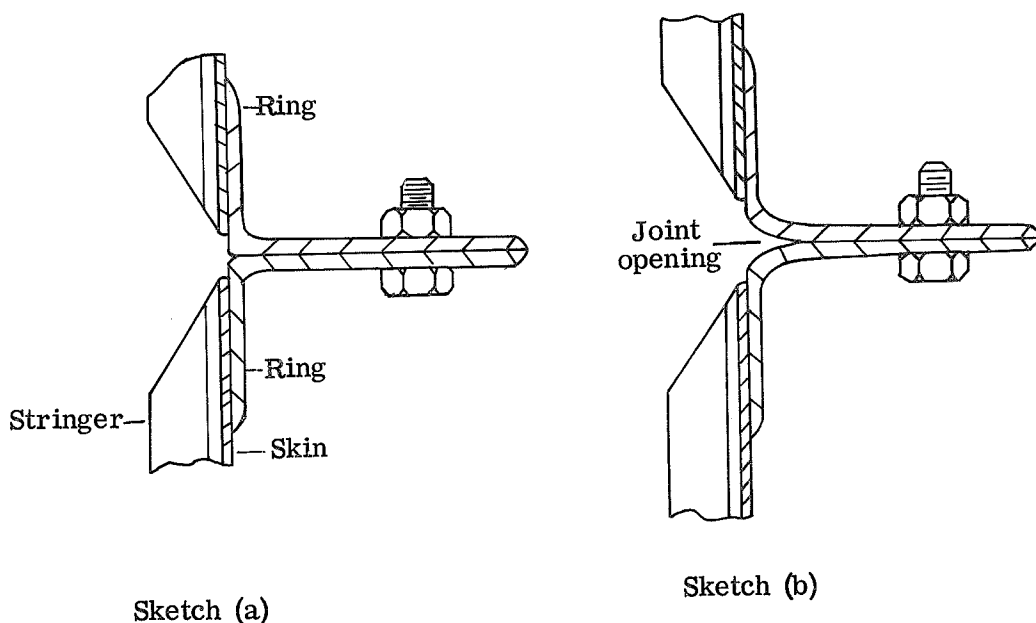
Preliminary Studies

Several tests were conducted to establish the effects of the simulation equipment, to tune the frequencies of the modes of concern, and to define the structural dynamic

properties of the full-stack model prior to conducting the flight-loads simulation test. Results of these preliminary tests are discussed.

Static acceleration load effects.- Since it was impractical to subject the entire model to the desired steady axial acceleration level, a static loading system was designed to apply the simulated acceleration loads to only the SLA and LM components of the structure. (See chapter III.)

Vibration tests using low-level input sinusoidal forces were conducted on the full-stack configuration to determine effects of the pulley attachment ring and compressive acceleration loads. The results indicate that the static load ring did not significantly alter the pitch response of the vehicle; however, the static g-loads, especially those applied to the LM, increased the frequency of the first longitudinal mode. This trend indicates an increase in the effective stiffness of the model. Correlation between previously presented analysis and test data revealed that the flexibility of the joints in the 1/10-scale Saturn model is not the same as that of the full-scale Saturn (ref. VI-1). In this reference it is pointed out that the joint longitudinal flexibility exhibited by the 1/10-scale model could be explained if the joints are assumed to behave as in the following manner:



A fully effective joint is shown in sketch (a) where the stiffness of the joint is representative of the assumed full-scale structure. However, in sketch (b) an opening occurs at the surface of the joint interface because of imperfections which result either from tolerance

limitations or machining errors. The stiffness of this imperfect joint is nonlinear and tends to increase with an increasing load until the surface opening is closed. This phenomena may be related to the increase in the resonant frequency of the first longitudinal mode which varied as a function of the simulated axial acceleration level in the following manner:

Simulated axial acceleration, g . . .	1	10	15	25	35
Longitudinal frequency, Hz	54.5	57.0	57.5	58.0	59.0

The frequency of the lateral mode of interest remained relatively constant throughout these tests.

Model tuning.- The vibration tests just discussed were conducted with the S-IC engines removed, the first stage (S-IC) empty, and the second stage (S-II) lox tank one-half full of simulated propellants. This configuration had been found to have a fourth lateral bending mode, the first longitudinal mode, and LM pitch mode frequencies near 55 Hz. However, when the load simulating 35g acceleration was applied to the SM, SLA, and LM, the first longitudinal mode frequency increased to 59 Hz and was higher than the frequency of the LM pitch mode. Hence, for accurate simulation of flight conditions, it was necessary to reduce the frequency of the first longitudinal mode of the model without affecting the LM pitch mode. This frequency reduction was accomplished by adding simulated propellant in the S-II stage lox tank.

Longitudinal-lateral coupling.- In order to attain adequate representation of flight stresses on the model SLA, the dynamic-loads simulation required that the LM respond with equal amplitudes in the longitudinal and pitch directions. Earlier studies established that the vehicle could be tuned so that the first longitudinal mode, a lateral mode wherein the response of the vehicle above the S-IVB stage resembled the fourth bending mode, and a local LM-SLA pitch mode nearly coincided at approximately 55 Hz. However, a response ratio, that is, the ratio of the pitch amplitude to the longitudinal amplitude, of unity at the center of the LM model was not obtained. Therefore, studies of some of the potential coupling mechanisms which could affect the response ratio were conducted at low input force levels. The mechanisms investigated include asymmetries in the LM, a force unbalance in the longitudinal excitation at the base of the vehicle, eccentricities of the SM tanks, and combined excitation in the longitudinal and pitch directions.

The basis of comparison between the various configurations was the response ratio of the LM center at the frequency of the peak pitch response near 55 Hz. Some ratios were also obtained at the frequency of the peak longitudinal response, which did not necessarily coincide with the pitch peak frequency.

The response ratios are presented in table VI-1 for the LM models investigated with the SLA-1 and SM-2 components. One electromagnetic shaker located at the S-IC center engine gimbal plane excited the vehicle longitudinally with a vibratory force of ± 10 pounds (44.5 N). Both symmetric and asymmetric LM-1 models were tested to determine the effect of LM symmetry on the response ratio. On the asymmetric uncoupled model, the masses were not equidistant radially and the model did not produce a lateral force from longitudinal excitation. A detailed description of the LM models is presented in chapter II. The largest response ratio, 0.258, was obtained with the model having symmetric weights and responding at the pitch-peak-response frequency of 54.5 Hz. The response ratios obtained at the longitudinal peak response frequency of 57.3 Hz for LM-1 with asymmetric weights and at 58.7 Hz for LM-1 with symmetric weights were lower than those obtained at the pitch peak response. The LM-2 model was designed to produce coupling between the pitch and longitudinal motions by using offset asymmetric weights as discussed in chapters II and IV. The response ratio measured for LM-2 when installed in the full-stack configuration was not, however, any higher than the ratio measured for LM-1.

The effect of off-center longitudinal excitation at the base of the vehicle was studied by using a full-stack configuration with the LM-2—SLA-1. Electromagnetic shakers were attached to the base of the vehicle near the location of fins A (midway between -Z and +Y axes) and C (between +Z and -Y axes), diametrically opposite from each other. The response ratios obtained for equal and unequal forces at fins A and C are presented in table VI-2. The maximum response ratio of 0.117 occurred with a vibratory force of 15 pounds applied at fin A and 5 pounds at fin C.

Data indicating the effects of flexible tank supports in the service module on the vibratory response of the LM are presented in figure VI-1 and table VI-3. The vehicle configuration included the coupled asymmetric LM-3, the SLA-2, and 50-percent-full S-II lox tank. The SM configurations were SM-1 with no tanks, SM-2 with flexible tank supports, and SM-2A with stiffened supports that increase tank frequencies out of the region of concern. Figure VI-1 presents frequency response curves of LM center-line acceleration and relative phase between the input force and the LM center-line acceleration in both pitch and longitudinal directions when excited by a ± 10 -pound (44.5-N) longitudinal force at the S-IC center engine gimbal block. Little change occurred in the amplitude or frequency of the longitudinal resonance for the three cases investigated. The single peak of the longitudinal response as well as the frequency coincidence of the 270° phase shift between input force and peak amplitude indicated negligible contributions to the response from other modes. However, figure VI-1(a) shows two peaks in the pitch response, at 51 and 54.5 Hz. Figure VI-1(b) shows that the amplitudes of response in the pitch direction had been significantly reduced when SM-2, with flexible tank supports,

replaced SM-1. Two resonant conditions were still present, the weaker response at 49 Hz and the stronger response at 54.5 Hz. The effect of increasing the stiffness of the tank supports with SM-2 is shown in figure VI-1(c). The frequency response curves and the phase curves for SM-1 and SM-2a have similar shapes, resonances occurring at approximately the same frequencies. As shown in table VI-3, the maximum response ratio value of 0.61 occurred at 51.0 Hz for SM-1, and the minimum value of 0.129 occurred at 54.5 Hz for SM-2. Thus, the flexible tank supports in SM-2 caused a significant reduction in pitch response amplitude and had less coupling effect than the configuration with stiffer tank supports.

Since none of the mechanisms involving internal components of the vehicle investigated provided a response ratio approaching unity, use of combined longitudinal and pitch inputs were employed to determine the forces required to drive the vehicle so that a response ratio of unity was obtained. The first vehicle configuration investigated included SLA-2, the coupled asymmetric LM-3, and SM-2, and had the S-II lox tank 50-percent full, and the S-IC propellant tanks empty. A longitudinal shaker was attached at the S-IC center engine gimbals attachment and a pitch shaker was attached to the end of the LM-3 cruciform at the +Z axis. The frequency of the input force from the pitch shaker used to excite the LM-SLA resonance was adjusted to 54.5 Hz where it produced a 90° phase difference between input pitch force and LM center-line pitch acceleration. The longitudinal force was maintained at ±10 pounds (44.5 N) and the same frequency. By using the variable-phase oscillator, the phase between the two input forces was adjusted to obtain maximum amplitude in the pitch acceleration. Data were recorded for several pitch input force levels and the resulting response ratios are plotted against pitch shaker force in figure VI-2. The ratio of pitch force to longitudinal force required to obtain a 1:1 response ratio for this vehicle configuration and mode shape was 1:10. The acceleration level reached by using ±1-pound (4.45-N) pitch force and ±10-pound (44.5-N) longitudinal force was ±0.35g. The data also show that the response ratio increased linearly with increasing pitch force.

Similar procedures using two orthogonal shakers were followed for the configuration consisting of the SLA-2, SM-2A, and coupled asymmetric LM-3 that was used in the final loads-simulation test. The S-II lox tank was full and a simulated 35g static load was applied to the LM-SLA structure. The resulting response ratios are plotted in figure VI-2 as squares. For this configuration at a frequency of 55 Hz, the ratio of pitch force to longitudinal force required to obtain a 1:1 response ratio was 12:1000. The acceleration level for a ±10-pound (44.5-N) longitudinal force and a 0.12-pound (0.53-N) pitch force was ±0.18g. As in the prior configuration, there is a linear increase in the response ratio for an increasing pitch force.

None of the configurations studied had 1:1 response ratio at the LM center with pure longitudinal excitation. This investigation demonstrated the necessity and feasibility of using combined pitch and longitudinal excitation at the LM-SLA pitch resonant frequency.

Model dynamic characteristics.- The preliminary studies established that the full-stack configuration for the combined acceleration-loads simulation would have SLA-2, LM-3, and SM-2A model components; no simulated propellants in the S-IC stage; the lox tank of the S-II stage full of simulated propellant; and combined pitch-longitudinal vibration excitation. Prior to combined acceleration-loads simulation, the characteristics of the tuned vehicle were determined with simulated 35g acceleration loads applied to the SM, SLA, and LM and with low-level dynamic loads applied in the longitudinal and pitch directions in the appropriate ratio. The response shapes measured during these tests are presented in figure VI-3. These data were measured at a frequency of 55.1 Hz with a 10-pound (44.5-N) sinusoidal longitudinal force applied at the S-IC center engine gimbal and with 0.12-pound (0.53-N) sinusoidal force applied in the pitch direction at the LM attach point. The LM response ratio approaches unity. These data are used subsequently for comparison with the flight-loads simulation.

Results from vibration tests on the short-stack configuration of the full-size Saturn V at the NASA Manned Spacecraft Center indicated that the SLA was responding as a shell at the LM-SLA pitch resonance so that 10 nodes ($n = 5$) were located around its circumference at the LM attachment station. A similar response shape was measured on the 1/10-scale SLA-2 model and is shown in figure VI-4. These data were recorded for the same conditions where the longitudinal and pitch modes were measured. The results of a harmonic analysis of this wave form is presented in table VI-4. A significant component of the wave is the fifth harmonic with significant contributions from the first and third harmonics. This response again indicates the similarity of dynamic model and the full-scale vehicle.

Test Procedure for Loads-Simulation Tests

The previous section discussed preliminary studies that established the model configuration. For the loads-simulation tests, the model was subjected to dynamic forces that approached the vibratory flight load acceleration levels incrementally. Each of these tests was performed with simulated 35g static acceleration load on the SM, SLA, and LM. Data were recorded with the center of the LM responding dynamically at approximately 0.5g, 1g, 2g, 4g, and 6g in the pitch and longitudinal directions. For a given level of LM response, the test procedure was as follows:

- (1) The first longitudinal mode of the model was excited by adjusting the frequency of the longitudinal force so that a 90° phase difference between the force and the LM center longitudinal acceleration was obtained.

(2) The longitudinal force was increased until the desired longitudinal acceleration was obtained at the LM center.

(3) The pitch input force was increased until the desired pitch acceleration was imposed at the LM center.

(4) The phase of the pitch input force relative to the longitudinal input force was varied until the LM center pitch acceleration was a peak.

(5) The LM center accelerations were then readjusted to the desired levels and a 40-second tape record of the output from selected vehicle transducers was obtained.

For each of the low-level-acceleration tests (0.5g, 1g, 2g, and 4g at the LM center in the longitudinal and pitch direction), data were recorded at the frequency of the first longitudinal mode. However, it was not possible to generate sufficient force to obtain 6g on the LM center in the pitch direction as required for the flight-loads simulation because of shaker amplifier limitations. Therefore, the frequency of the excitation forces was changed to correspond to the LM pitch mode. At this frequency, 54.1 Hz, the fundamental test conditions were still present and no difficulty was encountered in exciting the LM at the required levels. The test procedure discussed previously was followed except that in step 1 the frequency of the longitudinal input force was adjusted to the LM pitch mode instead of the first vehicle longitudinal mode.

Results and Discussion of Combined Loads Tests

Results of combined dynamic and static acceleration loads simulation on the LM-SLA section of the 1/10-scale Apollo Saturn V dynamic model are presented. Response data obtained during the simulation are presented and compared with responses measured during low-level dynamic tests.

Model component response data for the high force tests with nominal 0.5g, 1g, 2g, 4g, and 6g response at the LM center are presented in table VI-5. The SLA shell was not instrumented for measurement of its vibratory motion during these tests. The input longitudinal and lateral sinusoidal forces are also given. The tests conducted with LM center dynamic motions nominally at 0.5g, 1g, 2g, and 4g were conducted at the vehicle first longitudinal mode frequency of about 56 Hz. However, the tests with LM center dynamic motions of 6g were conducted at the LM pitch resonant frequency of 54.1 Hz as discussed previously.

During the high force-level tests, most of the available data channels were allotted to transducers located in the model payload region. As a result, the total model response shapes were not identified in detail. In order to ascertain that the model responses were the same as those observed during the low-force-level tests, the high- and low-force-level response data were normalized to the LM center acceleration in the pitch and longitudinal

directions and the two sets of data are compared in figure VI-5. Figure VI-5(a) is the comparison of the normalized pitch data which show that the high-force-level data compare favorably with those previously measured and that the model payload area is responding in a shape similar to the fourth vehicle bending mode. The longitudinal data, shown in figure VI-5(b), although not in as good agreement as the pitch data, do show that the model was responding with a shape similar to the first longitudinal mode.

The primary purpose of the high-force-level tests was to verify the structural integrity of the LM-SLA interface hardware and the adjacent SLA sandwich structure under the combined dynamic and static loads. Data analysis and post-test inspection of the SLA showed that no failures occurred during these tests.

Concluding Remarks

Results are presented of a simulation on the 1/10-scale Apollo-Saturn V dynamic model of combined loads that occurred on the LM-SLA structure during the AS-502 anomaly. For the simulations, the frequencies of the first longitudinal mode, a lateral mode (fig. VI-3) and the LM-SLA pitch mode of the model were tuned to be nearly coincident and representative of the flight condition. The LM-SLA and SM structures were subjected to scaled combined static and dynamic loads equivalent to flight acceleration loads resulting from 3.5g thrust acceleration and 5.3 Hz oscillatory accelerations of 0.6g in the longitudinal and lateral directions at the LM center. As a result of these studies, the following comments can be made:

1. It has been demonstrated that frequencies and mode shapes of specified responses of the upper part of the 1/10-scale dynamic model of the Apollo-Saturn V launch vehicle adequately simulate desired flight resonant conditions.
2. A harmonic analysis of the mode shape of the SLA shell during vibrations at the frequency of the simulation shows that the primary circumferential component of the wave form is a shell mode having ten nodes on its circumference.
3. The model withstood combined static and dynamic acceleration loads derived from those imposed on the full-scale structure during flight without failure. Therefore, no failure mechanism related to the AS-502 flight structural anomaly could be identified.

Reference

- VI-1. Grimes, P. J.; McTigue, L. D.; Riley, G. F.; and Tilden, D. I.: Advancements in Structural Dynamic Technology Resulting From Saturn V Programs. Vol. II. NASA CR-1540, 1970.

TABLE VI-1.- LM RESPONSE RATIOS WITH VEHICLE
LONGITUDINAL EXCITATION

Frequency, Hz	Pitch/Longitudinal ratio for -		
	LM 1		LM 2
	Symmetric	Asymmetric uncoupled	Asymmetric coupled
54.5	0.258	0.110	-----
56.1	-----	-----	0.0691
*57.3	-----	.027	-----
*58.7	.0651	-----	-----

*Data taken at longitudinal response peak.

TABLE VI-2.- LM RESPONSE RATIOS WITH OFF-CENTER
LONGITUDINAL EXCITATION

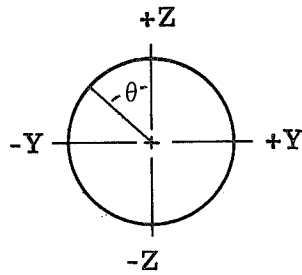
Force at S-IC base, lb	Force at fin A, lb	Force at fin C, lb	Frequency of peak response, Hz	LM center-line response		Pitch/Longitudinal ratio
				Pitch, g	Longitudinal, g	
10	--	-	56.1	0.047	0.680	0.0691
--	10	-	57.0	.067	.720	.094
--	5	5	57.2	.062	.610	.102
--	10	5	56.4	.079	.750	.105
--	15	5	57.4	.117	1.00	.117
--	20	5	57.0	.150	1.50	.100

TABLE VI-3.- LM RESPONSE RATIOS WITH
SM TANK FLEXIBILITY

Frequency, Hz	Pitch/Longitudinal ratio for -		
	SM-1	SM-2	SM-2a
51.0	0.61	-----	0.476
54.5	.383	0.129	.321

TABLE VI-4.- RESULTS OF HARMONIC ANALYSIS OF
SLA SHELL RESPONSE

$$\left[\text{Response at } \theta = A_0 + \sum_{n=1}^{n=12} (A_n \cos n\theta + B_n \sin n\theta) \right]$$



n	A _n	B _n
0	4.38	-----
1	-47.64	-11.73
2	1.71	1.58
3	-31.01	6.58
4	1.17	.87
5	-63.12	-19.21
6	2.00	1.58
7	-8.30	-1.12
8	-.75	2.45
9	-.49	-4.58
10	-.46	2.01
11	3.06	.01
12	-.54	0

TABLE VI-5.- SOME COMPONENT RESPONSES OF 1/10-SCALE APOLLO SATURN V MODEL

Nominal test g levels	Frequency, Hz	Input force, lb (N), for -		LM center-line response, g, for -			Engine response level, g, for -				Model station 416 response, g, for -	
		Longitudinal	Pitch	Longitudinal	Pitch	Yaw	S-IVB pitch	S-IVB yaw	S-II pitch	S-II yaw	Longitudinal	Pitch
0.5	^a 55.9	18.6 (82.7)	1.23 (5.48)	0.461	0.521	0.312	2.21	0.390	0.791	0.424	0.367	0.286
1.0	^a 56.4	44.0 (196)	3.66 (16.3)	.912	1.01	.438	3.40	----	----	----	----	0.546
2.0	^a 56.2	98.4 (438)	7.99 (35.5)	1.60	1.98	1.16	6.45	----	----	----	----	1.09
4.0	^a 56.3	185 (824)	15.8 (70.4)	3.72	3.53	1.56	10.6	----	----	----	----	1.79
6.0	^b 54.1	517 (2200)	35.1 (156)	5.95	5.98	2.10	^c 27.5	----	----	----	----	3.06

^aResonance tuned to first longitudinal mode.

^bResonance tuned to fourth bending mode.

^cThe response decreased 10 percent after 50 seconds of excitation.

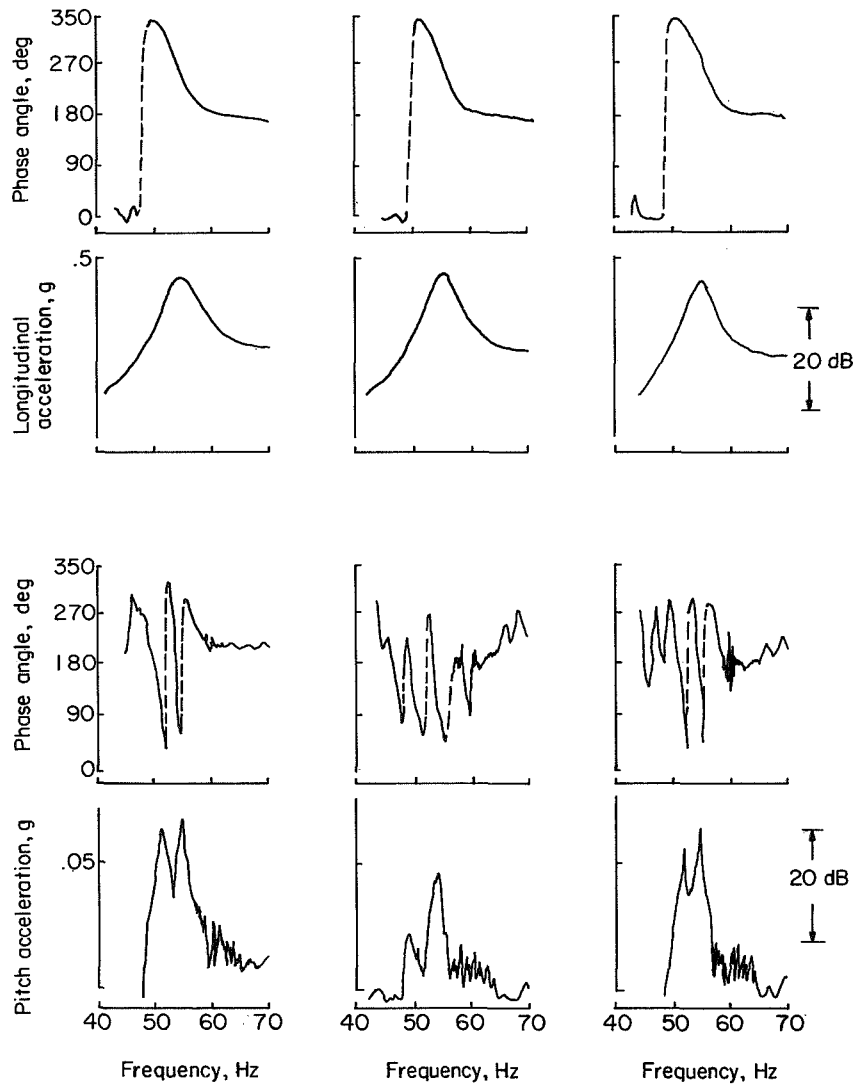


Figure VI-1.- Acceleration response amplitude and phase angle for LM center in full-stack configuration with 10-pound (44.5-N) longitudinal input sinusoidal force (phase referenced to force).

Configuration

- SM-2, SLA-2, coupled asymmetric LM-3, S-II Lox
50% full
 - SM-2A, SLA-2, coupled asymmetric LM-3, S-II Lox
100% full
- 35-g static axial load on SLA-2/LM-3

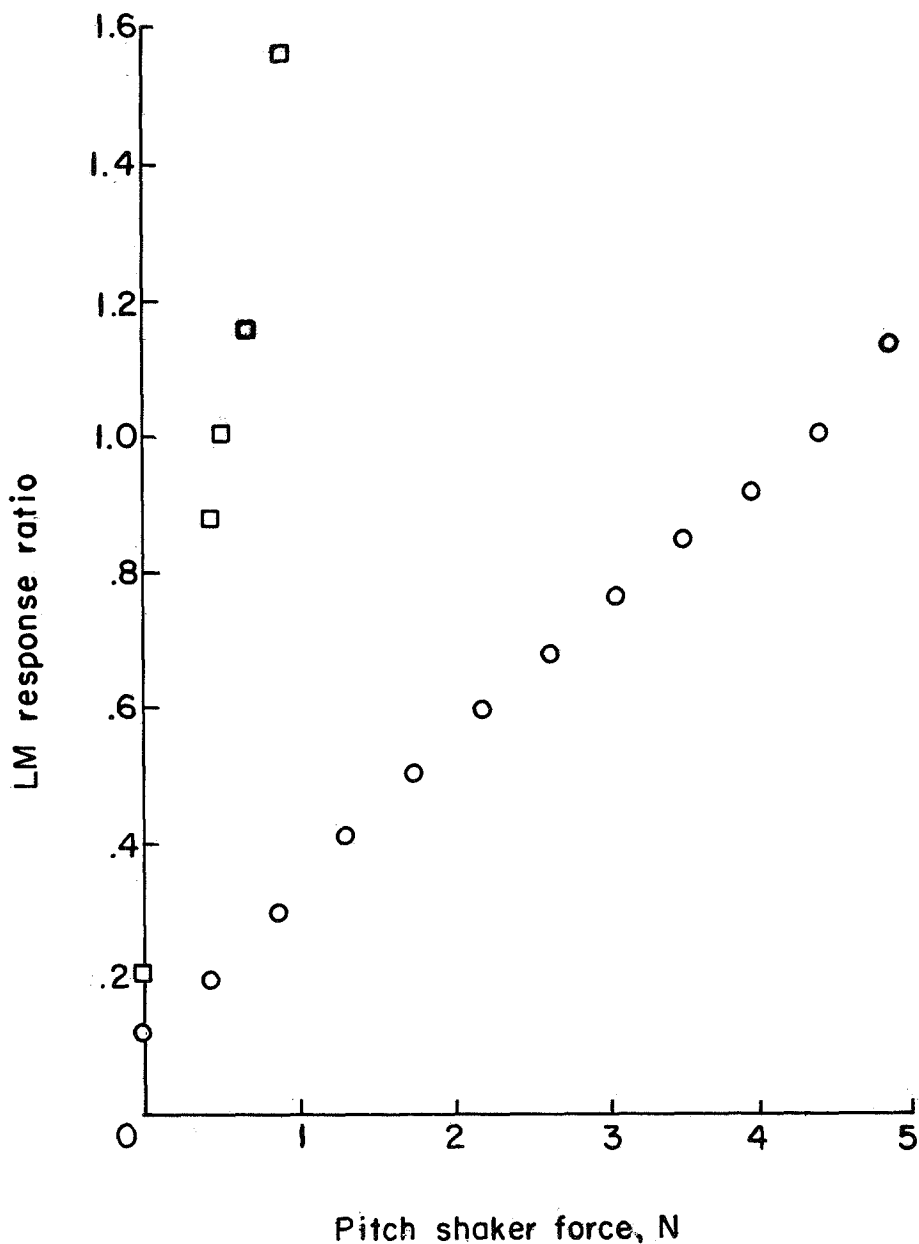


Figure VI-2.- Variation of LM response ratios with pitch input force. Longitudinal input force constant at ± 10 pounds (44.5 N).

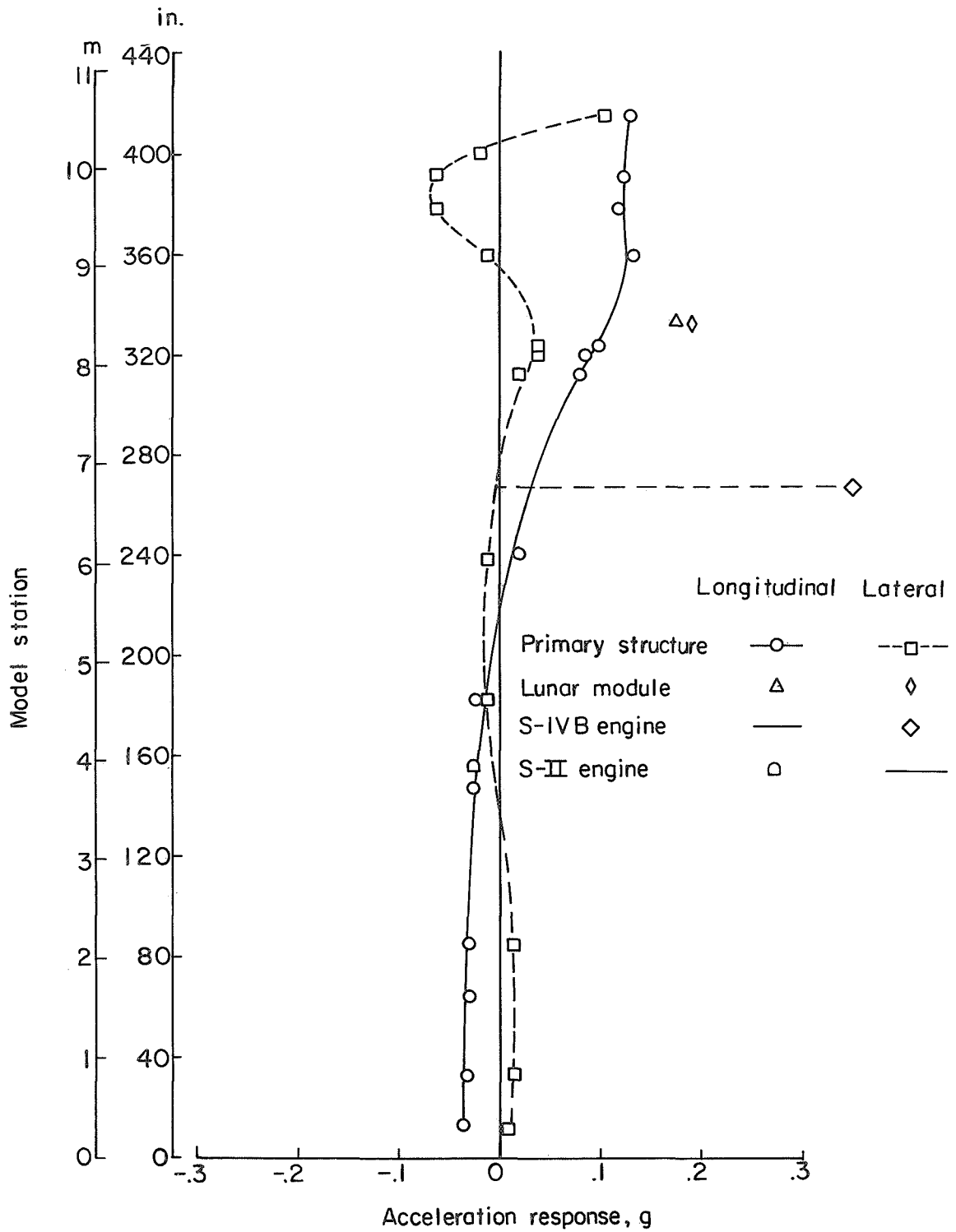


Figure VI-3.- Response shapes from 1/10-scale full-stack model with combined lateral and longitudinal excitation and 35g simulated static load on LM-SLA.

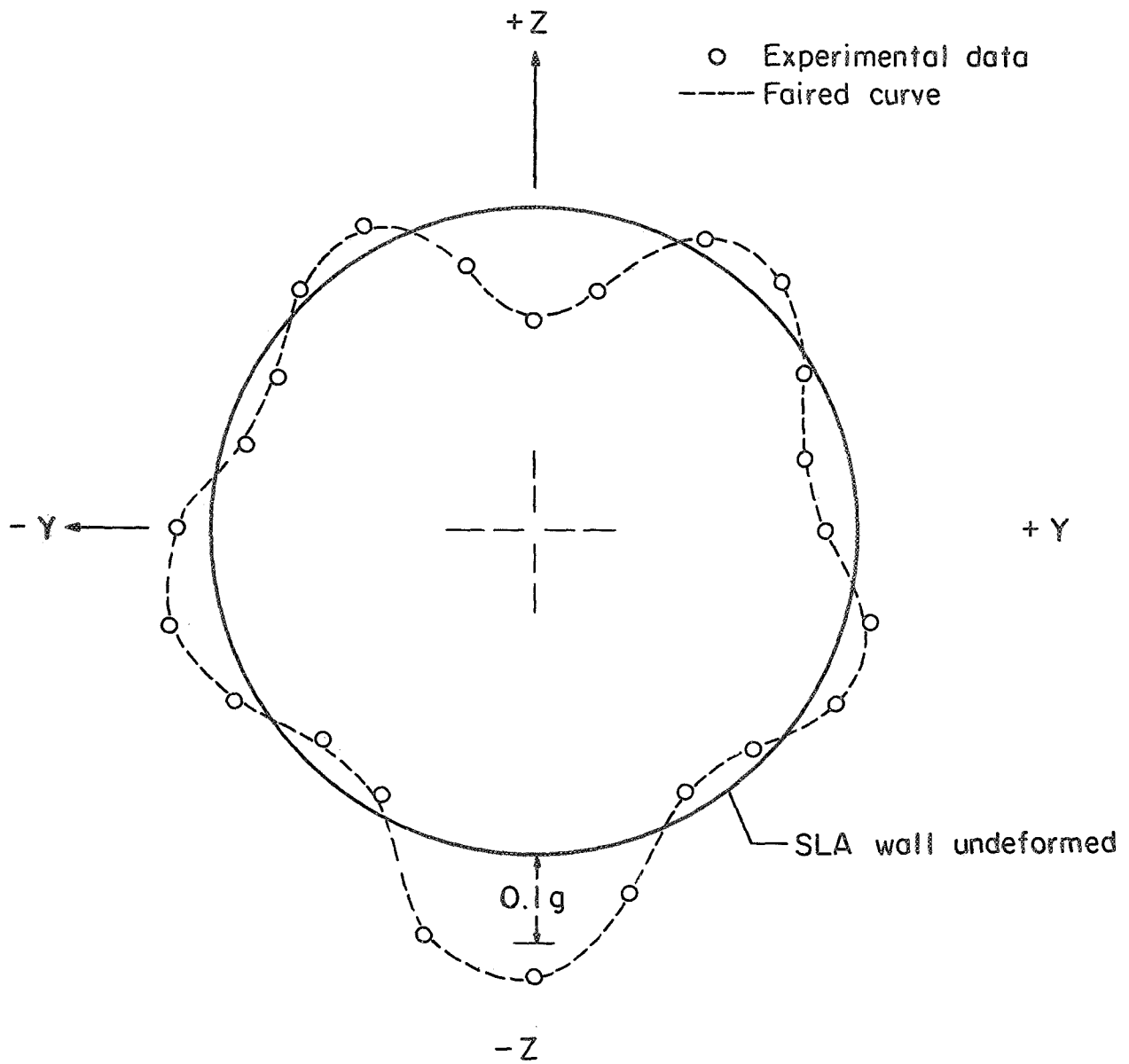
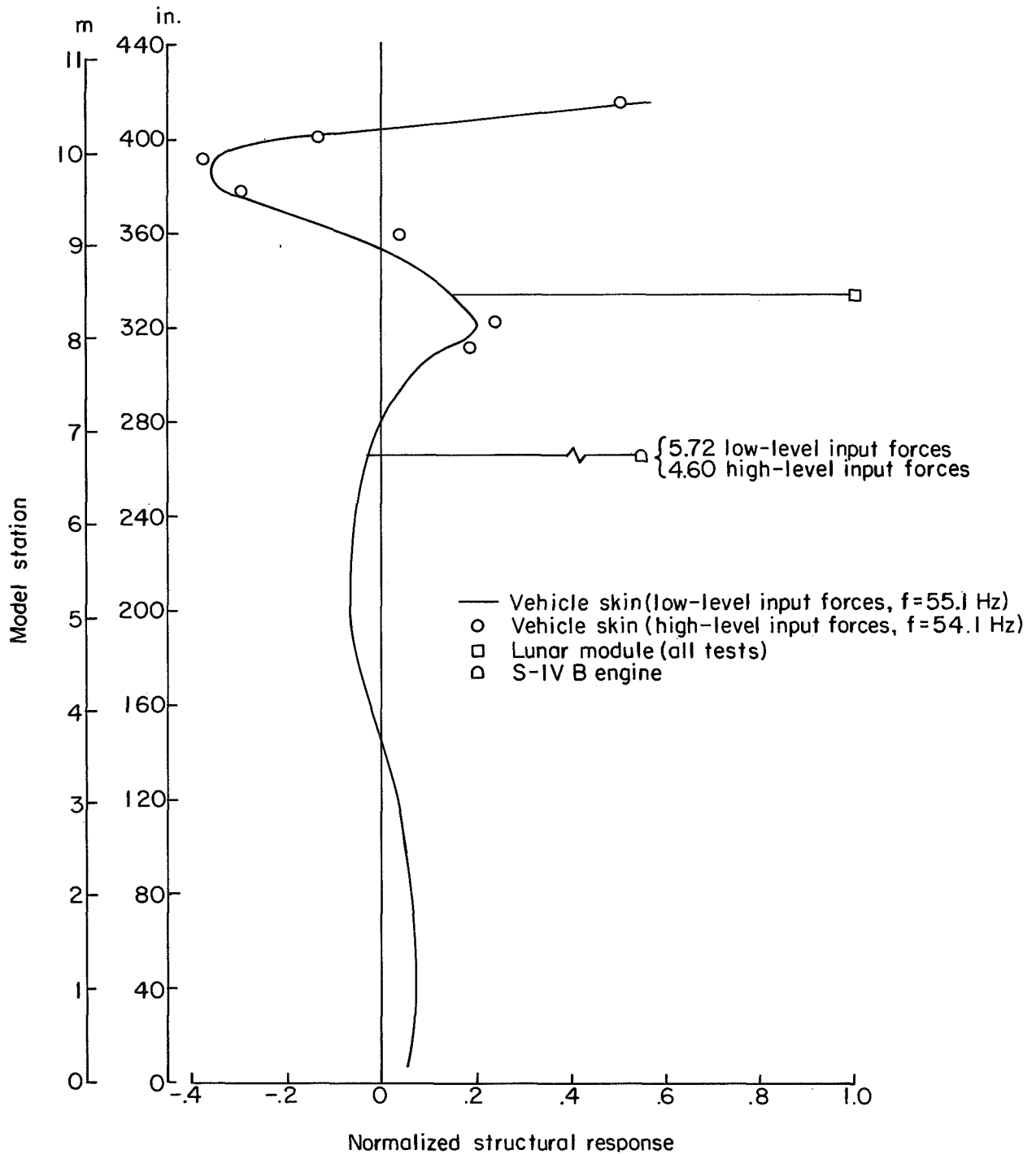
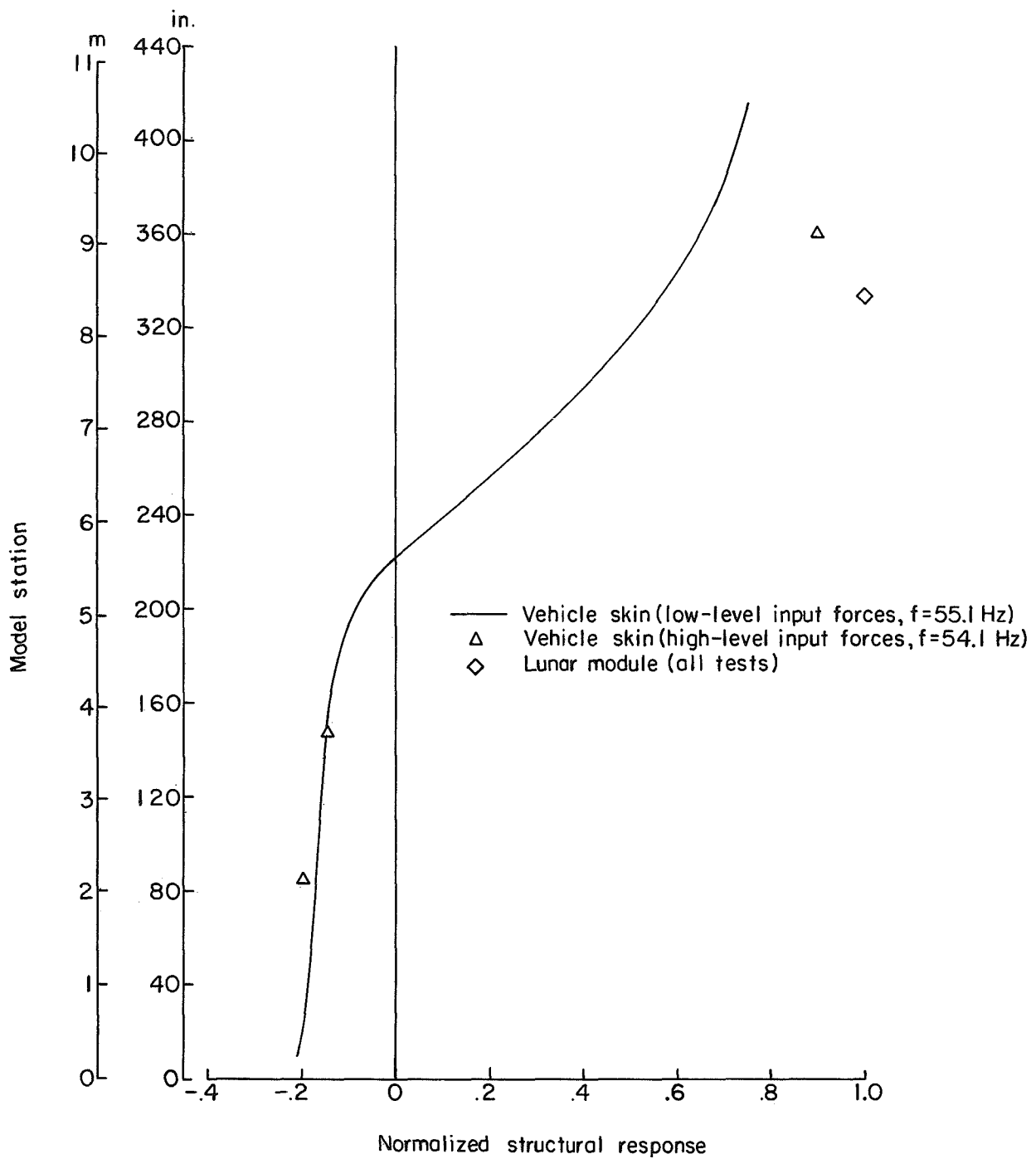


Figure VI-4.- Radial response shape of SLA-1 at LM attach plane. Full-stack model with 35g simulated static load and combined lateral and longitudinal excitation.



(a) Pitch.

Figure VI-5.- Comparison of model response data from low-force and high-force full-stack tests. All data normalized to LM center-line response.



(b) Longitudinal.

Figure VI-5.- Concluded.

VII. GENERAL CONCLUDING REMARKS

By Sumner A. Leadbetter
Langley Research Center

This paper has presented results from analytical and experimental investigations of potential structural dynamic problems that could contribute to structural malfunctions in the payload section of a launch vehicle. The studies reported were conducted at Langley Research Center in support of extensive investigations at other NASA Centers and contractor facilities of an unmanned Apollo Saturn 502 structural anomaly. Presented are results of greatest significance that cover LM-SLA dynamic characteristics, ability of a short-stack configuration (partial vehicle) test to simulate a full-stack configuration (total vehicle) test, potential coupling mechanisms between longitudinal and lateral response, and combined static and dynamic flight loads simulation on a dynamic model. This section discusses salient results from the investigation.

A significant feature of this investigation was the simultaneous application of analytical and experimental techniques to solve an operational problem, wherein the experimental data were obtained on a carefully scaled structural dynamic model. Previous applications of dynamic models have been made during the prototype development cycle before full-scale hardware was available. In this case, time precluded use of full-scale hardware and the existing detailed 1/10-scale dynamic model was a natural source of data for validating mathematical models that had to be developed for studying unanticipated dynamic problems. Thus, dynamic models should be considered as relatively inexpensive and quick sources of experimental data for operational troubleshooting.

Two analytical procedures were used, one to obtain a definition of the overall structural dynamic characteristics of the Apollo-Saturn V short-stack (partial vehicle) and full-stack (total vehicle) model configurations and the other to define the mode shapes and frequencies of the LM-SLA structure. Although the first, a transfer matrix approach, did prove to be a versatile tool for parametric studies of overall vehicle dynamic properties, it did not provide the detailed modal definition that was needed and that the shell analysis and involved component mode analysis could provide. These analyses did provide valuable insight into complex structural dynamic problems such as the behavior of a complex shell structure having attached asymmetric flexible structures.

The nature of the flight structural anomaly, involving higher mode vibrations, required that the dynamic behavior of the launch vehicle and payload be thoroughly understood before corrective measures could be attempted. The Langley studies contributed to this understanding in a timely manner because of three factors: First, the parallel approach of analysis and experiment insured that all important factors were being

considered. Second, the use of dynamic models permitted the experimental program to be conducted quickly, inexpensively, and with maximum flexibility. Finally, the component mode analytical approach developed confidence in the analytical tools on simple structures before more complex configurations needed to be analyzed. For example, these studies showed that the LM and SLA interact in a very complex fashion that involves asymmetric deformations of the LM. Since the actual LM is a much more complex structure than the simplified 1/10-scale model, even more complex interactions could be expected on the flight vehicle.

Analytical parametric studies of model overall structural dynamic characteristics revealed significant factors. The importance of branch component response in the vehicle frequency range of interest was investigated by altering the magnitude of the involved component stiffness and it was found that the second- and third-stage engine dynamics produced a greater effect on the overall model response than the SM or the LM component did. Another factor noted was that doubling the damping in the SM tanks affected the ratio of the lateral to longitudinal coupling more than doubling the damping in the LM did.

The attempts to develop a boundary-restraint system for the short-stack configuration that duplicated boundary conditions of the same components when installed in the full-stack vehicle were only partially successful. During an analytical study, displacements at the base of the short-stack configuration were matched to displacements of the same component installed in the full-stack configuration for vibrations in the modes of interest. Results from these studies indicated that failure to match rotation, shear, and moment boundary conditions can lead to serious discrepancies between vehicle motions at other points in the full- and short-stack configurations. Thus, without considerable additional effort to match all boundary conditions, short-stack tests cannot be expected to produce motions representative of a full-stack test. In spite of this limitation, short-stack tests were shown to be valuable for understanding dynamic behavior and for validating mathematical models that could, in turn, predict behavior of the full-stack configuration.

The mechanism by which responses of the elastic structure were coupled to generate 0.6g acceleration in the LM at 5.3 Hz in both the pitch and longitudinal directions on the flight vehicle was not conclusively determined. Such coupling can arise from asymmetries in stiffness, mass, or force inputs. Any stiffness asymmetries should have been inherent in the dynamic model structure but were found to be not sufficient to produce the observed coupling. Mass asymmetries of the LM were simulated analytically and on the model. Under some conditions, a ratio of pitch to longitudinal response of one under longitudinal excitation could be achieved. However, for the most realistic conditions – using the assembled dynamic model – this 1:1 ratio could not be attained with longitudinal excitation without supplementing the longitudinal input force with a lateral input force at the

same frequency. As part of these studies, the SM tanks were found to influence the ratio of pitch to longitudinal coupling of the LM. The four SM tanks were offset from the vehicle center line and thus couple the pitch and longitudinal motions directly. In addition, they behave as branches off the main structure with frequencies near the anomaly frequency. Therefore, these SM tanks can tend to behave as vibration absorbers at the frequencies of interest. These findings indicated that the SM tanks had a significant role in the coupling mechanism on the flight vehicle. However, the response at these frequencies was extremely sensitive to the tank-mounting flexibilities and flight configurations could not be duplicated on the model with any confidence.

The climax of the studies reported herein was the simulation of combined static and dynamic flight loads on the LM-SLA section of the 1/10-scale Apollo Saturn V model. Excluding thermal loads, the model successfully sustained stresses corresponding to full-scale conditions, namely, static stresses from 3.5g axial acceleration and dynamic stresses corresponding to 0.6g longitudinal and lateral vibratory acceleration at 5.3 Hz. This simulation is believed to be the first application of dynamic models for demonstrations of structural integrity under combined static and dynamic flight loads. No attempt was made to simulate loads that could result from any temperature change. The loading techniques developed could have application in future combined loads studies on both dynamic models and full-scale vehicles.

These studies of the Apollo Saturn 502 structural anomaly have contributed to the conclusion by other groups that the structural failure did not result from pogo-induced flight loads. In addition, the Langley investigation has contributed substantially to the understanding of the behavior of complex structural systems. The combined application of analysis and experimental methods, the application of combined flight loads simulation techniques to dynamic models, and the utility of dynamic models in operational problem solving have been demonstrated.

Langley Research Center,
National Aeronautics and Space Administration,
Hampton, Va., February 27, 1970.



"The aeronautical and space activities of the United States shall be conducted so as to contribute . . . to the expansion of human knowledge of phenomena in the atmosphere and space. The Administration shall provide for the widest practicable and appropriate dissemination of information concerning its activities and the results thereof."

— NATIONAL AERONAUTICS AND SPACE ACT OF 1958

NASA SCIENTIFIC AND TECHNICAL PUBLICATIONS

TECHNICAL REPORTS: Scientific and technical information considered important, complete, and a lasting contribution to existing knowledge.

TECHNICAL NOTES: Information less broad in scope but nevertheless of importance as a contribution to existing knowledge.

TECHNICAL MEMORANDUMS: Information receiving limited distribution because of preliminary data, security classification, or other reasons.

CONTRACTOR REPORTS: Scientific and technical information generated under a NASA contract or grant and considered an important contribution to existing knowledge.

TECHNICAL TRANSLATIONS: Information published in a foreign language considered to merit NASA distribution in English.

SPECIAL PUBLICATIONS: Information derived from or of value to NASA activities. Publications include conference proceedings, monographs, data compilations, handbooks, sourcebooks, and special bibliographies.

TECHNOLOGY UTILIZATION PUBLICATIONS: Information on technology used by NASA that may be of particular interest in commercial and other non-aerospace applications. Publications include Tech Briefs, Technology Utilization Reports and Notes, and Technology Surveys.

Details on the availability of these publications may be obtained from:

**SCIENTIFIC AND TECHNICAL INFORMATION DIVISION
NATIONAL AERONAUTICS AND SPACE ADMINISTRATION
Washington, D.C. 20546**